Improved Estimation of Transport Parameters in the Dermis

A dissertation submitted to the

Division of Research and Advanced Studies
of the University of Cincinnati

in partial fulfillment of the requirements
for the degree of

DOCTOR OF PHILOSPOPHY

in the Division of Pharmaceutical Sciences
of the James L. Winkle College of Pharmacy

2012

by

Rania Ibrahim

M.S University of Cincinnati
June 2000

Committee Chair: Gerald B. Kasting, Ph.D.

ABSTRACT

An improved model of dermal concentrations and clearance is presented. This was accomplished by refining the assumptions in the current computational model and by developing and analyzing additional data. Accurate values of partition and diffusion coefficients within the lower skin layers are among the information required in order to estimate skin concentrations of permeants following topical application. For highly lipophilic compounds these parameters also play a significant role in determining systemic absorption rates. A modified in vitro experimental methodology was employed to measure the transport parameters of 3 solutes varying in lipophilicity, namely, DEET, diclofenac and parathion. Isolated human dermis obtained from surgical reduction was mounted in side-by-side diffusion cells in the presence and absence of a dialysis membrane (5000 MW cutoff) placed between the dermis and the donor solution. The results indicate that for permeants such as diclofenac and parathion, that are more than about 87% bound to soluble proteins in the dermis, the dialysis membrane method is important in order to obtain accurate estimates of transport and partitioning parameters in dermis.

A computational model for estimating dermal clearance in humans of arbitrary, non metabolized solutes was developed. The blood capillary component employed slit theory with contributions from both small (10 nm) and large (50 nm) slits. The lymphatic component was derived from previously reported clearance measurements of dermal and subcutaneous injections of ^{131}I-albumin in humans. Model parameters were fit to both blood capillary permeability data and lymphatic clearance data. Small molecules are

cleared largely by the blood and large molecules by the lymph. The combined model showed a crossover behavior at approximately 29 kDa, in acceptable agreement with the reported value of 16 kDa. When combined with existing models for stratum corneum permeability and appropriate measures of tissue binding, the developed model has the potential to significantly improve tissue concentration estimates for large or highly protein bound permeants following dermal exposure.

The dermal clearance model combined with existing models for stratum corneum permeability and appropriate measures of protein binding were used to analyze *in vivo* concentration data from the literature and compare it to predictions made by the current mathematical model. All data were analyzed using the modified mathematical model; however, for permeants with reported absorption data, a curve-fitting spreadsheet was also used which took into account both skin concentration profiles and absorption profiles in urine. For most permeants the model predicted a steeper slope and hence a quicker decrease in the skin concentration with depth than the observed data. Acceptable predictions were made for Econazole, Methoxsalen, Flurbiprofen and ketoprofen with adjustments to the diffusivity of the stratum corneum. The revised computational model is able to make predictions for topically applied permeants, yet further work can be done to better improve the predictive capability of the model.

Mom, Dad, Nisreen, Omar and Mostafa

ACKNOWLEDGMENTS

I have had the opportunity and pleasure to interact with many individuals during my years in the graduate program at the University of Cincinnati. Several individuals have had a great impact on my journey through the program and I would like to take this opportunity to acknowledge them

First and foremost, I would like to take the opportunity to acknowledge my committee members for serving on this committee, their time, input and advice.

I would like to thank Dr. G. B. Kasting, the committee chair and advisor. Dr. Kasting, has been invaluable through out this whole process. Not only has he been an extraordinary mentor, but also a friend, a confidant and one of my greatest supporters. Through all the highs and lows of this journey, he has always been there for me. There was never a time where he did not make himself available to me to discuss both my professional and personal life. He has taught me so much and no words can describe my immense gratitude for his support and mentorship. He is truly an extraordinary individual and I have been blessed to have him as my advisor.

I would like to thank Dr. R. R. Wickett, for all of his advice and input. It was Dr. Wickett's classes that made me realize my career path and passion. I would also like to thank him for helping me acquire my dream job. He had the faith in my capabilities and highly recommended me for a position that I could of only dreamed about. He continues to be a mentor for me in my career and for that I will always be grateful.

I would like to thank Dr. K. Li for his support in this program and his invaluable input and advice. His suggestions always incited a very interesting debate and provided a alternative approach to my research which I greatly appreciate.

I would like to thank Dr. P. Desai for his time and input in my research. He was a source of encouragement during this journey and provided me with great advice during the process of putting my research proposal together.

I would also like to thank Dr. J. Fried for his support in this program. He accepted me into the IGERT program which paid for my tuition and stipends during the first three years of the program. To be given the opportunity to be a part of IGERT and the skills I developed through the program were invaluable. I am forever grateful to him for the opportunity.

Lastly, I would like thank Dr. A. Sakr, who took the time to talk to me about the program and introduced me to Dr. Wickett and Dr. Kasting.

I would also like to thank the organizations, IGERT, NIH and COLIPA for financially supporting me and my research and making my graduate career possible. The James L. Winkle College of Pharmacy was also integral part of my academic career. They allowed me the opportunity to travel to conferences and present my work. It was at one of these conferences where I met my present employer. So for that, I am extremely grateful.

I would like thank Bill Pickens for providing me with the skin samples during my research. Also, the generous donation from the Musculoskeletal Tissue Foundation made it possible for me to continue my research when skin samples were scarce.

The staff and professors at the department have all touched my life in various ways and will always have a special place in my heart.

I would like to give a huge thanks to Matthew Miller for all of his help. I am pretty sure that I talked his ear off most of the time, but he has been a huge support for me in my research. He took the time to teach me the ins and outs of the lab, the inner workings of the model and without him I would not be where I am today.

I want to thank my dear friends and colleagues Jennifer Karr and Poonam Chopra for being there for me and for their friendship. All the laughs and tears were worth it and they will forever be a part of my life. Big thanks to all the other students in the program who have made a lasting impression on me.

Last but not least, I would like to thank my family who has supported me through out this whole process. My parents are my role models and I am who I am today thanks to them and their support and guidance. If only I were a fraction of who they are I would truly be an extraordinary individual. My sister and brothers were a source of comic relief for me during the rough times when there didn't seem to be a light at the end of the tunnel. Thanks Omar for the tutoring in Chemistry when I first started the program. I'm sure it wasn't the most exciting chapter in your life.

Thank you to everyone from the bottom of my heart!

TABLE OF CONTENTS

LIST OF TABLES

LIST OF FIGURES

1. INTRODUCTION

The skin constitutes the primary barrier to the absorption of chemicals into the body. It consists of three main regions which collectively control the overall absorption of a solute into the body. These regions include a highly lipophilic stratum corneum which is considered the primary barrier, a hydrophilic epidermal layer whose role is increased as the lipophilicity of the permeant increases,(Gupta, Wientjes et al. 1995) and finally the dermal layer whose vascular nature leads to the clearance of solutes into the systemic circulation or surrounding tissues as well as tissue retention of the solute due to protein binding. Knowledge of the rate and extent of dermal absorption is of great importance in the cosmetic and transdermal drug delivery industry.(van der Merwe, Brooks et al. 2006) Another pressing need has been in the area of dermal risk assessment in occupational, environmental and leisure settings.(Kruse, Golden et al. 2007)

In the case of topical drug delivery; lag times, skin concentrations in the dermal tissue and clearance to its targeted sites, are all important factors that determine the efficacy of the drug. With regards to dermal risk assessment, these same factors give insight into the exposure effects of toxins on the skin and the body as a whole. In principal, the study of chemical penetration in humans *in vivo* would provide us with the most relevant values of the transport parameters associated with absorption. Yet, such studies are expensive and may be unethical. *In vivo* animal studies have also become less popular due to ethical and economic reasons. Thus, *in vitro* studies utilizing human skin and animal skin have become the standard in permeation studies, the former being preferred due to differences

in skin characteristics between species. To experimentally predict the absorption of every permeant would be extremely time consuming and expensive.(Kruse, Golden et al. 2007) Thus alternative methods have become popular in these fields. The most promising methods available are predictive models developed to estimate the transport parameters of a permeant based on its physicochemical properties and the properties of the skin layers. The quality of these models often depends on the quality of the experimental data to which they have been fitted. Ideally, these models would accurately mimic the transport properties of the different layers of the skin in order to estimate the absorption profiles of varying solutes. However, they have not fully reached this level of sophistication. Further refinement is required concerning the physiological basis of the models as well as the experimental methods utilized to develop calibration data.

1.1 Predictive models

Many articles in the literature have been devoted to the description of skin absorption models. These models can be divided into two main types:(van der Merwe, Brooks et al. 2006)

- Quantitative structure-activity relationship (QSAR) models. These models predict the steady-state permeability constant of molecules based on physical-chemical properties of permeants, solvents and chemical mixtures.
- Mathematical models that simulate the effects of partitioning and transport processes involved in absorption. These models vary according to how they are correlated to the physiology of the skin.

- Compartmental Models: Such models may be traditional compartmental models that are not physiologically relevant. These models solve rate equations and describe solute transport in terms of pharmacokinetic parameters.
- Diffusion Models: These models account for descriptions of body compartments and tissues based on the physiology of these components. The transport parameters derived by these models are based on diffusion equations and not rate equations used in pharmacokinetics.

There are, however, limitations associated with most of these models in terms of their predictive power. QSARs do not predict absorption outside of the steady-state portion of the absorption/time curve. Also, Cleek and Bunge(Cleek and Bunge 1993) have demonstrated that the absorption of the solute as described by steady-state parameters may be highly underestimated in comparison to the actual absorption of the permeant as seen in the figure below.

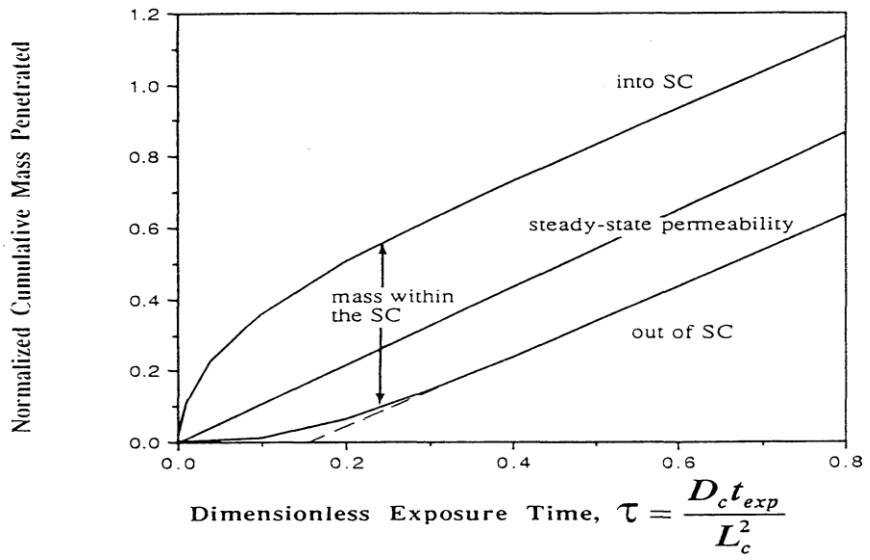

Figure 1.1 Cumulative mass of chemical penetrating into and out of the stratum corneum normalized by ($AL_cK_{cv}C_v^0$) as a function of dimensionless t_{exp}.(Cleek and Bunge 1993) (Source: Cleek R and Bunge A.1993. *Pharm Res*. **10:** 497-506)

Simplistic compartmental models that do not account for the physiology and anatomy of the skin give rough estimates of the transport parameters associated with dermal absorption and thus are poor as predictive tools.(van der Merwe, Brooks et al. 2006)

Scheuplein(Scheuplein 1965; Scheuplein 1967) was among the first to quantitatively model the skin barrier. The stratum corneum (SC) was assumed to be a uniform diffusion medium with parallel follicular pathways. The viable tissue (VT) was established as the rate limiting barrier for highly lipophilic compounds. Michaels et al.(Michaels, Chandrasekaran et al. 1975) modeled the SC as a brick and mortar structure with molecules diffusing intercellularly or interstitially. However, the model was deemed conceptual rather than predictive due to the fact that it required exacting information that

was unavailable. Berner and Cooper(Berner and Cooper 1987) assigned parallel lipodal pathways and polar pathways. A third pathway, a heterogeneous oil-water multi-laminate pathway was added. Yet the parameters required for the model lacked physiological and/or experimental basis. Albery and Hadgraft(Albery and Hadgraft 1979) had a similar model to Berner and Cooper(Berner and Cooper 1987) and thus were faced with the same limitations. Kasting et al.(Kasting, Smith et al. 1987) described skin permeation as a simple passive diffusion process. The SC was considered the rate limiting barrier and was treated as a homogeneous layer. Solubility limitation for the permeant in the SC and the molecular size dependence for the diffusivity were incorporated into the model. Flynn(Flynn 1990) also recognized the dependence of the diffusivity on molecular weight (MW) and classified permeability coefficients according to chemical polarity such that hydrophilic compounds used polar pathways. Guy and Hadgraft(Guy and Hadgraft 1988) and Potts and Guy(Potts and Guy 1992) challenged the polar pathway idea and theorized that the higher permeability k_p for the smaller polar compounds (low MW) was due to their high diffusivity specifically that the normalization of k_p by K_{OCT} leads to an inverse dependence on the MW. A concise summary of the above developments may be found in (McCarley and Bunge, 2001).(McCarley and Bunge 2001)

1.1.1 Pharmacokinetic models

In these models the body is represented by one or more well-stirred compartments. Most commonly found in the literature are one-compartmental and two-compartmental skin models. Kruse et al.(Kruse, Golden et al. 2007) developed a four-compartmental skin model and Higaki et al.(Higaki, Asai et al. 2002) developed a six-compartmental model

representing the muscles and underlying tissues affected by systemic clearance and direct penetration from the dermis. It should be noted that the literature at times may be confusing due to the lack of clarity when referring to the viable tissues (VT). Some models consider the VT as the epidermis sans the SC, while others consider it as the combination of epidermis sans the SC and dermis. For simplification, compartmental models consider average concentration across the skin layer rather than position-dependent concentration, which in itself may be considered a limitation since the concentration of the permeant varies with position and tissue layer.

The common theme observed in all of these models is that the viable epidermis and dermis are treated as a single aqueous homogenous layer, with complete clearance of the permeant at the base layer. This serves as less than satisfactory for the following scenarios: (a) when the SC barrier has been compromised; (b) topical application of vasconstrictive agents with the permeant; (c) contact sensitization thresholds; (d) effects of age and environmental/pathological conditions.(Kretsos, Miller et al. 2008)

Another common problem associated with compartmental models is the fact that they are adequate in describing the absorption of permeants to which the model has been fitted, yet are unable to describe the absorption of new permeants. Thus, the use of such models as predictive tools is unsuitable for hypothesis generation and testing.(van der Merwe, Brooks et al. 2006)

McCarley and Bunge(McCarley and Bunge 2001) published a review on one-compartmental and two-compartmental models available in the literature. The authors stated that in the process of their research, although hundreds of papers had been dedicated to compartmental model representations of the skin, the majority of these

papers estimated values for rate constants from the experimental data without relating these values to the physiological and physical parameters of the skin. Also, several of the models did not state the assumptions built into their development, nor did they clearly define the relationship between the rate constants and physicochemical properties of the skin and permeant. Another issue that arose was the fact that skin layers included in the models were not always clear. Such models are inadequate for use in predicting new permeants since the unknowns are too numerous and cannot be explained or used by anyone other than the authors of the respective models. The objective is to develop a model that can be easily used by any individual.

1.1.2 One-compartment models

One-compartmental models can be grouped into three main categories:

- The compartment represents the SC or the viable epidermis (VE) alone. The assumption put forth in such models is that other skin layers do not contribute significantly to the storage capacity and overall resistance.(McKone 1993; Bunge, Flynn et al. 1994; Bunge, Cleek et al. 1995; McCarley and Bunge 1998) For example: the rate limiting barrier to the penetration of a highly lipophilic permeant would be the aqueous viable epidermis. These simplistic models do not account for parameters of the excluded skin layer which may have implications on factors other than resistance such as lag times, tissue concentrations and systemic clearance.
- The compartment represents all skin layers.(McDougal, Jepson et al. 1986; Kubota and Maibach 1992; Rao and Brown 1993; Blancato and Chiu 1994;

Kubota and Maibach 1994; Singh and Roberts 1994) It may or may not include the dermis.

- The compartment represents a hybrid, such that the penetration of the solute is limited by the SC, but the storage capacity is controlled by the VE.(Guy, Hadgraft et al. 1982; Guy and Hadgraft 1985; Brown and Hattis 1989)

Several assumptions are built into the development of these models: (a) equilibrium between the skin and blood (b) equilibrium between the skin and vehicle (c) rate of mass transfer into the skin from the vehicle is proportional to the steady-state permeability coefficient k_p (d) rate of removal from the skin is controlled by the solubility of the solute in the blood and the blood flow rate.

Table 1. Category and Common Assumptions of Several One-Compartment Models

Model #	Model	Category	Equilibrium between Skin and Vehicle	Equilibrium between Skin and Blood	k_1^A Proportional to $P_{skin,v}$	k_2^A Estimated Assuming Blood Flow Limited	Rate Constant Neglected	Used Membrane Model to Estimate Rate Constants
1	McKone[9]	1 (sc)	✓		✓		✓ (k_{-2}^A)	
2	McCarley[10]	1 (sc or ve)		✓				✓
3	Rao[11]	2	✓	✓	✓	✓		
4	Blancato[12]	2	✓	✓	✓	✓		
5	McDougal[13,14]	2	✓	✓	✓	✓		
6	Kubota[15,16]	2					✓ (k_{-2}^A)	✓
7	Singh[17]	2			✓		✓ (k_{-2}^A)	
8	Guy[19–21]	3		✓			✓ (k_{-1}^A)	
9	Brown[18]	3		✓	✓	✓		

Table 1.1 Category and common assumptions of several one-compartmental models.(McCarley and Bunge 2001) Source: McCarley KD, Bunge AL. 2001. *J Pharm Sci* **90(11)**:1699-1719

Guy et al. model: (Guy, Hadgraft et al. 1982; Guy and Hadgraft 1985) This model is different from other one-compartmental models in the sense that the chemical being absorbed is in a solid form as opposed to a solution. Therefore, the cumulative amount of permeant crossing the skin is proportional to the mass remaining on the skin. The rate constant representing the transfer from skin to vehicle was neglected in this model. When compared to the 2-membrane model, which is a more realistic model and also accounts for the changes in concentration with position, the cumulative amount of chemical crossing the epidermal-blood interface was overestimated, especially for more lipophilic compounds. Also the predicted values of the cumulative mass in the epidermis and cumulative mass crossing the epidermal-blood interface were independent of K_{oct}.

Singh and Roberts model:(Singh and Roberts 1994) This model assumes that the transfer rates from epidermis to vehicle and epidermis to blood are based on the steady-state concentration of the epidermis. The rate constant representing the transfer from blood to skin is neglected. When compared to the 2-membrane model, the cumulative amount of chemical crossing the epidermal-blood interface was overestimated for lipophilic compounds.

Kubota and Maibach model:(Kubota and Maibach 1992; Kubota and Maibach 1994) Rate constants were derived by forcing the model to match the behavior of the one-membrane model. The model does not clearly define which skin layers are included. Also, the rate constant representing the transfer from blood to skin was neglected. When

compared to the two-membrane model it was a better predictor of the transport parameters due to the fact that it was based on the one-membrane model.

McCarley and Bunge model:(McCarley and Bunge 1998) Similar to the Kubota and Maibach model, this model was matched to the one-membrane model where 11 different one-compartmental models were developed. However, unlike the Kubota and Maibach model, the authors suggested the use of only one skin layer, i.e., the SC, for moderately lipophilic chemicals and the use of two separate one-compartmental models for highly lipophilic solutes representing the SC and VE. The model neglects the mass transfer resistance in the vehicle. This model underestimates the mass of absorbing chemical in the epidermis and overestimates the cumulative mass of chemical crossing the vehicle-epidermal interface. Yet, like the Kubota and Maibach model, this model was a better predictor when compared to the two-membrane model. It should be noted that all the models were used to predict chloroform data and compared to experimental data except for this model. This was attributed to the fact that the model's development had not been based on experimental data for chloroform and thus could not be used as a predictor for this permeant. This highlights the issue with compartmental models not being adequate for the prediction of new permeants.

Brown and Hattis model:(Brown and Hattis 1989) This model includes an adjustable parameter that accounts for uncertainties in estimating permeability and partition coefficients, blood flow rates, skin thickness and deviations from Fick's law. The effect of solute size on the diffusivity in the viable epidermis D_{VE} was neglected and it was

assumed that $D_{VE} = 6x10^{-6}$ cm^2/s. The model was inappropriate for use when the receptor compartment had no flow, due to the fact that the model in this limit predicts that there is no flux from the skin to the receptor compartment.

McKone model:(McKone 1993) includes an adjustable parameter that accounts for "exposure conditions", yet it does not define the term and what it encompasses. When compared to the two-membrane model, the mass of absorbing chemical in the epidermis was underestimated and the cumulative mass of chemical crossing the vehicle-epidermal interface was overestimated.

Roberts and Cross model: (Roberts and Cross 1999) The single compartment represents the viable epidermis and dermis. Changes in the amount of solute in the tissue compartment are described in terms of exponential absorption kinetics. Single pass hind limb perfusions using male Wistar rats were used to develop the experimental data for comparison with the model predictions. Perfusates of both dextran and bovine serum albumin (BSA) were used to show the effects of protein binding of diclofenac (DCF) in both tissue and blood on respective tissue and concentrations as well as on clearance of the solute. The predicted clearance values in the presence of BSA were higher than the observed values, yet were of the same order of magnitude. The authors claimed that the absorption of a solute into the dermis from an aqueous solution is independent of the protein binding and K_{OCT} of the solute. Our results shown later contradict this claim. The authors also state that the use of a one-compartmental model is inadequate since the solute concentrations in the tissues are not uniform.

1.1.3 Two-compartment models

In these models, one compartment represents the SC and the other compartment represents the VT. McCarley and Bunge(McCarley and Bunge 2001) found that there were only 2 models that were clearly defined in terms of physicochemical and physical properties of the skin. The assumptions built into these models is as follows: (a) penetration into the SC is proportional to the steady-state permeability k_p^{SC} of the SC (b) clearance is controlled by the solubility of the permeant in the blood and the blood flow rate (c) penetration into the VE is proportional to the steady-state permeability k_p^{VT} of the VT.

Shatkin and Brown model:(Shatkin and Brown 1991) The rate constant representing transfer from the SC to the vehicle includes an arbitrary factor of 2. Estimates of the individual components of k_p^i were used, that is, diffusivity D_i, partition coefficient K_i and thickness h_i where i corresponds to the respective skin layer. This model like the Brown model neglected the effect of solute size on diffusivity in the VT. This model was a better predictor of the experimental data for chloroform when there was no blood flow, however, it did not adequately predict the experimental data when blood flow was present and was deemed inappropriate for use in such scenarios.

Chinery and Gleason model:(Chinery and Gleason 1993) Unlike the Shatkin and Brown model, estimates of k_p^i were used as opposed to its individual components. This model was also considered inappropriate for use when there is no flow in the receptor compartment.

1.1.4 Four layer diffusion model

The compartments represent the donor, the SC, the VE and the receptor. The model parameter for the diffusivity coefficient (D_i) is dependent on the molecular weight (MW) of the chemical and the distribution between the layers is determined by the partition coefficient (K_i) which is dependent on the lipophilicity and composition of the tissue.(Kruse, Golden et al. 2007) It is a one-dimensional model that describes the mass flows between the different compartments. For computational purposes the skin layers are divided into multiple sub-layers, such that the SC is divided into six sub-layers and the VE into five sub-layers. Diffusion in the individual sub-layers is described by a numerical approximation to Fick's 1st law that is, using concentration differences between the sub-layers. The effects of clearance out of the tissue and volume are represented by an additional receptor compartment. Skin hydration is not accounted for in this model. The model was used to predict transport for 5 compounds (triclosan, testosterone, malathion, parathion and caffeine). Experimental data were collected from in vitro experiments utilizing both finite and infinite doses for each of the compounds. The model predictions were than compared to the experimental data. Model parameters were fitted to the data, however, due to the limited availability of data, the assumption was made that the most critical parameters were those of the SC. Thus, the partition coefficient K_{SC} and diffusivity D_{SC} were utilized as the fitted parameters of this model. Several limitations were observed. The biggest limitation was that two sets of fitted parameter values were obtained depending on the input starting values chosen. The better parameter set was then chosen by either seeing which set best fit the finite dose experimental data or the set that was closest to the QSAR based approximation. A

problem arises for new permeants for which experimental data are not available- the issue of selecting the better parameter set becomes difficult. Also the model generated profiles that fit the data at long times well, yet did not match the non-steady-state regions. Model predictions for finite dose only fit the experimental data well for time periods less than 5hrs, thus the authors stated that the model was not an adequate predictor of finite doses absorption for long time periods. For lipophilic compounds, the predicted values of the permeability coefficient k_p were larger than those determined experimentally. This could possibly be attributed to inadequate experimental techniques as discussed later.

1.1.5 Six-compartment model

This model(Higaki, Asai et al. 2002) consists of 6 compartments, the donor, the VT (includes the dermis), the muscle directly below the site, plasma, contralateral muscle, contralateral tissue. The SC was not included in this model. The model was initially developed based on experimental data for antipyrine. The model was then used to predict the transport parameters for 10 other drugs, however, the model equation used to calculate the distribution volume of the plasma was changed since the original equation only gave valid solutions for antipyrine and not the other 10 drugs. This is a an example of how these compartmental models are difficult to generalize for new permeants unless modified, which would be difficult for anyone other than the developers of the model. This model predicted that the drug reaching the muscle was mainly derived from direct penetration from the skin as opposed to the systemic circulation. The direct delivery increased with an increase in the unbound fraction of the drug.

1.1.6 Isolated diffusion model

This model describes the decline of drug concentration with depth as a function of diffusion and capillary membrane clearance, such that the decline in the concentration is exponential with depth.(Gupta, Wientjes et al. 1995) The authors suggest that the SC and epidermis can be explained by simple diffusion models, whereas, the dermis is better explained by the distributed model described above. The assumptions made in this model are that (a) metabolism is negligible (b) capillaries are uniformly distributed (c) capillary wall transport is a passive process. The predicted parameters from the distributed model and simple diffusion model were compared to both in vitro and in vivo experimental data. The distributed model was a better predictor and better fit to the experimental data, showing that incorporation of clearance in a predictive model is necessary. However, this model does not account for the effects of the stratum corneum on the overall transport process. Also, the simplistic representation of the capillaries in the dermis may provide inaccurate predictions of clearance and ultimately tissue concentrations in the dermis since an increase in clearance would reduce the tissue concentration and vice versa.

1.1.7 Bunge et al. model(Bunge, Cleek et al. 1995)

This model is currently in use as the predictive tool at the Environmental Protection Agency (EPA). In this model the dermis and epidermis are lumped as single homogeneous layer. As mentioned earlier, they thus assume absolute dermal clearance which may serve as an inadequate assumption in certain situations. The model predicts the mass of solute absorbed by using estimates of diffusivity D_i, partition coefficient K_i and thickness of the skin layer h_i instead of the steady-state permeability k_p^i which lumps

all three parameters together. The possible limitation here may be in the limited availability of these separate parameters, since most experimental data represent a combination of D_i and K_i and an exact thickness of the various skin layers is not completely known. Also, the author states that the model should not be used to predict the absorption of permeants that are highly hydrophilic, specifically permeants that have a K_{OCT} less than 1.8. The effects of systemic clearance and lymphatic clearance are not accounted for in this model.

1.1.8 Transient distributed-diffusion model

Here the skin is represented in three separate layers, the SC, the viable epidermis and the dermis where the epidermis is presently treated as unperfused dermis. The model is a transient one-dimensional skin permeation model that can predict transport from a finite dose. As mentioned previously, several models assume absolute clearance which is not a valid assumption under certain conditions. Thus, the dermal clearance here is modeled realistically as it would appear *in vivo*, specifically as a distributed phenomenon modulated by diffusion.(Kretsos, Kasting et al. 2004) The model does not include the hypodermis, since its incorporation into the model had negligible effects on the predicted parameters of the dermis. The assumptions built into the model include partitioning equilibrium and continuity of flux at the interfaces and a uniform first-order clearance in the dermis. Clearance via the lymphatic system is ignored. Although the exact contribution of lymphatic clearance is unclear, it has been established that large hydrophilic macromolecules are taken up primarily by the lymphatic system. This limitation is further implied by the inability of the model to predict parameters for highly

bound lipophilic compounds such as retinoic acid due to the absence of lymphatic clearance.(Kretsos, Miller et al. 2008) Also one study of stripped skin has shown that direct penetration from the dermis to the underlying tissues is predominant over systemic clearance; thus the assumption that all clearance occurs via the blood may be inadequate.(Higaki, Asai et al. 2002) The model predicts an exponential decay in permeant concentration with depth in the dermis and a linear decay in the SC and epidermis. With regards to protein binding, the model assumes that most of the solute binding occurs to albumin which is present in the dermis and makes up 2.7% w/v.(Bert, Mathieson et al. 1982) The model neglects the mobility of the albumin and limits the contribution of the dermal lipids which may serve as a limitation and is a possible explanation to why our current model under predicts the skin concentrations when compared to those measured *in vitro*. A recent study by the Novartis Pharma group examined the binding of two highly lipophilic drugs, pimecrolimus and tacrolimus, to soluble skin proteins and plasma proteins. With regards to soluble skin proteins, both drugs were bound to an unidentified protein with a molecular weight of approximately 15 kDa, possibly corresponding to macrophilin 12.(Weiss, Fresneau et al. 2008) For plasma proteins, the study showed, that binding was highest to lipoproteins, particularly high-density lipoproteins (HDL) followed by α1-acid glycoprotein and γ-globulins. Albumin was less relevant to the overall plasma protein binding of the drugs as shown in Figure 2.(Weiss, Fresneau et al. 2008) This study contradicts our assumption that most protein binding in the skin occurs with albumin. The clearance values of the dermis predicted by the model were not as accurate when compared to in vivo data. This can be attributed to

the underlying assumption of the steady-state distribution of the permeant in the tissue and also the assumption of uniform clearance with depth.

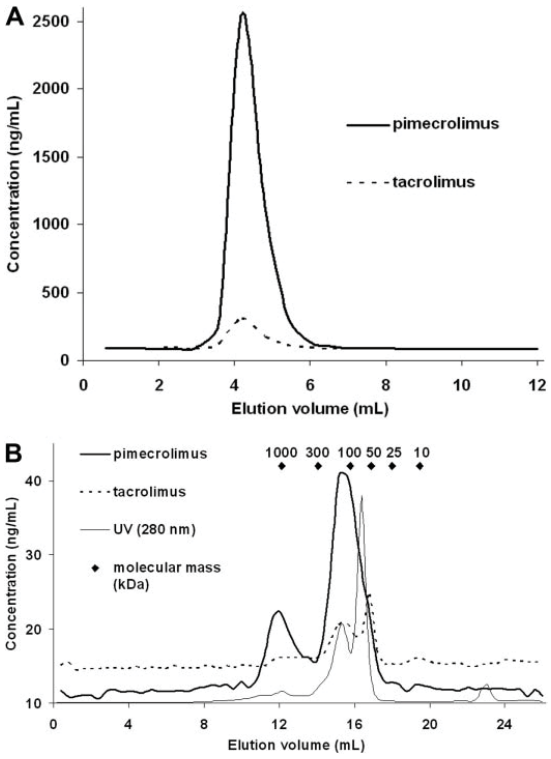

Figure 1.2 Binding of pimecrolimus and tacrolimus to human plasma proteins. Plasma(100 _l) was loaded onto a gel filtration column equilibrated with either pimecrolimus or tacrolimus. A, total binding to plasma proteins analyzed on a HiTrap column at actual free concentrations of 88 and 87 mg/ml for pimecrolimus and tacrolimus, respectively. B, binding to human plasma proteins separated on a Superose 6HR 10/300 column. The major UV peak at approximately 70 kDa corresponds mainly to albumin, and neither pimecrolimus nor tacrolimus coelutes strongly with this peak. The major peaks for pimecrolimus correspond to the expected elution volumes of HDL (_170 kDa) and LDL (approximately 3500 kDa); the major peaks for tacrolimus correspond to the expected elution volumes of _1-acid glycoprotein (approximately 43 kDa) and HDL (_170

kDa). Elution profiles in B are from one representative of three experiments; the UV signal is in arbitrary units. (Source: Weiss et al. 2008. *Drug Metab Disp*. **36**: 1812-1818).

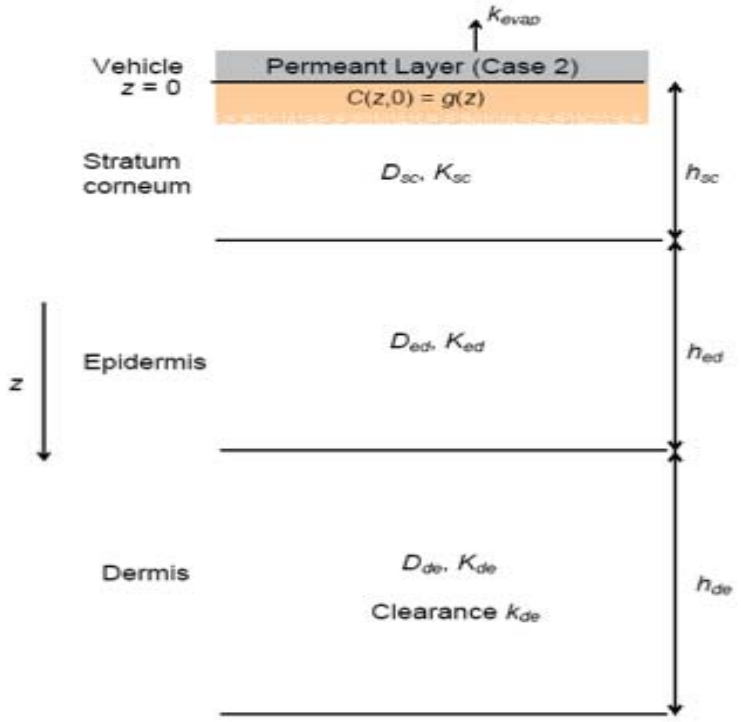

Figure 1.3 Current Kasting et. al computational model. Kasting GB, Miller MA, Bhatt VD. 2008. *J Occup Environ Hyg* **5**:633-644

1.2 BLOOD CAPILLARIES

1.2.1 Blood capillary structure

The blood capillary wall in most tissues consists of a three-layered structure. The endothelial glycocalyx layer (EGL) found on the luminal side of the capillary, the basement layer found on the albuminal side, and the endothelial cell lining found between

the basement membrane and glycocalyx layer.(Sarin 2010) The blood capillary can be classified as non-sinusoidal or sinusoidal, where the distinguishing factor is the presence or absence of a continuous basement membrane, respectively. Furthermore, these capillaries are classified as fenestrated or non-fenestrated. There are 2 main types of capillaries found in all organs with the exception of the kidney, liver and bone marrow as described below.

(a) Non-sinusoidal non-fenestrated blood capillary/continuous capillary: both the basement membrane layer and endothelial cell lining layer are continuous.(Sarin 2010) The interendothelial clefts, which are the clefts between 2 adjacent endothelial cells, constitute the primary transport pathways due to the absence of fenestrations. Although the reported width of the interendothelial cleft is approximately 20 nm, the actual available width for transport through the cleft is much narrower due to the presence of junction strands with a resulting effective diameter of 4-10 nm.(Sarin 2010) These capillaries have a high permeability to water and small solutes, yet a low permeability to proteins and macromolecules.

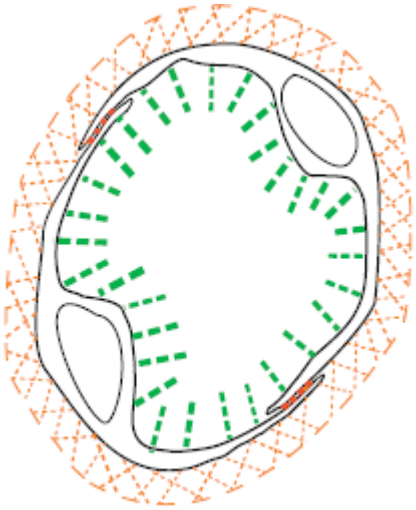

Figure 1.4 Non-Sinusoidal Non-Fenestrated Blood Capillary. The green pillars represent the individual mucopolysaccharide fibers of the EGL. The orange hatched region represents the basement membrane. (Courtesy of Sarin, 2010).

(b) Non-sinusoidal fenestrated blood capillary: the basement membrane layer is continuous; however, the endothelial cell lining is fenestrated. In all organs except for the kidney, these fenestrations and diaphragmed, such that they are not completely open, but are covered with plate-like sieves believed to be about 2-7 nm wide.(Sarin 2010) These capillaries have a higher permeability to water and small solutes than non-fenestrated capillaries, yet they exhibit a similar permeability to proteins and macromolecules.

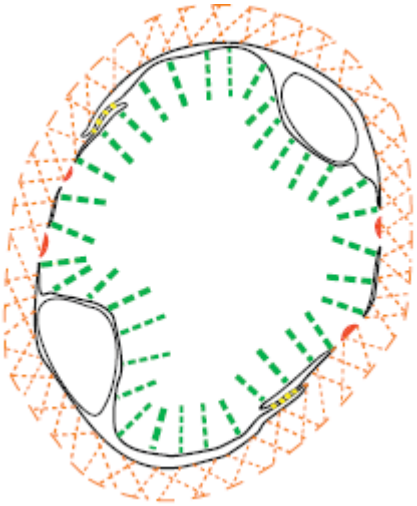

Figure 1.5 Non-Sinusoidal Fenestrated (Diaphragmed Fenestrae) Blood Capillary. The green pillars represent the individual mucopolysaccharide fibers of the EGL. The orange hatched region represents the basement membrane. The endothelial cell lining contains diaphragmed fenestrae depicted by the red plates. (Courtesy of Sarin, 2010).

With regards to skin capillaries, there is no general agreement on the type of capillaries found in the dermis. Some have reported that only continuous capillaries are found in the skin,(Imayama 1981) while others have reported the presence of both fenestrated and non-fenestrated capillaries. Braverman and Yen (Braverman and Yen 1977) suggested that majority of the capillaries found in the skin are continuous, yet fenestrated capillaries can be found in certain skin regions such as the fingertips and heels that have highly developed rete ridges. A study by Imayama (Imayama 1981) on the walking pads of rats demonstrated that the capillaries further away from the epidermis were continuous, whereas, the capillaries closer to the dermal-epidermal junction and those close to the dermal papillae were fenestrated in nature.

Endothelial Glycocalyx Layer (EGL)

In the 1940s Danielli (Danielli 1940) and Chambers and Zweifach (Chambers and Zweifach 1947) first proposed the possibility that a thin layer may cover the entire endothelial cell lining. By 1966 Luft (Luft 1966) was able to detect the presence of this layer in rat intestinal mucosa. In 1979, Klitzman and Duling (Klitzman and Duling 1979) detected a much thicker layer than observed by Luft. Although, the function of the EGL was not completely understood at the time of these discoveries, in 1994, Pries et al. (Pries, Secomb et al. 1994) were able to demonstrate that the EGL contributed to the microvascular flow resistance of the capillary. The EGL consists of a matrix of proteoglycans, namely heparan and heparan sulfate; and glycosaminoglycans (GAGs), specifically hyaluronan and chondroitin sulfate that contain sialic acid residues that impart a net negative charge on the EGL,(Weinbaum, Tarbell et al. 2007; Flessner 2008) Although, the EGL is not completely understood, it is believed that plasma proteins such as albumin absorb into the side chains of the GAGs forming a fiber matrix with a gap spacing between fibers equivalent to the diameter of albumin.(Sugihara-Seki and Fu 2005) Studies have shown that the thickness of the EGL is about 100 -500 nm.(Weinbaum, Tarbell et al. 2007)

The EGL is believed to be the primary molecular sieve for plasma proteins and macromolecules, but in turn allows the free exchange of water and small lipid-insoluble solutes. This hypothesis was confirmed when observing the permeabilities of both fenestrated and non-fenestrated blood capillaries. Although the hydraulic conductivities of fenestrated capillaries are higher than non-fenestrated capillaries, their permeability to

plasma proteins and macromolecules are remarkably similar.(Berg, Nieuwdorp et al. 2006; Weinbaum, Tarbell et al. 2007)

1.2.2 Transport Pathways

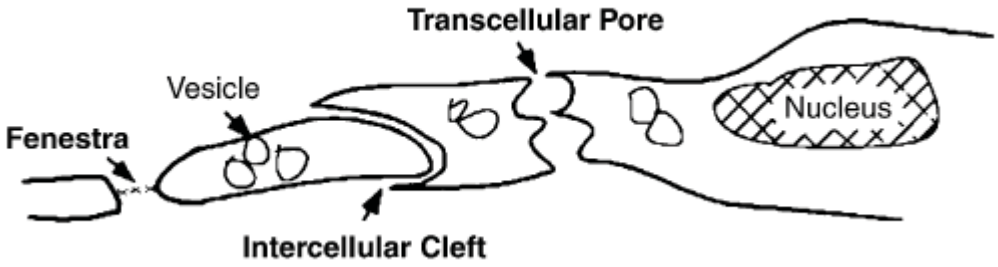

Figure 1.6 Transvascular pathways in the microvascular wall.(Sugihara-Seki and Fu 2005) (Courtesy of Fu, 2001).

(a) Cell membrane: consists of 3 barriers. The cell membrane, cytoplasm and plasma membrane. Small lipophilic solutes as well as water may use this pathway.

(b) Interendothelial cleft: may be the primary pathway for water, hydrophilic solutes and plasma proteins. Although the cleft is reported as 20 nm wide, the presence of junction strands within the cleft make the available area of the cleft much narrower with a resulting effective diameter of 4-10 nm.(Renkin 1977; Levick and Michel 2010) Adamson and Michel (Adamson 1993) studied frog mesenteric capillaries and demonstrated that the junction strand exhibited infrequent breaks that were on average 150 nm long, spaced about 2-4 um apart along the length of the strand. Some investigators believe that larger pores or clefts, of about 50-70 nm in width are present much less frequently than the smaller pores and generally

are attributed to the transport of proteins and macromolecules (Audus and Borchardt 1991). The width of these large pores may be reduced to 20-30 nm depending on the narrowness of the stricture. (Audus and Borchardt 1991) It should be noted that there is no solid evidence to support this theory.(Sarin 2010)

(c) Vesicles: are believed to be the major pathway for the transport of plasma proteins and macromolecules. They operate in a shuttling mode (transcytosis) similar to Brownian movement and their transport characteristics are those of diffusion. (Renkin and Curry 1982; Renkin 1985) The contribution of vesicular transport is of some controversy. Rippe and Haraldsson (Rippe and Haraldsson 1994) and Taylor and Granger (Taylor and Granger 1984) found little or no positive evidence to support the importance of transcytosis when analyzing large-solute transport. Furthermore, Rosengren et al. (Rosengren, Rippe et al. 2006) studied protein transport in mice completely lacking vesicles and found that the transport of proteins actually increased, suggesting that transcytosis does not in fact contribute to the transport of macromolecules.

(d) Fenestrae: believed to be an additional pathway for water, ions and small lipid-insoluble solutes, but not necessarily for proteins.(Sugihara-Seki and Fu 2005; Sarin 2010) These openings may be open or closed based upon the presence of a diaphragm, a sieve-like plate. Open fenestra are specific to renal glomerular capillaries.(Audus and Borchardt 1991; Sugihara-Seki and Fu 2005; Sarin 2010)

(e) Transcellular pore: is an additional pathway for the transport of macromolecules that may be opened in response to inflammation and/or local injury.(Sugihara-Seki and Fu 2005)

Based on the physiology of the blood capillaries and the various transport pathways, several investigators have developed models to describe the transport of water, ions, small lipid-insoluble solutes and macromolecules. The earliest and most basic of all models was the simple "pore/slit theory". (Wilschut, ten Berge et al. 1995) As understanding and knowledge of the capillary structure progressed, so did the complexity of models.

1.2.3 Blood capillary models

Membrane transport is described by the Kedem-Katchalsky equations derived from the principles of irreversible thermodynamics,(Kedem and Katchalsky 1958)

$$J_s = P\Delta C + (1-\sigma_f)J_v C \tag{1.1}$$

$$J_v = L_p(\Delta P - \sigma_d \Delta\pi) \tag{1.2}$$

where J_s is the solute flux; J_v is the fluid flux; P is the diffusive permeability to solutes; ΔC is the concentration difference across the membrane; σ_f is the solvent drag due to membrane restriction; C is the mean intramembrane solute concentration; L_p is the hydraulic conductivity which describes the membrane permeability to water; ΔP is the difference between local capillary blood pressure and interstitial hydrostatic pressure; σ_d is the reflection coefficient which describes the selectivity of the membrane to solutes; and $\Delta\pi$ is the difference between colloid osmotic pressure in plasma and the underside of glycocalyx. For ideal solutions σ_f is equal to σ_d and is represented by σ, the reflection coefficient.(Curry 1983; Michel and Curry 1999)

1.2.3.1 Pore theory

The permeability of the capillary wall is described in terms of flow through a water-filled cylindrical pore, which is the cleft between 2 adjacent endothelial cells.

The hydraulic conductivity L_p can be calculated from Poiseuille's Law (Michel and Curry 1999; Sugihara-Seki and Fu 2005)

$$L_p = \frac{N\pi R^4}{8\mu\Delta x} \tag{1.3}$$

where N is the number of pores per unit surface area of the capillary wall; R is the pore radius; μ is the water viscosity at 37 °C; and Δx is the depth of the cleft from lumen to tissue.

The solute permeability within the pore P_{pore} is

$$P_{pore} = N\pi R^2 \times D_{pore} \times \frac{\Phi}{\Delta x} \tag{1.4}$$

where D_{pore} is the solute diffusion coefficient within the pore; and Φ is the solute partition coefficient. Respectively,

$$D_{pore} = D_{aq}\left(1 - 2.1044\lambda + 2.08877\lambda^2 - 0.94813\lambda^5 - 1.372\lambda^6\right) \tag{1.5}$$

$$\Phi = (1-\lambda)^2 \tag{1.6}$$

$$\lambda = \frac{r_s}{R} \tag{1.7}$$

$$D_{aq} = \frac{7.4\times10^{-8} T(MW_{water}\cdot\phi_{water})^{1/2}}{\mu V_A^{0.6}} \tag{1.8}$$

where r_s is the solute radius; D_{aq} is the aqueous diffusivity calculated at 37°C using the Wilke-Chang relationship; T is the temperature in K; ϕ_{water} is the solvent association

parameter for water; μ is the viscosity of water at 37 °C; and V_A is the molar volume of the solute at boiling point.

1.2.3.2 Slit theory

The interendothelial cleft is modeled as a slit instead of a cylindrical pore. It seems more likely that the cleft resembles a rectangular slit, more so than a cylindrical pore.(Rippe and Haraldsson 1994)

The hydraulic conductivity L_p can be calculated from Poiseuille's Law(Michel and Curry 1999; Sugihara-Seki and Fu 2005)

$$L_p = \frac{LfW^3}{12\mu\Delta x} \tag{1.9}$$

where L is the total slit length per unit area of vessel wall; W is the width of the slit, f is the fraction of the length of the slit open to a width W; μ is the water viscosity at 37 °C; and Δx is the depth of the cleft from lumen to tissue.

The solute permeability within the slit P_{slit} is (Michel and Curry 1999; Sugihara-Seki and Fu 2005)

$$P_{slit} = fWL \times D_{slit} \times \frac{\Phi}{\Delta x} \tag{1.10}$$

where D_{slit} is the solute diffusion coefficient within the slit; and Φ is the solute partition coefficient. Respectively,

$$D_{slit} = D_{aq}(1 - 1.004\lambda + 0.418\lambda^3 + 0.210\lambda^4 - 0.1696\lambda^5) \tag{1.11}$$

$$\lambda = \frac{r_s}{(W/2)} \tag{1.12}$$

$$r_s = \left(\frac{3V_A}{4\pi}\right)^{1/3} \tag{1.13}$$

$$\Phi = (1 - \lambda)$$

$$\sigma = (1 - \Phi)^2$$

(1.14)

(1.15)

$$D_{aq} = \frac{7.4 \times 10^{-8} T (MW_{water} \cdot \phi_{water})^{1/2}}{\mu V_A^{0.6}} \quad (1.16)$$

where D_{aq} is the aqueous diffusivity calculated at 37°C using the Wilke-Chang relationship; λ is the ratio of the solute radius r_s and half-width of the slit; T is the temperature in K; Φ_{water} is the solvent association parameter for water; μ is the viscosity of water at 37 °C; and V_A is the molar volume at boiling point.

1.2.3.3 Fiber matrix theory

The glycocalyx is considered to be the primary molecular sieve to plasma proteins and macromolecules. Luft (Luft 1966) was the first to describe the presence of the glycocalyx on the luminal side of the interendothelial cleft based on staining experiments using ruthenium red and Alcian blue for cell surface glycoproteins. These studies suggested that the glycocalyx extended into the outer regions of the cleft. Curry and Michel (Curry and Michel 1980) were the first to provide a quantitative description of the fiber matrix model using the stochastic theory of Ogston et al (Ogston, Preston et al. 1973). Solute exclusion was accounted for be a network of fibers characteristic of glycoproteins on the endothelial cell surface. The solute partition coefficient Φ, and ratio of the solute diffusion coefficient of the matrix to the free diffusion coefficient D_{fiber}/D_{free} were described in terms of the fraction of the matrix volume occupied by the fiber S_f and the fiber radius r_f. This initial fiber matrix theory assumed that the matrix occupied the entire length of the cleft. The resistance of the fibers to water flow K_p was calculated using the

Carman Kozeny equation.(Curry and Michel 1980; Michel and Curry 1999; Sugihara-Seki and Fu 2005)

Upon the discovery of junction strands within the cleft by Adamson and Michel(Adamson 1993) and their observations that only a maximum of 20-30% of the junction is effectively opened, the initial assumption of fiber matrix occupying the entire length of the cleft showed that water flows would be underestimated by at least 3-fold. Thus a revised fiber matrix theory was established that incorporated the junction strand geometry and limited the presence of the fiber matrix to the cleft entrance. As a result, Tsay and Weinbaum (Tsay and Weinbaum 1991) introduced and an effective conductivity of the matrix K_{eff}, which was related to the value of K_p. It should be noted however that some investigators, namely Rippe et al. (Rippe 2008) who are responsible for the two and three Pore Theories are not advocates of the theory that the glycocalyx contributes to the size-selectivity of the capillary wall. They state that there is not enough evidence to collaborate the glycocalyx hypothesis.

$$\Delta = r_f \left[\left(\frac{\pi}{S_f} \right)^{0.5} - 2 \right] \tag{1.17}$$

where Δ is the gap spacing between the fibers; r_f is the fiber radius; and S_f is the fraction of the matrix occupied by the fiber. The Darcy hydraulic conductance K_p is

$$K_p = 0.0572 r_f^2 \left(\frac{\Delta}{r_f} \right)^{2.377} \tag{1.18}$$

This is related to the effective conductivity of the matrix K_{eff} by

$$K_{eff} = K_p \left[1 - \frac{\tanh\left[(W/2)/\sqrt{K_p} \right]}{(W/2)/\sqrt{K_p}} \right] \tag{1.19}$$

where W is the width of the slit/interendothelial cleft.

The solute partition coefficient Φ and the D_{fiber}/D_{free} for an ordered fiber arrangement are as follows

$$\Phi = 1 - S_f \left(1 + \frac{a}{r_f}\right)^2 \tag{1.20}$$

$$\frac{D_{fiber}}{D_{free}} = 1 - \left[\sqrt{1 - S_f}\left(1 + \frac{2a}{\sqrt{\pi} r_f}\right)\right] \tag{1.21}$$

where a is the solute radius and D_{free} is the aqueous diffusivity at 37°C is calculated as described above for the Slit Theory.

Thus the solute permeability P_{fiber} and the hydraulic conductivity L_p are

$$P_{fiber} = \frac{A_{fiber}}{L} \frac{D_{fiber}}{D_{free}} \phi \tag{1.22}$$

$$L_p = \frac{A_{fiber}}{L} \frac{K_{eff}}{\mu_{eff}} \tag{1.23}$$

where A_{fiber} is the area of the fiber filled pathway; L is the depth of the pathway; and μ_{eff} is the effective viscosity related to the viscosity of water μ at 37°C.

$$\mu_{eff} = \mu \frac{\left[(W/2)/\sqrt{K_p}\right]^3}{3\left[(W/2)/\sqrt{K_p} - \tanh\left[(W/2)/\sqrt{K_p}\right]\right]} \tag{1.24}$$

1.2.3.4 Two-pore and three-pore theory

This theory was developed by Rippe et al. (Rippe and Haraldsson 1987; Rippe and Haraldsson 1994).The principal hypothesis underlying this theory is that there are essentially 2 types of pores. Small pores with radiuses of 4.5 nm, and less frequent large pores with radiuses of 25 nm. It is believed that the frequency of the large pore may be as such that there are approximately 200-10,000 small pores to every large pore (Renkin, Watson et al. 1977; Rippe and Haraldsson 1987). Hence, in this theory a ratio of 95:5 of small pore to large pore was chosen. Rippe et al. (Rippe and Haraldsson 1987; Rippe, Rosengren et al. 2002) challenge the idea of vesicular transport (transcytosis) of macromolecules due to the fact that in true capillaries, these channels cannot be found by electron microscopes. They believe that the passive convection of macromolecules across large pores can account for the bulk transfer of the major plasma proteins from the blood to tissue, although albumin and smaller solutes can also permeate the capillary membrane by diffusion through the smaller pores.

The three-pore theory is an extension of the two-pore theory such that a water-only conductive pathway, specifically the aquaporin, was introduced (Rippe et al, 2000, Venturoli and Rippe, 2001). The small pore radius was set to 4.3 nm and the large pore radius to 25 nm. The ratio of the small pore: large pore: aquaporin is 90:7:3. Furthermore, the three-pore theory was further modified to include a fiber matrix model to represent the interstitium. (Rippe and Venturoli 2007)

The reflection coefficient σ is

$$\sigma = 1 - \frac{(1-\lambda)^2 \cdot \left[2-(1-\lambda)^2\right] \cdot \left(1-\frac{\lambda}{3}\right)}{1-\frac{\lambda}{3}+\frac{2}{3}\cdot\lambda^2} \tag{1.25}$$

where λ is the ratio of the solute radius to the pore radius. A reflection coefficient for each pore radius is calculated such that a total reflection coefficient σ_{cap} is

$$\sigma_{cap} = \alpha_s \sigma_s + \alpha_L \sigma_L \tag{1.26}$$

where α_L is the area fraction of large pores and α_s is the area fraction of small pores (1-α_L).

The permeability-surface area product PS is

$$\frac{A}{A_o} \cdot \frac{A_o}{\Delta x} \cdot D_{aq} \tag{1.27}$$

where A/A_o is the diffusive restrictive function, $A_o/\Delta x$ is the total unrestricted area of exchange per unit diffusion path length and D_{aq} is the aqueous diffusivity calculated using Stokes-Einstein relationship.

$$D_{aq} = \frac{RT}{6\pi\mu N_A r_s} \tag{1.28}$$

$$\frac{A}{A_o} = \frac{(1-\lambda)^{9/2}}{1 - 0.3956\lambda + 1.0616\lambda^2} \tag{1.29}$$

where RT is the product of the gas constant and absolute temperature in Kelvin; μ is the viscosity of water μ at 37°C; N_A is Avogadro's number; and r_s is the solute radius.

The total permeability-surface area product PS_{cap} and total hydraulic conductance are

$$PS_{cap} = D_{aq} \frac{A_o}{\Delta x} \cdot \left[(1 - A_L) \cdot \left(\frac{A}{A_o} \right)_s + A_L \cdot \left(\frac{A}{A_o} \right)_L \right] \tag{1.30}$$

$$L_p S_{cap} = \frac{A}{\Delta x} \frac{r_s^2}{8\mu} \frac{\alpha_L}{(1-\alpha_L)} \tag{1.31}$$

1.2.3.5 1-D and 3-D models

Hu and Weinbaum (Hu and Weinbaum 1999) had developed a sophisticated 3-D model with five separate regions to describe the transport of solutes across the glycocalyx, cleft and junction strands within the blood capillary wall. This model was far to complicated for most investigators to use and required considerable computer time for the numerical solutions to converge (Zhang, Adamson et al. 2006). As a result, they developed a simpler 1-D model such that each of the five regions of the 3-D model was described by a 1-D convection-diffusion equation. The key simplification of the1-D model was the conversion of the tight junction strands with periodic breaks into a single continuous slit. This continuous slit was modeled to provide the same permeability and hydraulic conductivity as predicted by the 3-D model. The values and parameters used for this model were taken from the literature of rat mesenteric microvessels (Zhang, Adamson et al. 2006). This model provides the user with 13 different equations that can be solved simultaneously and in much less time than the 3-D version.

1.3 LYMPHATIC CAPILLARIES

1.3.1 Structure and function

The lymphatics serve various functions in the body. Amongst these functions are: (Strand and Bergqvist 1989)

(a) The production and transport of thymus-dependent small lymphocytes that play a role in cellular immunity.

(b) Production of large lymphocytes and plasma cells which then produce antibodies.

(c) Filtration of body fluids through nodal sinuses.

One of the most important functions of the lymphatics is the return of larger proteins and lymphocytes from the interstitium to the blood. About 20-40 L/day of fluid is filtered into the interstitium and of that volume, about 2-4 L/day is carried away by the lymphatics.(Ryan 1978) Due to the unidirectional flow of lymph, the fluid is recovered from the periphery and then finally to the major lymphatic vessel, the thoracic duct, which in turn returns the fluid to the vasculature. (Porter and Charman 2000) In the skin, the lymphatic vasculature begins in the subpapillary layer of the dermis.(Schmid-Schonbein 1990) Joory et al.(Joory 2004) studied the depth of lymphatics in the human forearm and found that the highest density was found at 250 μm from the dermal-epidermal junction. The initial lymphatics found in the subpapillary layer of the dermis are closely interconnected in a hexagonal pattern and connect through a set of precollectors with deeper layers of lymphatics.(Schmid-Schonbein 1990) The lymphatic capillaries in the skin are 100 μm wide and consist of a single layer of overlapping endothelial cells that are joined together by large intercellular junctions.(Modi, Stanton et al. 2007) The basement membrane in these capillaries is discontinuous or absent and are noncontractile.(Swartz 2001) Anchoring filaments attach to the lymphatic capillary wall and to the collagen fibers of the interstitium which maintain the structure of these capillaries. Both the anchoring filaments and overlapping endothelial cells provide an endothelial microvalve that allows the unidirectional flow of lymph.(Schmid-Schonbein

1990; Swartz 2001) The endothelium of the lymphatics poses very little hindrance to solute uptake, yet, the protein concentration in lymph fluid is inversely dependent on the flow rate.(Swartz 2001) Larger solutes are preferentially absorbed by the lymphatics, yet, the larger the solute, the slower the uptake into the lymphatics. Uptake by the initial lymphatics is not only a function of size, but also shape, charge and lipophilicity.(Swartz 2001) The initial lymphatics drain into thicker-walled collecting ducts which are not only comprised of an inner endothelial layer, but are covered by a connective sheath containing elastic and muscular cells. The contraction of these muscle cells allows for the propulsion of the lymph through the vessels, lymph nodes and ultimately to the thoracic duct and systemic circulation. In addition to the contraction and relaxation of the muscle cells, other factors affect the propulsion of lymph through the vessels such as muscular activity, respiratory movement, massage, heat, and venous pressure.(Swartz 2001)

1.3.2 Effect of molecular weight on lymphatic absorption

The blood capillaries are poorly permeable to large hydrophilic macromolecules, as a result, these larger molecules are primarily transported via the lymphatics. Supersaxo et al.(Supersaxo, Hein et al. 1990) studied the effect of molecular weight on lymphatic absorption following subcutaneous injection. 4 compounds, namely, 3H-Fluorodeoxyuridine (^{3}H-FUDR) (246.2 Da), ^{3}H-Inulin (5200 Da), ^{14}C-Cytochrome c (12,300 Da) and Interferon alpha-2a (19,000 Da) were injected subcutaneously into the hind leg of White Alpine and Black Jura sheep. The efferent duct of the popliteal lymph node was cannulated and samples of the lymph were collected for 24 hrs. The concentration of the Interferon alpha-2a was measured by an enzyme-linked

immunosorbent assay, and the remaining compounds were analyzed via a scintillation counter.

The recovery of the compound in lymph was expressed as a percentage of the administered dose and was calculated as the product of the concentration in the lymph and the volume of lymph collected at each time interval. The cumulative recoveries were:

- FUDR(246.2Da): 4 ± 1.5 %
- Inulin (5200Da): 21.0 ± 7.1 %
- Cytochrome c (12,300Da): 38.6 ± 6.7%
- Interferon alpha-2a (19,000Da): 59.5 ± 7.7%

A linear relationship was found between the molecular weight and the proportion of dose lymphatically absorbed, such that for compounds with a molecular weight of 16,000 Da and above, more than 50% of the administered dose was being transported via the lymphatics.

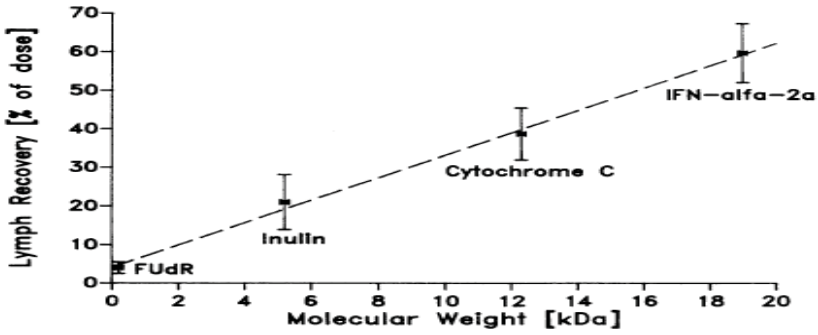

Fig. 2. Correlation between the molecular weight and the cumulative recovery of rIFN alpha-2a (MW 19,000), cytochrome *c* (MW 12,300), Inulin (MW 5200), and FUDR (MW 246.2) in the efferent lymph from the right popliteal lymph node following s.c. administration into the lower part of the right hind leg. Each point and bar show the mean and SD of three experiments performed in three separate sheep. The line drawn is the best fit by linear regression analysis calculated with the four mean values. The points have a correlation coefficient r of 0.998 ($p < 0.01$).

Figure 1.7 Correlation between molecular weight and the cumulative recovery in the lymph.(Supersaxo, Hein et al. 1990) Source: Supersaxo A, Hein WR, Steffen H. *Pharm Sci*. 1990. 7: 167-169.

Cross and Roberts(Cross and Roberts 1993) also studied the absorption kinetics of interferon alpha-2a in female Sprague Dawley rats *in vivo*. An incision on the lower abdomen was made to the level of the subcutaneous tissue. The skin was separated from the subcutaneous layer and an absorption cell was then fixed to the moist tissue. The cell was clamped in position and maintained at 37ºC. Radiolabeled albumin and PBS solution was introduced into the absorption cell and the experiment was carried out to 6 h. Blood samples were collected from the tail vein at the end of the study, and the tissue below the absorption cell was removed and analyzed for radioactivity. Nor-adrenaline was administered with interferon in some cells to observe its effect on the overall clearance. Nor-adrenaline is a vasoconstrictor and had no effect on the clearance of interferon. This is a strong indication of the fact that interferon is cleared mainly via the lymphatics,

hence a constriction in the blood capillaries had no effect on its clearance. The clearance of interferon was 1.41 ± 0.38 x 10^{-3} mL min^{-1} and the absorption half-life from the solution was 3.8 ± 1.1 h. Furthermore, at 2 h, a loss of 38.9 ±10.3% of interferon from the cell was measured and at 6 h was 57.5 ± 11.9%. Only 1% of this dose was recovered in the tissues directly below the cell. These results are in close agreement with the *in vivo* values observed by the Supersaxo group in sheep.

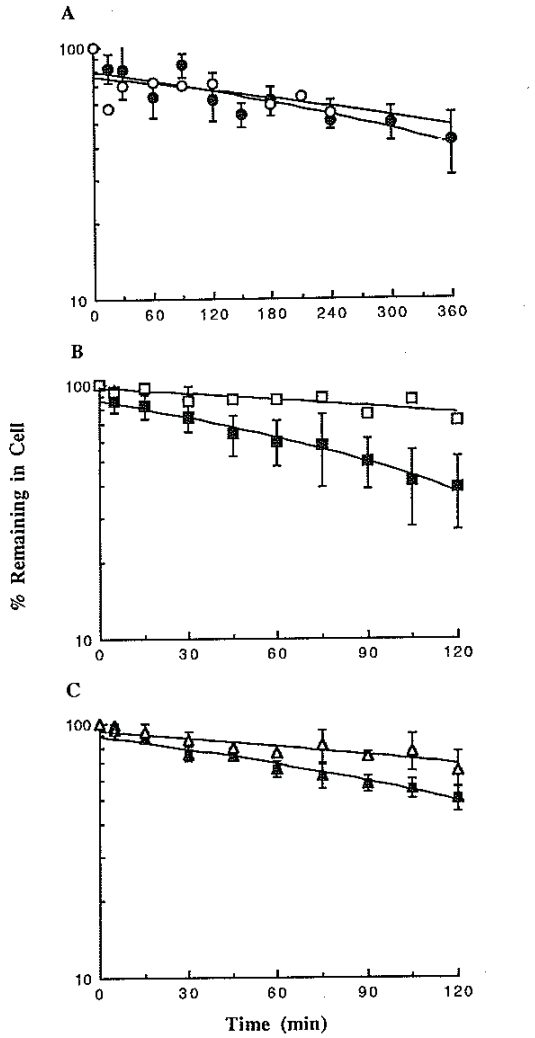

FIG. 1. Effect of noradrenaline on the absorption of (A) interferon g, (B) water and (C) lignocaine. Open symbols are experiments in the absence of noradrenaline, closed symbols are experiments in the presence of 1 μM noradrenaline.

Figure 1.8 Cross SE, Roberts MS. *J Pharm Pharmacol*. 1992. **45**: 606-609.

These studies demonstrate the important role played by the lymphatic capillaries with regards to the clearance of macromolecules. Yet, questions regarding the transport rate of these macromolecules cannot be answered by such studies. Instead, these queries are answered by studying how quickly these macromolecules move out of the injection site and into the lymph and plasma.

1.3.3 Lymphatic capillary flow studies

The measurement of lymph flow has been of great importance in the characterization and understanding of clinical diseases such as edema and lymphedema which are primarily a consequence of impaired lymphatic drainage and flow.(Modi, Stanton et al. 2005; Modi, Stanton et al. 2007) Many methods for the study of lymph flow rate are available, however, only a few of these studies are noninvasive. The most widely used method involves an injection of a radioactive macromolecule into the dermis or muscle of subcutis followed by the measurement of the rate of disappearance from the injection site.(Modi, Stanton et al. 2007) This method is referred to as quantitative lymphoscintagraphy. Different methods available for the assessment of lymphatic function *in vivo* are as follows:(Modi, Stanton et al. 2007)

(i) Direct lymphangiography: small lymphatic collectors are visualized by a subcutaneously-injected dye. These lymphatics are then dissected under local anesthesia, cannulated and then infused with a radiopaque contrast agent. This technique provides anatomical information yet very little functional information and is no longer used because it may exacerbate lymphedema.

(ii) Indirect lymphangiography: involves the injection of a large molecular weight contrast medium interstitially, which is taken up by the lymphatic capillaries and then enters the main collecting ducts. Both some anatomical and functional information can be deduced from such studies.

(iii) Fluorescence microlymphography: a small bolus of fluorescein-labeled dextran is injected intradermally. The drainage of the solution into the lymphatic network can be visualized by fluorescence microscopy. These studies provide information regarding the number of capillaries, their diameters, lengths etc. but do not measure lymph flow.

(iv) Direct lymph collection: lymphatic collector vessels in the limbs of healthy subjects are cannulated and the lymph flow and lymphatic pumping pressure are measured directly.

None of the described methods above measure lymph flow except for direct cannulation. Although, some of these methods provide information on lymph velocity, that parameter can not be used to determine lymph flow due to the fact that the lymphatic cross-sectional area is unknown.

1.3.3.1 Cannulation studies

In these studies the test molecules are injected intravenously or intramuscularly in the test subject. A lymphatic duct such as the thoracic duct or popliteal duct is cannulated and regular samples of lymph are collected. The state of the subject varies from one study to the other, such that lymph flow rates may be measured under physical activity, passive movement, anesthesia or conscious subjects, increases in venous pressure and increases

in temperature of the site. A comprehensive summary of these various studies can be found in the table below. The flow rate from the cannulated vessel is a function of the pressure at the outflow end of the vessel.(Laine, Allen et al. 1987) The height and resistance of the cannula has significant effects on the pressure at the outflow end, hence significant effects on the lymph flow rates being measured, such that the flow rate measured in a cannulated lymph vessel is not equal to the flow rate had the vessel not been cannulated. (Laine, Allen et al. 1987) Furthermore, the changes in the lymph flow rate measured in the cannulated vessel are not proportional to the total tissue lymph flow.(Laine, Allen et al. 1987) Additionally, studies involving the cannulation of the thoracic duct may be misleading because although most lymph vessels run from an organ through the lymph nodes and then finally into the thoracic duct which then empties into the veins in the neck; some lymph vessels from some tissues enter the veins by routes other than the thoracic duct.

Table 1.2 Cannulation studies in various species with varying conditions of subject

Species	**Site**	**Method of Measurement**	**Lymph Flow (Q) Original Units**	**Lymph Flow (Q) s^{-1} x 10^6**	**Reference**
Dog	Hind leg	Cannulation (Anesth)	2 x 10^{-5} mL $g^{-1}s^{-1}$	20	(Garlick and Renkin 1970)
Dog	Thoracic duct	Cannulation (Anesth)	2 mL kg^{-1} h^{-1}	0.556	(Lesser 1871)

Dog	Thoracic duct	Cannulation (Anesth)	32.54 uL min^{-1} kg^{-1}	0.543	(Schad and Brechtelsbauer 1977) *Looked at dogs that were conscious at rest, and conscious with walking and dogs under ansesth*
Dog	Lung	Cannulation (Anesth)	0.1 mL min^{-1} $100g^{-1}$	16.7	(Gabel and Drake 1979)
Cat	Calf Muscle	Cannulation (Anesth)	0.013 mL min^{-1}100 g^{-1} *(passive movements)* 0.02 mL min^{-1}100 g^{-1} *(induced movements)*	2.17	(Jacobsson and Kjellmer 1964)
Rabbit	Hind limb Muscle	Cannulation (Anesth)	21 µL min^{-1} $100g^{-1}$	3.5	(Bach and Lewis 1973)
Rabbit	Hind Limb Skin	Cannulation (Anesth)	240 µL min^{-1} $100g^{-1}$	40	(Bach and Lewis 1973)
Horse	Abdomen (jejunum)	Cannulation (Anesth)	5.1 ± 1.7 µL min^{-1} kg^{-1}	0.085	(Dabareiner, White et al. 2005)
Sheep & Lamb	Thoracic duct	Cannulation (Anesth)	0.157 ± 0.033 mL min^{-1} kg^{-1} *(lamb)* 0.046 ± 0.018 mL min^{-1} kg^{-1} *(sheep)*	2.62 (lamb) 0.767 (sheep)	(Harake and Power 1986)
Dog	Thoracic duct	Cannulation (Non-Anesth)	49.3 ± 26.2 µL min^{-1} kg^{-1} *(at rest)*	0.822	(Schad and Brechtelsbauer 1977)
Dog	Thoracic duct	Cannulation (Non-Anesth)	98.6 µL min^{-1} kg^{-1} *(walking)*	1.64	(Schad and Brechtelsbauer 1977)

1.3.3.2 Disappearance studies (lymphoscintigraphy)

This method is the most widely used technique to assess lymph flow rates primarily due to its noninvasiveness. Typically, these studies involve the subcutaneous or intradermal injection of radiolabeled albumin or other radiolabeled macromolecules. The disappearance of the solute from the injection site is then measured externally via a Geiger Counter and the appearance of the radiolabeled compound in the blood is measured from collected plasma samples. The clearance of these injected solutes from the injection site is not only site specific, but is greatly affected by physical activity, heat and venous pressure.(Olszewski, Engeset et al. 1977) The type of injection employed (subcutaneous, intradermal, skeletal muscle) may also have a significant affect on the lymph flow rates being measured. Intradermal injections are cleared much faster than subcutaneous injections due to the high lymphatic density in the dermis. A few of these studies will be discussed further. It should be noted that many of these studies observed the transport rate in both healthy patients and patients with an impaired lymphatic system. In the interest of my work, only data from radiolabeled-albumin injected into normal human subjects will be discussed.

Ellis et al.(Ellis, Marks et al. 1970) studied the clearance rate of ^{131}I-albumin from 3 different intradermal injection sites in 20 healthy subjects; the dorsum of the index finger in the midline 2 cm proximal to the nail fold (proximal finger), the dorsum of the other finger 0.5 cm proximal to the nail fold (distal finger), and the cheek 3 cm below and 2 cm medial to the lateral orbital tubercle on the outer margin of the of the orbit. The disappearance rate of ^{131}I-albumin from the injection site was measured externally via a

Geiger Counter for 24 h. For the majority of patients, the radioactivity fell exponentially and the clearance rate of ^{131}I-albumin varied with site. The clearance half-time ($T^{1/2}$) was calculated from the radioactivity detected at the injection site versus time, such that $T^{1/2}$ was 0.693 divided by the slope as depicted in Figure 1.9

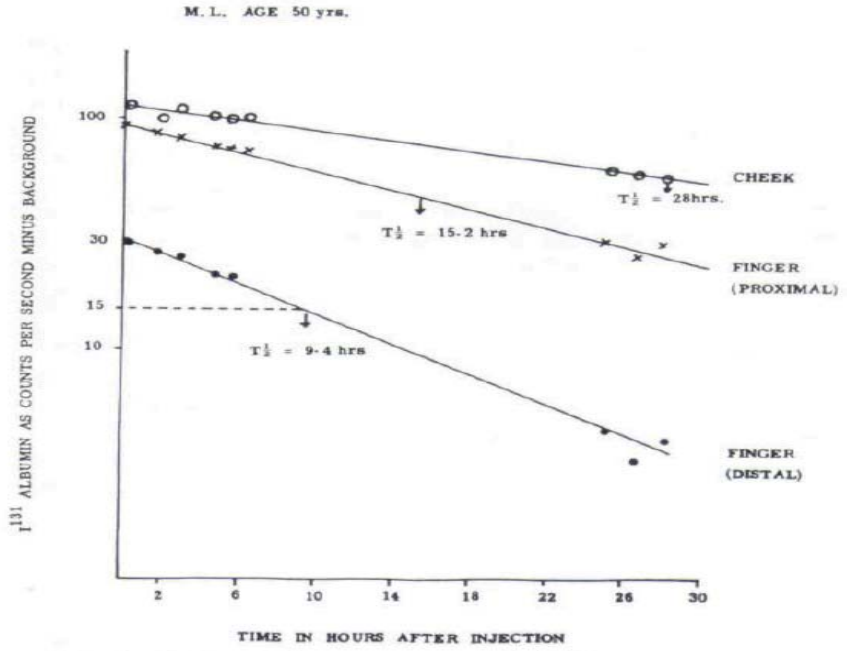

FIG. 1.—Rate of disappearance of ^{131}I human serum albumin injected intradermally into 3 different sites. Residual radioactivity plotted on semi-logarithmic graph paper. Calculation of the clearance half-time $T_{\frac{1}{2}}$.

Figure 1.9 Source: Ellis JP, Marks R, Perry BJ. *Br J Derm*. 1970. **82**: 593-599.

The highest clearance rate half-time was observed in the distal finger, 8 ± 2.8 h (mean ± SD), followed by the proximal finger 12.9 ± 3.8 h, and finally the cheek 33.5 ± 25.1 h. The effects of movement were also studied in some of the subjects, such that the right and left fingers were both injected at the proximal site. The left hand was splinted and the

right hand remained free. The clearance rates for both fingers were very similar ($T^{1/2}$ left= 18 h, $T^{1/2}$ right=20 h).

Hollander et al. (Hollander, Reilly et al. 1961) studied the clearance rate of ^{131}I-albumin when injected subcutaneously in the limbs of 15 healthy subjects. The disappearance rate of radioactivity was measured externally at the injection site using a scintillation counter. Blood and urine samples were also collected. The clearance half-time $T^{1/2}$ in the limb averaged 33.4 ± 9.3 h (mean ± SD) and ranged from 18 – 48 h. In the forearm, the average $T^{1/2}$ was 23.1 ± 2.1 h and ranged from 19 – 27 h. Figure 1.10 shows the disappearance rate of ^{131}I-albumin from the limb of a healthy subject.

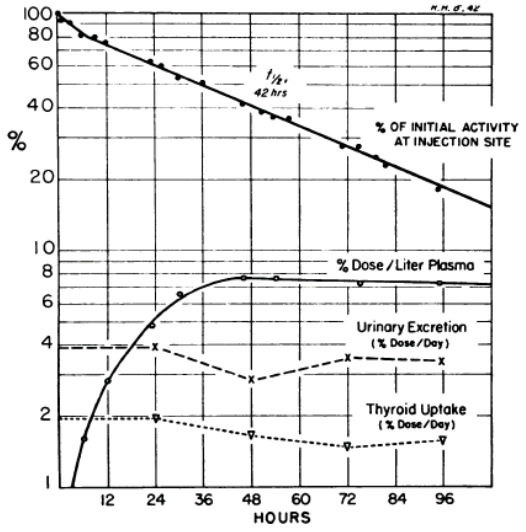

FIG. 1. THE DISAPPEARANCE OF I^{131}-ALBUMIN FROM THE SUBCUTANEOUS TISSUE OF A NORMAL LEG.

Figure 1.10 Source: Hollander W, Reilly P, Burrows BA. *J Clin Invest*. 1961. **40**: 222-233.

Taylor et al.(Taylor, Kinmonth et al. 1957) studied the disappearance rate of ^{131}I-albumin when injected subcutaneously in the limbs of 6 healthy subjects. The effects of physical activity were observed on the clearance rate of ^{131}I-albumin from a highly active

individual to a subject confined to bed rest. The disappearance rate from the site of injection was measured externally via a scintillation counter and blood samples were also collected. Results showed that the clearance rate from the site of injection increased with increasing physical activity as shown in Table 1.3.

Table 1.3 Source: Taylor et al. Br Med J. 1957.

TABLE I.—*Results of Local Counting Over Injection Site in Human Subjects*

Subject	Degree of Physical Activity	Removal Rate of R.P.P. (Percentage of Dose Removed per Hour)
	Control Group	
J.R.	Very active	3·9
F.S.	Active	2·2
F.B.	Slight	1·2
M.A.H. ..	Bed	2·5
E.W.H. ..	,,	1·o
E.J.	,,	1·7
Mean ..		2·2±0·4

Similarly, physical activity had a significant effect on the concentration of ^{131}I-albumin reaching the systemic circulation, such that an increase in physical activity led to an increase in ^{131}I-albumin detected in the blood stream. However, physical activity had no effect on the time taken for ^{131}I-albumin to initially enter the blood stream as shown in Table 1.4.

Table 1.4 Source: Taylor et al. Br Med J. 1957.

TABLE II.—*Estimation of Arrival in Blood of R.P.P. Injected Subcutaneously in Human Subjects*

Subject	Initial Delay (in Hours)	Initial Rate of Rise of Radioactivity in Blood. (10^{-4}% of Dose ml. of Blood/Hour)
	Control Group	
J.R.	0·5	9·3
F.S.	0·9	6·3
F.B.	1·0	2·5
E.W.H.	0·7	1·6
E.J.	0·8	0·8
Mean ..	0·8 ± 0·1	4·1 ± 1·6

Staberg et al. (Staberg, Klemp et al. 1983) studied the disappearance rate of both ^{131}I-albumin and ^{125}I-albumin injected intradermally in 9 patients with psoriasis vulgaris. Both the diseased and normal limb in each subject was injected with a different tracer so that the appearance of each could be distinguished in the blood samples collected. External measurements at injection sites were made via a scintillation counter. The average clearance half-time was 29.1 ± 9.6 h. Figure 1.11 shows the disappearance rate of ^{131}I-albumin and ^{125}I-albumin in one patient.

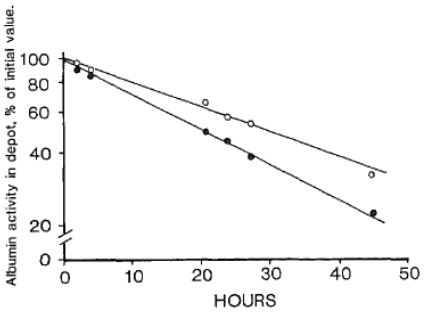

Fig. 1. An example of the local clearance of radiolabelled albumin from uninvolved (o) and involved (•) skin of a patient with psoriasis. The ordinate is in log scale.

Figure 1.11 Source: Staberg et al. *J Amer Acad Derm*. 1983. **9**: 857-861.

The effect of physical activity on the clearance rate of albumin was observed such that the subjects were allowed to walk around 3 h after the injection had been administered. A steep increase in the radiolabeled albumin in the blood was observed as shown in Figure 1.12.

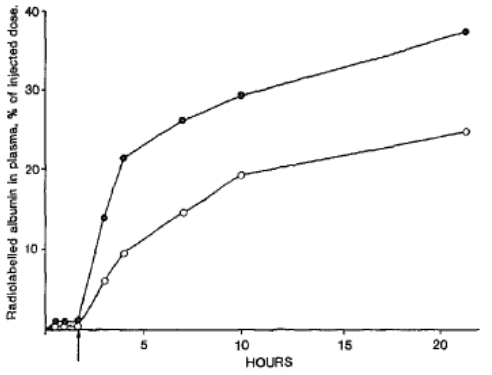

Fig. 4. An example of the plasma appearance of radiolabelled albumin injected intradermally in uninvolved (o) and involved (●) skin of a patient with psoriasis. The arrow indicates the time when the patient was allowed to move.

Figure 1.12 Source: Staberg et al. *J Amer Acad Derm*. 1983. **9**: 857-861.

From these studies one can conclude that the clearance rate of macromolecules via the lymphatic capillaries, specifically albumin, is very site specific. These variations from site to site are not completely understood, however, they may be due to variations in lymphatic drainage, differences in blood and lymphatic flow, differences in the thickness and density of the dermis and subcutaneous tissues, differences in pressure or differences in the lymphatic capillary network. Irrespective of which of these may have an effect, variations in the clearance rate of albumin from one site to another must be considered and taken into consideration. Also, the effects of physical activity on the clearance rate of albumin are significant and should also be taken into consideration.

1.4 DERMAL TRANSPORT STUDIES

1.4.1 *In vitro* human dermal permeability studies

The development of predictive models stems largely from theory and experimental data. The experimental data are utilized to fit parameters in the model and ultimately fit the model to explain the experimental data adequately. Thus, the quality of these models and their ability to predict transport parameters of solutes is dependent on the quality of the experimental data. If the data are lacking or are not a clear representation of what is occurring in the skin layers, then predictive models will fail. Many studies have been dedicated to the characterization and study of the stratum corneum. Simple models such as Potts-Guy (Potts and Guy 1992) and variations thereof have been developed. Although, these models are adequate for predicting the steady-state transdermal flux and overall skin permeability of moderately lipophilic permeants, they underestimate lag time after application, half life of the permeant and tissue concentrations, the knowledge of which is valuable in dermal risk assessment and transdermal drug delivery.(Kretsos, Kasting et al. 2004) Thus, the study of the lower skin layers is essential for providing an encompassing model to accurately describe the overall transport of a solute in skin. As mentioned earlier, several models treat the epidermis and dermis as a single aqueous homogeneous layer. Yet, studies have shown that the permeation of solutes in the epidermis can be explained by a simple diffusion model where a linear concentration profile is observed whereas, and the dermis better explained by a distributed model that accounts for clearance and an exponential decay of solute with depth is observed.(Gupta,

Wientjes et al. 1995) Treating both these layers as one and in the same can be misleading and may lead to less accurate predictions. Thus the refinement of these predictive models requires the separate characterization of these layers since they display different transport properties. Khalil et al. (Khalil, Kretsos et al. 2006) reported that the diffusivity of glucose in the dermis was D_{de}= 2.64 ± 0.42 x 10^{-6} cm^2/s whereas values for the viable epidermis ranged from D_{ve}= 0.037 x 10^{-6} cm^2/s to 1.0 x 10^{-6} cm^2/s depending upon the estimation method. Differences between the tissues in permeability as well as the product of diffusivity and partition coefficient were also observed. This suggests that the idea of treating both tissues as a single homogenous layer may not be valid. Studies of the viable epidermis are very limited. This is primarily due to the difficulty in obtaining this tissue and studying it *in vitro*. In order to obtain the viable epidermis, the stratum corneum must be removed via tape stripping or dermatoming, both of which have limitations. A fundamental limitation of tape stripping is that the SC cannot be totally removed and that some of this layer remains attached to the epidermal surface as "islets".(Touitou, Meidan et al. 1998) Also, one cannot determine whether part of the viable epidermis has been removed. Dermatoming also has its limitations since one is not entirely sure of how much of the viable epidermis is being removed. Unless sufficient data are available about the exact thickness of each layer, preliminary experiments are required to determine this parameter.(Touitou, Meidan et al. 1998) The dermis can be removed by heat separation (Kilgman and Christophers 1963). Yet, the remaining tissue, the viable epidermis is a soft gooey substance that can be physically difficult to work with. *In vivo* dermis studies are relatively rare, whereas *in vitro* dermis studies are more numerous, yet not as common as stratum corneum studies. Understanding permeation through the dermis gives insight into

important factors such as skin concentrations, clearance and protein binding which are important in risk assessment and topical drug delivery.

1.4.2 Tissue sample preparation for *in vitro* studies

Tissue samples may either be obtained as human cadaver skin or from surgical procedures such as abdominoplasties and breast reduction surgeries. A review of dermal penetration studies in the literature show that a wide variety of sample preparations have been used. Some studies use dermis tissue from human split-thickness skin and derive transport parameters based on these samples that are then implemented into predictive models. The problem that arises here is that the dermis layer is not complete, thus the transport parameters being derived do not correlate to a full dermis layer, although the predictive model describes a full thickness dermal tissue. This problem can also be observed with skin from breast reduction surgeries that has been dermatomed to remove the subcutaneous fat layer where a portion of the dermis may also been removed. Although assumptions can be made that the differences in the transport parameters of full and partial dermal tissue may not be significant, there is no real evidence to support this assumption.

Another question that arises in tissue handling is whether the process of heat separation has an effect on the transport properties and integrity of the dermis. A study by Liu et al. (Liu, Higuchi et al. 1994) set out to answer this question. A comparison was made between the transport parameters of heat separated dermis and dermatomed dermis. No significant differences were observed between the different preparations, showing that the heat separation process did not affect the integrity of the dermal tissue. The same

study compared the transport parameters of fresh dermal tissue to that of stored dermal tissue and also found that there were no significant differences between the two preparations. One issue that is yet to be addressed is the effect of dermal tissue thickness on the transport properties of diffusivity, D_{de} and partition coefficient, K_{de}. A significant thickness effect would imply that careful consideration must be taken when selecting tissue samples for *in vitro* dermal penetration studies.

Table 1.5 Represents a compilation of some of the *in vitro* literature data studying human dermis. Variability in tissue source and handling is shown in this table.

Authors	Skin Source	Dermis Preparation	Experimental Setup	Permeant
(Khalil, Kretsos et al. 2006)	Split thickness cadaver skin from back, thigh and abdomen.	Dermis obtained by heat separation.	Side-by-side diffusion cells. (PBS)	Glucose
(Liu, Higuchi et al. 1994)	Surgical skin from abdominoplasty. Skin was dermatomed (partial dermis).	Dermis obtained by heat separation or dermatoming. Partial dermis was used.	Horizontal diffusion cells. (Saline)	B-estradiol (E2)
(Hansen, Henning et al. 2008)	Surgical skin from abdominoplasty. Full thickness dermis, i.e. no dermatoming.	Dermis obtained by heat separation. Full thickness dermis was used.	Franz cells. (PBS)	Flufenamic acid and caffeine
(Kruse, Golden et al. 2007)	Surgical skin from breast reductions.	Dermatomed to contain full epidermis and upper dermis.	Modified Franz cells.(5% BSA)	Triclosan, testosterone, malathion, parathion and caffeine
(Siddiqui, Roberts et al. 1989)	Abdominal skin from cadavers with subcutaneous fat layer attached.	No real detail.	Permeation cell which was immersed in a water bath.	Hydrocortisone, triamcinolone, prednisolone, corticosterone, triamcinolone acetonide and betamethasone-17 valerate

1.4.3 Experimental setup

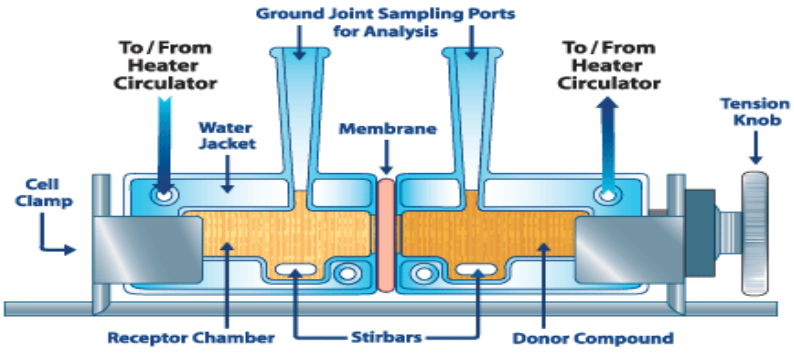

Figure 1.13 Side-by-side diffusion cell. (Source: www.permegear.com)

Studies of dermis transport employ side-by side diffusion cells or Franz diffusion cells. The side-by side cells provide more of a uniform environment for the tissue sample since it is sandwiched between well-stirred aqueous solutions. In the Franz cell only the underside of the dermal tissue is exposed to an aqueous solution. Also, stirring is poor in the receptor solution and non existent in the donor solution. The side-side diffusion cells were chosen for our work due to full hydration, better stirring and better temperature control than Franz cells. Some studies maintain the temperature of the cells at 32ºC, while others at 37ºC. For stratum corneum studies, the former temperature is adequate since the surface of the skin has a lower temperature than the lower skin layers. However, for lower skin layer studies such as the dermis, 37ºC is a more realistic temperature. Thus predictive models relying on data collected at 32ºC should be corrected for this difference in temperature. Several studies do not correct for the aqueous boundary layer (ABL) contribution to the overall resistance of the tissue. Although, the contribution of these layers may be quite small, its determination can only enhance the accuracy of the transport parameters obtained experimentally and thus enhance the predictive capability

of the model. The most significant limitation observed in the literature is the lack of consideration for the fact that albumin and other soluble proteins present in the tissue may diffuse into the donor compartment. Let us consider the implications of such a scenario. If the soluble proteins present in the dermis diffuses out into the donor compartment, then some of the permeant present in this compartment may bind to the albumin and soluble proteins. The more strongly protein bound the permeant, the larger the effect. As a result, the available free concentration of the solute would be lowered. This in turn would lower the effective concentration gradient. Thus less of the solute would partition into the tissue, implying that the tissue has a higher resistance than what is actually true. Thus, the data collected from such an experiment would not accurately depict the transport parameters of that solute in the dermis. Analysis shows that the effective dermis partition coefficient measured in such a study would be reduced from the true value by a factor f_u^{donor}, where f_u^{donor} is the unbound fraction of permeant in the donor solution. If these data were then used to calibrate a model, an inaccurate prediction would result. Permeability and tissue concentrations would be artificially low. This phenomenon would be enhanced in situations where the permeant is highly lipophilic or strongly protein bound. Therefore, this scenario requires further probing. It suggests that some of the data available in the literature today is inaccurate and must be revised.

1.4.4 Simplified analysis of albumin effect in donor solution

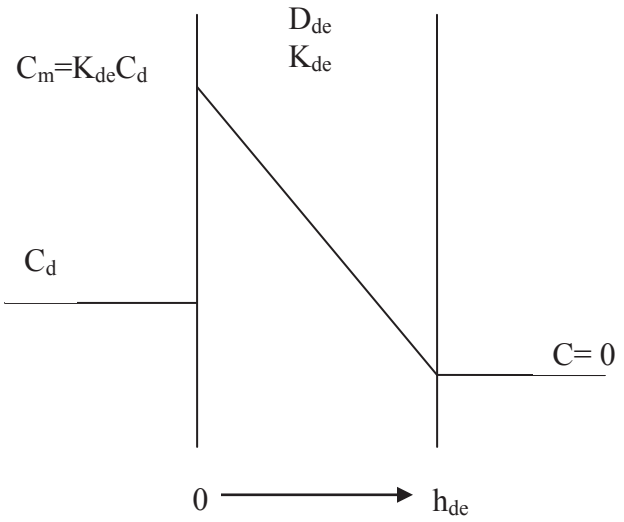

C_m= membrane concentration
C_d= donor concentration
K_{de}= dermis partition coefficient
D_{de}= dermis diffusivity
H_{de}= dermis thickness
C_{avg}= average concentration

Figure 1.14 Simplified depiction of solute partitioning through the dermis from the donor compartment into the receptor compartment.

Scenario 1: No diffusion of albumin into the donor solution

The steady-state flux is defined as the product of the permeability coefficient k_p and the concentration difference ΔC across the isolated dermis membrane in the diffusion cell

$$J_{ss} = k_p \times \Delta C \tag{1.32}$$

The permeability coefficient k_p is the product of the diffusivity in the dermis D_{de} and the partition coefficient in the dermis K_{de} divided by the thickness of the dermis h_{de}. Thus the steady-state flux can be defined as

$$k_p = \frac{D_{de} \times K_{de}}{h_{de}} \tag{1.33}$$

$$J_{ss} = \left(\frac{D_{de} \times K_{de}}{h_{de}} \right) \times C_d \tag{1.34}$$

To account for binding effects that may in turn alter the diffusivity and partitioning in the dermis the diffusivity D_{de} and partition coefficient K_{de} can be expressed in terms of the binding factor BF where we assume that the solute will partition into the albumin-inaccessible fluid region with a partition coefficient of 1 and into the albumin-accessible fluid region with a partition coefficient of $1/f_u$, where f_u is the fraction unbound in the donor solution, and into the lipid fraction with a partition coefficient equal to the octanol-water partition coefficient K_{oct} multiplied by the nonionized fraction f_{non}. It should be noted that based on equilibrium partitioning studies conducted by Bert et al. (1982), the albumin-accessible and albumin-inaccessible regions of the fluid fraction of the dermis were considered to be proportioned in the ratio of 0.32:0.68.

$$BF = 0.68 + \frac{0.32}{f_u} + 0.001 f_{non} K_{oct} \tag{1.35}$$

$$D_{de} = \frac{D_{free}}{BF} \tag{1.36}$$

$$K_{de} = K_{free} \times BF \tag{1.37}$$

where D_{free} is the diffusivity in the absence of binding, K_{free} is the partition coefficient in the absence of binding.

Thus the steady-state flux can be expressed as

$$J_{ss} = \left(\frac{D_{free} \times K_{free}}{h_{de}} \right) \times C_{free}(x = 0) \tag{1.38}$$

where C_{free} is the free available donor concentration.

(Source:(Kretsos, Miller et al. 2008))

Scenario 2: Albumin diffuses into the donor compartment

The albumin present in the donor compartment will bind to the solute concentration dependent on the binding affinity of the solute. Thus, the available free concentration of the solute will be lowered and the steady-state flux J_{ss} would be expressed as

$$J_{ss} = k_p \times \Delta C_{free} \tag{1.39}$$

where ΔC_{free} represents the free available concentration of the solute present in the donor compartment. The steady-state flux can be expressed as

$$J_{ss} = k_p \times f_u C_d \tag{1.40}$$

Due to the binding effects of albumin to the solute in the donor compartment, the permeability coefficient k_p expressed in Equation 2, will be reduced by a factor of the fraction unbound in the donor compartment, f_u^{donor}. Thus the effective permeability coefficient k_p^{eff} will be

$$k_p^{eff} = \left(\frac{D_{de} \times K_{de}}{h_{de}} \right) \times f_u^{donor} \tag{1.41}$$

The apparent diffusivity D_{de} will be unaffected, whereas the apparent Kde will be reduced by a factor of the fraction unbound in the donor compartment such that the experimental partition coefficient $K_{de}^{\exp}$ will be

$$K_{de}^{\exp} = \frac{\overline{C_{de}}}{C_d} = \frac{\overline{C_{free}} \times BF}{C_{free} / f_u^{donor}} = f_u^{donor} \times \frac{BF}{2} \tag{1.42}$$

where $\overline{C_{de}}$ and $\overline{C_{free}}$ represent the average concentration in the dermis and the average free concentration in the donor solution.

2. HYPOTHESIS

An improved model of dermal concentrations and clearance can be developed by refining the assumptions in the current computational model by developing and analyzing additional data.

Specific aims

Aim 1 To develop improved methodology for determining transport parameters of lipophilic compounds in dermis.

Hypothesis: Improvement of the existing experimental methodology used to study dermis *in vitro* will lead to significantly better skin concentration predictions.

The improvement of the existing experimental methodology in studying the dermal tissue *in vitro* was deemed necessary due to our underlying hypothesis that the albumin present in the tissue diffuses out, thus binding to the permeant and as a result lowering the available free concentration. This in turn would lead to an inaccurate quantification of the diffusing and partition coefficients of the compound in question. This hypothesis led to the idea that the use of a barrier membrane in conjunction with the dermal tissue would eliminate this issue.

1.1 Selection of an adequate and appropriate barrier membrane and determination of barrier membrane resistance.

1.2 To determine the contribution of the Aqueous Boundary Layer (ABL) to the overall resistance in a side-by-side diffusion cell.

1.3 Test the influence of diffusible protein on permeant transfer.

1.4 To quantify the presence of protein in the donor compartment in the absence or presence of dialysis membrane.

1.5 To determine the binding affinity of the permeant to lower molecular weight proteins diffusing out of the dermis in the presence of the barrier membrane.

1.6 Theoretical determination and calculation of coupled transport of mobile and bound protein.

Aim 2 To utilize the developed methodology to determine the diffusivity and partition coefficients of selected permeants in excised human dermis.

Hypothesis: Improved methodology will lead to better estimations of transport parameters for permeants of varying lipophilicity.

Our hypothesis of the necessity of a barrier membrane to prevent the diffusion of protein through the tissue will be tested using permeants of varying lipophilicity. We predict that for moderately lipophilic compounds such as DEET, the absence of the dialysis membrane will not significantly affect the transport parameters tabulated from the experimental data. However, it is believed that this will be quite the contrary for more lipophilic compounds, respectively DDT, parathion and diclofenac.

2.1 DEET

2.2 Diclofenac.

2.3 Parathion.

Aim 3 To use the developed data and literature results to improve the current computational model for solute transport in the dermis.

Hypothesis: Improvement of the current computational model leading to more accurate estimations of the transport parameters for permeants of varying lipophilicity.

The overall main goal is to improve the current computational model and determine its functionality in accurately calculating transport parameters for all permeants. Consolidating the *in vitro* data collected from the previous Aims can aid in better understanding how the model can be modified to better represent the effects of the dermis. Comparison however, of previous in vivo data to the model will give us a clearer representation of how well the model is able to calculate the transport parameters of the permeants in question.

3.1 Collect permeability and tissue concentration data from relevant sources.

3.2 Compare the collected data for tissue concentrations and permeability parameters to the calculated values using the current computational model.

3.2.1 *In vitro*

3.2.2 *In vivo*

3.3 To estimate the transport rate of albumin in human dermis *in vivo*.

3.4 Modify model to better describe and predict the data.

3. IMPROVED METHOD FOR DETERMINING DIFFUSION AND PARTHION COEFFICIENTS IN HUMAN DERMIS

Ibrahim, R. Kasting, G.B. Improved method for determining diffusion and partition coefficients in human dermis. 2007. J Pharm Sci 99: 4928-2939

3.1 INTRODUCTION

It is well established that the stratum corneum dominates the skin's barrier to transport of polar and moderately lipophilic compounds due to its unique brick-and-mortar structure including a continuous lipid barrier. However, highly lipophilic compounds (those with an octanol/water partition coefficient greater than about 1000) experience significant diffusive resistance in the lower skin layers during absorption due to the water-continuous structure of these layers.(Cleek and Bunge 1993) Representing these layers as an unstirred aqueous layer of about 200 μm thickness has proven to be satisfactory to describe many features of steady-state skin permeation of lipophilic compounds.(Scheuplein 1978; Kasting, Smith et al. 1992; Cleek and Bunge 1993; Basketter, Pease et al. 2007) However, this representation fails to account for the magnitude of lipophilic permeant concentrations in the dermis following topical administration. High concentrations arise due to binding of these compounds to lipids and proteins within the tissue,(Cross, Magnusson et al. 2003; Cross and Roberts 2006; Kretsos, Miller et al. 2008) including a substantial contribution from hair follicles.(Illel, Schaefer et al. 1991; Grams and Bouwstra 2002; Grams, Alaruikka et al. 2003) It is of interest to better estimate skin concentrations of topically-applied compounds for several

applications including dermatological drug development(Mehta, Afouna et al. 1997) and skin sensitization risk assessment.(Basketter, Pease et al. 2007)

Capillary clearance profoundly affects permeant concentrations in dermis in vivo, leading to steady-state concentration profiles that approximate exponential decays.(Gupta, Wientjes et al. 1995; Kretsos, Kasting et al. 2004; Kretsos, Miller et al. 2008) In vitro experiments with isolated dermis can determine solute diffusivities and partition coefficients in this skin layer in the absence of capillary clearance. The combination of a steady-state permeability experiment with an equilibrium partitioning experiment suffices to yield both parameters.(Khalil, Kretsos et al. 2006; Kretsos, Miller et al. 2008) Binding of solutes to extravascular albumin and other soluble proteins in the dermal matrix is thought to contribute appreciably to the partitioning of lipophilic compounds.(Cross, Magnusson et al. 2003; Kretsos, Miller et al. 2008; Weiss, Fresneau et al. 2008) The total concentration of serum proteins in dermis is 11 mg/g, based on Bert and coworkers' measurements in postmortem human dermis.(Bert, Pearce et al. 1986) The concentration in the albumin accessible regions (approximately 32% of the fluid fraction)(Bert, Mathieson et al. 1982) has been estimated to be 2.7% w/v.(Kretsos, Miller et al. 2008) It is furthermore evident that albumin and other serum proteins can migrate slowly through the tissue; otherwise, they would accumulate in dermis rather than being cleared in the lymph. This phenomenon presents a challenge to conducting accurate experiments in vitro. In particular, if albumin or other soluble proteins migrate into the donor solution during a side-by-side diffusion cell experiment, and the test permeant binds to the protein, then an artificially low dermis permeability would be obtained. A similar limitation applies to equilibrium partition coefficients determined by immersing tissue

samples in an aqueous buffer. The method described in this paper removes this uncertainty by preventing the diffusion of macromolecules into the donor solution. The cost is that the permeability of the barrier membrane providing this function must be accurately known in order to estimate the dermis permeability. The method is illustrated using DEET, a moderately lipophilic compound that binds moderately to albumin, and diclofenac, an ionizable and therefore water-soluble drug that is nevertheless highly protein bound.

3.2 MATERIALS AND METHODS

3.2.1 Materials

Dialysis membrane (5000 Da cutoff) was purchased from Bel-Art Products, Pequannock, NJ. PharmElast™ medical grade silicone (PDMS) membrane, 0.020" (~500 μm) in thickness, was obtained from SF Medical (now Trelleborg Sealing Solutions US, Bloomfield Hills, MI). Additional dialysis membrane (3500 Da cutoff) and dialysis tubing (100-500 Da cutoff) were purchased from SpectrumLabs, Rancho Dominguez, CA. Unlabeled DEET (97.3%) and diclofenac were purchased from Sigma-Aldrich, Atlanta, GA. [Carbonyl-^{14}C] DEET (52mCi/mmol, radiochemical purity >99%) was purchased from Vitrax, Placentia, CA. [Carbonyl-^{14}C] diclofenac (55mCi/mmol, radiochemical purity >99%) was purchased from American Radiolabeled Chemicals, St. Louis, MO. Ultima Gold™ XR scintillation cocktail and Soluene®-350 were purchased from Perkin-Elmer, Boston, MA. A Micro BCA™ protein assay kit was purchased from Thermo Scientific, Rockford, IL. Skin from abdominoplasty (3 donors) and mammoplasty (4 donors) was obtained from the University of Cincinnati Academic

Health Center. Phosphate-buffered saline (PBS), bovine serum albumin (BSA) and sodium azide were purchased from Sigma Chemicals.

3.2.2 Barrier membrane and aqueous boundary layer studies

Dialysis membrane (5000 Da cutoff) and PDMS sheets were considered as possible barrier membranes. Membranes were mounted in water-jacketed side-by-side diffusion cells (1.77 cm^2) maintained at a temperature of 37ºC. Multiple membranes were mounted in some experiments to probe the contributions of aqueous boundary layers. Each donor compartment (6 mL) of the diffusion cells was filled with PBS solution to which sodium azide (0.02%) had been added to inhibit microbial growth. The receptor compartments (6 mL) were filled with either PBS or 2% BSA-PBS solution, both supplemented with sodium azide. Both compartments were magnetically stirred using synchronous motors operating at 600 rpm. After a 24-h equilibration the donor compartment was spiked with 100 μL of ^{14}C-DEET + unlabeled DEET in ethanol yielding a 10 μg/mL DEET solution containing 0.56 μCi of ^{14}C DEET. The donor and receptor compartments were sequentially sampled (0.1 mL donor; 0.5 mL receptor), and the receptor solution was replenished with an equal volume of fresh solution after each sampling. More consistent values for the initial donor concentrations were obtained by extrapolation of later time points (1, 1.5 and 6h) back to time zero than by taking early time points. All collected samples were mixed with scintillation cocktail (5 mL) and analyzed by liquid scintillation counting. For dialysis membrane similar experiments were carried out using 7.5 μg/mL (0.56 μCi) of ^{14}C-diclofenac in the donor solution.

For all experiments the cumulative amount of solute passing through unit area of membrane $M(t)$ was plotted versus time. The steady-state flux J_{ss} was calculated as the

slope of the linear portion of the graph, and the time lag T_L was calculated as the intercept of the regression line on the time axis. The permeability coefficient k_p and its reciprocal, the total diffusive resistance R_{tot}, were calculated as

$$k_p = \frac{1}{R_{tot}} = \frac{J_{ss}}{\Delta C} \approx \frac{J_{ss}}{C_d}. \quad (3.1)$$

where C_d is the donor solution concentration. The approximation $\Delta C \cong C_d$ was justified since the concentration of permeant in the receptor solution never exceeded 13% of that in the donor solution.

The assumption was made that the membrane system under study was surrounded by two potentially unsymmetrical, unstirred aqueous layers (aqueous boundary layers or ABLs) having resistances R_1 (donor solution) and R_2 (receptor solution). The membrane resistance was determined by subtracting their sum from R_{tot}:

$$R_{mem} = R_{tot} - (R_1 + R_2) \quad (3.2)$$

The value of $R_1 + R_2$ for the symmetrical case in which both donor and receptor solutions contained PBS (thus, $R_1 = R_2$) was determined from a ^{14}C-DEET experiment in which N = 1, 2 and 3 dialysis membranes were mounted in series. A linear regression was performed on a plot of R_{tot} versus the number of membranes in each cell according to Eq. 3.3:

$$R_{tot} = (R_1 + R_2) + NR_{Dial} \quad (3.3)$$

The boundary layer thickness h_{ABL} was then calculated from Eq. 3.4 using the Wilke-Chang relationship (Eq. 3.5) to estimate the aqueous diffusivity D_{aq} for DEET.

$$h_{ABL} = D_{aq} R_1 \tag{3.4}$$

$$D_{aq}(\text{cm}^2\text{s}^{-1}) = \frac{7.4\times10^{-8} T(M\cdot\phi)^{1/2}}{\eta V_A^{0.6}} \tag{3.5}$$

In Eq. 3.5 T is temperature in Kelvin, M is solvent molecular weight (18.01 for water), ϕ is the solvent association parameter (2.27 for water), η is solvent viscosity in centipoise (0.67 cp for water at 37°C) and V_A is the molar volume of the solute at the normal boiling point in $\text{cm}^3\text{mol}^{-1}$. V_A was estimated using Schröeders Method.(Poling, Prausnitz et al. 2001) Eq. 3.5 refers to the diffusivity of unbound permeant. For bound permeant, the diffusivity would be closer to that of albumin as explained in Appendix 1.

For experiments involving other permeants, and for those in which BSA was included in the receptor solution, the values of R_1 and R_2 were recalculated according to Eqs. 3.6 and 3.7,

$$R_1 = \frac{h_{ABL}}{D_{aq}} \tag{3.6}$$

$$R_2 = f_u \frac{h_{ABL}}{D_{eff}} \tag{3.7}$$

In these relationships, D_{aq} is the aqueous diffusivity of the test permeant estimated from Eq. 3.5 and h_{ABL} is aqueous boundary layer thickness determined from Eq. 3.4, a suitable choice since the viscosity of a 2% BSA solution is not appreciably different than that of

water (Rheosense 2008) and the aqueous diffusivities of the test permeants are comparable.(Pohl, Saparov et al. 1998) In Eq. 3.7, f_u is the unbound fraction of test permeant in the receptor solution and D_{eff} is the effective diffusivity of the test permeant in the receptor solution,

$$D_{eff} = f_u D_{free} + (1 - f_u) D_{bound} \tag{3.8}$$

Here D_{free} is the aqueous diffusivity of unbound permeant (equivalent to D_{aq} in Eqs. 3.5 and 3.6) and D_{bound} is that of permeant bound to albumin. The value of D_{bound} was taken to be 9.29×10^{-7} cm^2/s, the estimated diffusivity of BSA in water at 37°C.(Fardet, Hoebler et al. 1998) A justification for Eqs. 3.7 and 3.8 is given in Appendix 1.

3.2.3 Protein binding studies

These studies were carried out using dialysis membranes (5000 Da cutoff) mounted in side-by-side diffusion cells as described above with the exception that they were continued for 96 h to ensure equilibrium conditions. The donor solution contained radiolabeled DEET (10 μg/mL) or diclofenac (7.5 μg/mL) in PBS and the receptor solution contained PBS + 2% BSA. Both solutions were preserved with 0.02% sodium azide. The value for DEET was obtained in a previous study.(Kasting, Miller et al. 2008) The fraction of the drug unbound to protein f_u was calculated as the ratio of donor solution concentration to receptor solution concentration at 96 h.

An additional study was carried out in which donor solutions obtained from a protein diffusion experiment employing a dialysis membrane (5000 Da cutoff – see description below) in series with dermis were dialyzed against PBS using dialysis tubing (100-500

Da cutoff). This study was conducted in order to determine whether protein fragments which passed through the 5000 Da membrane were capable of binding diclofenac. The donor solution was placed inside the dialysis tubing, which was immersed in PBS solution. ^{14}C-diclofenac (7.5 μg/mL) was added to either the PBS or donor solution. The solutions were dialyzed for 31 days.

3.2.4 Dermis transport studies

Dialysis membranes (5000 Da cutoff) were prepared as previously described. In most cases skin was stored frozen at -80ºC and allowed to thaw before use. Limited testing of fresh versus frozen skin from the same donor did not show significant differences in transport parameters for DEET; however the supply of fresh skin was not sufficient to rigorously test this finding. Skin samples from abdominoplasty included some subcutaneous fat, which was cut away using surgical scissors prior to freezing. Skin samples from mammoplasty were thinner and contained no visible fat. The skin was then rinsed thoroughly in PBS solution to remove any traces of blood and cut into approximately 2.5 cm × 2.5 cm pieces. Any skin samples with visible tears were discarded. The epidermis was separated from the dermis by heat separation(Kilgman and Christophers 1963) using 57ºC water for 2 min. Excess water was then removed from the samples, which were placed on weighing paper and accurately weighed. A trace was made of each sample and used to quantify its area. The thickness of the sample was then determined assuming a density of 1.075 g/cm^3.(Kasting, Smith et al. 1992; Altshuler, Smirnov et al. 2005) The dermis sample was mounted in the diffusion cell in series with a dialysis membrane placed between the dermis and the donor solution. Test permeants were ^{14}C-DEET (10 μg/mL) and ^{14}C-diclofenac (7.5 μg/mL). The receptor solutions

were either PBS or 2% BSA-PBS solution, both supplemented with sodium azide. The BSA was added to maintain a physiological environment within the dermis. All DEET studies were carried out for 6 h and diclofenac studies were carried out for 48 h to attain steady-state conditions. The remainder of the experiment was conducted as previously described. Each dermis sample was dissolved in Soluene® (1 mL) and placed in an autoclave oven overnight. All collected samples and dissolved skin samples were analyzed by LSC. A separate study was conducted using dermis samples mounted without the dialysis membrane, and the results were compared.

Permeation data were analyzed according to Eqs. 3.1 and 3.2. The value of R_{mem} represented either the dermis resistance R_{de} or the sum of dermis plus dialysis membrane resistances R_{de} + R_{Dial}, depending on the type of study conducted. Permeant concentrations in the receptor compartment for DEET never exceeded 10% of the donor concentration. Those for diclofenac at the end of the study averaged 16% (dermis only) and 34% (dermis + dialysis membrane) of the donor concentration. The consequences of this level of accumulation are discussed later. For dermis + dialysis membrane studies, the value of R_{de} was thus calculated as:

$$R_{de} = R_{tot} - R_1 - R_2 - R_{Dial} \tag{3.9}$$

The product of dermis diffusivity and partition coefficient $D_{de}K_{de}$, often termed permeability P_{de} (Kretsos, Miller et al. 2008) was calculated from R_{de} and the thickness h_{de} of each sample according to Eq. 3.10:

$$P_{de} = D_{de}K_{de} = h_{de} / R_{de} \tag{3.10}$$

The value of the dermis/donor solution partition coefficient K_{de} was obtained from the average concentration measured in the dermis tissue sample $\overline{C_{de}}$ according to Eq. 3.11, which is justified in Appendix 2:

$$K_{de} = \frac{2\overline{C_{de}}}{C_d}\left(\frac{R_{tot}}{R_{tot} - R_1 - R_{Dial} + R_2}\right) \tag{3.11}$$

Dermis diffusivity D_{de} was then calculated as

$$D_{de} = P_{de} / K_{de} \tag{3.12}$$

For studies in which the dermis dominated the time lag T_L, D_{de} was also calculated from Eq. 3.13:

$$D_{de} = h_{de}^2 / 6T_L \tag{3.13}$$

Comparisons between diffusivities obtained from Eqs. 3.12 and 3.13 are discussed later. Corresponding formulas for dermis only experiments also employed Eqs. 3.9-3.13 except that the value of R_{Dial} was set to zero.

3.2.5 Protein diffusion studies

Human dermis was prepared and mounted in side-by-side diffusion cells as in the dermis transport studies. In some cells a dialysis membrane (either 3500 Da or 5000 Da cutoff) was inserted between the dermis and the donor solution. The donor solution was PBS and the receptor solution was PBS + 2% BSA. Both solutions contained 0.02% sodium azide to inhibit microbial growth. Five minutes after mounting the cells, and periodically thereafter, samples (200 μL) were withdrawn from the donor solution (with replacement

buffer added) and 150 μL of the sample was placed in a 96-well plate. In the case of the dermis only treatment, the sample was diluted by a factor of 5 prior to assay. The collected samples were analyzed for protein content using the Micro BCA™ assay kit. This method utilizes bicinchonic acid (BCA) as the detection reagent for Cu^{+1}, which is formed when Cu^{+2} is reduced by protein in an alkaline environment. It is a non-specific assay for protein. The assay was calibrated using solutions of BSA in PBS with varying concentration. Results were calculated as BSA-equivalents/mL and expressed following conversion by the cell parameters as BSA-equivalents/cm^2.

3.3 Statistical Analysis. For all experiments, results were calculated individually for each diffusion cell, then averaged to obtain a mean and standard error. Transport and partitioning parameters obtained by different methods were compared via 2-way ANOVA using donor as a blocking variable. The pairwise comparison test used was the Holm-Sidak method. *p*-values less than 0.05 were considered to be significant. For comparisons involving only two groups, a Student's t-test was employed. All tests were conducted using SigmaStat version 3.10 (SYSTAT, Chicago, IL).

3.4 RESULTS

3.4.1 Aqueous boundary layer study

Permeation profiles for ^{14}C-DEET across 1, 2 or 3 dialysis membranes into PBS are shown in Figure 3.1a. Total diffusive resistances calculated from these profiles based on the slopes from 0-3 h post-dose are plotted versus the number of membranes in Figure 3.1b. Linear regression of these data according to Eq. 3.3 yielded $R_1 + R_2 = (3950 \pm 120)$ s/cm and $R_{Dial} = (21{,}740 \pm 50)$ s/cm, with a squared correlation coefficient $r^2 = 0.995$.

Since the boundary layers were symmetrical in this study, $R_1 = R_2 = 1975$ s/cm. Further analysis according to Eqs. 3.4 and 3.5 led to $D_{aq}=8.54 \times 10^{-6}$ cm^2/s and $h_{ABL} = 0.0169$ cm or about 170 μm. The total unstirred layer thickness relevant to the diffusion cells is thus $2 \times h_{ABL} \approx 340$ μm. For diclofenac, Eqs. 3.5 and 3.6 yield $D_{aq} = 7.08 \times 10^{-6}$ cm^2/s and $R_1 = 2390$ s/cm for this slightly larger and more slowly diffusing permeant.

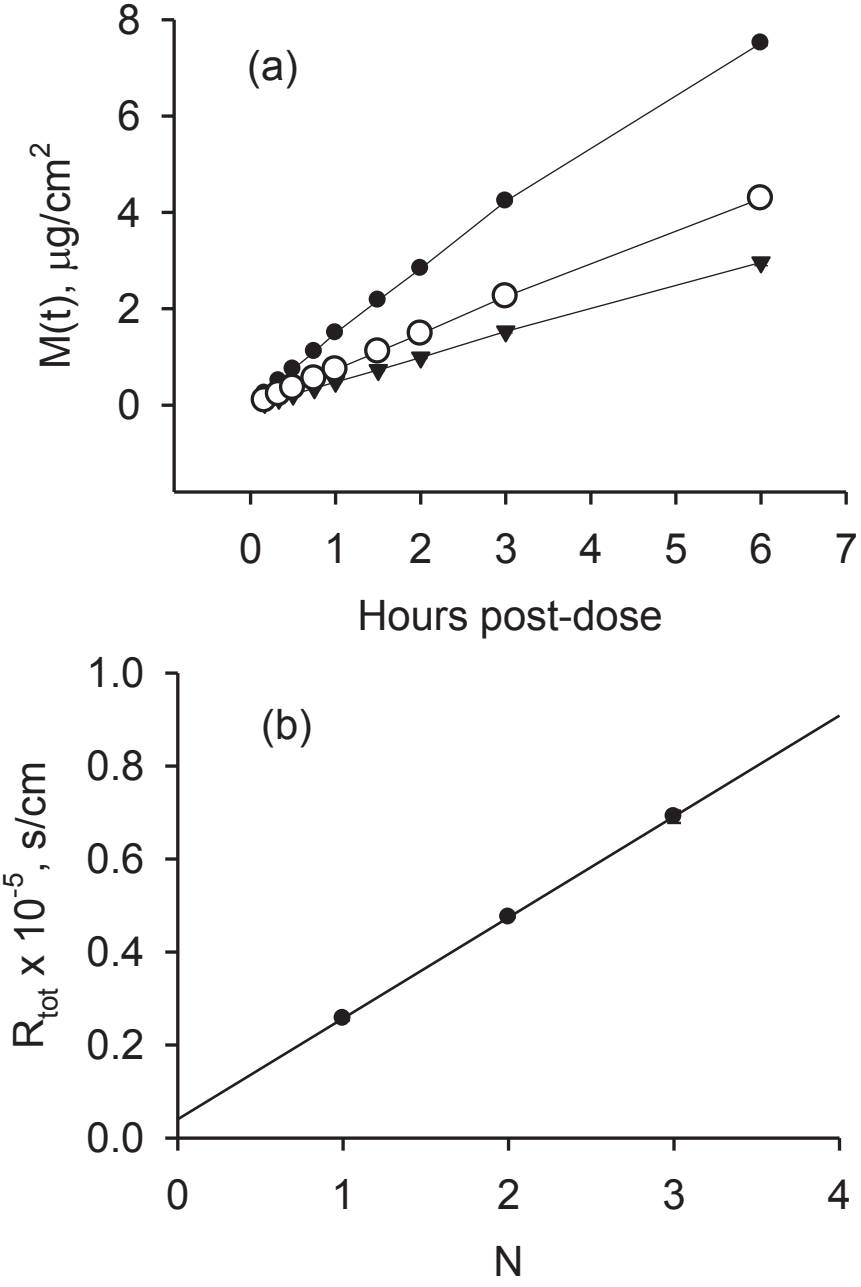

Figure 3.1 (a) Results of aqueous boundary layer study for ^{14}C-DEET permeating across 1 (●), 2 (○) or 3 (▼) dialysis membranes placed in series in the diffusion cells. Data shown are the mean ± SE of 9 determinations. (b) Analysis of data shown in panel (a) according to Eq. (3.3). In both panels, the error bars are smaller than the size of the symbols.

3.5.2 Protein binding studies

The percentages of ^{14}C-DEET and ^{14}C-diclofenac bound in a 2% BSA solution (mean ± SE, n = 4-5) were 81.1 ± 0.4% and 96.0 ± 0.5%, respectively, based on equilibrium concentrations at 96 h post-dose. Thus, f_u = 0.19 for DEET and 0.04 for diclofenac. These results were used in combination with those in the previous section and a published value of BSA diffusivity in water (Fardet, Hoebler et al. 1998) to estimate the aqueous boundary layer resistance in receptor compartments containing PBS + 2% BSA. Under these conditions, Eqs. 3.7 and 3.8 yield R_2 = 1370 s/cm for DEET and 580 s/cm for diclofenac.

Equilibration of ^{14}C-diclofenac between donor solutions containing small protein fragments (< 5000 Da) derived from dermis diffusion studies dialyzed against PBS using dialysis tubing (100-500 Da cutoff) was a slow process that was not complete within 31 days. However, since the approach to equilibrium was followed from both directions (i.e., the radiolabel was placed either inside or outside the dialysis tubing), limits to the true equilibrium could be established. An upper limit to binding of ~11% and a lower limit of ~2% were obtained, so that f_u for the donor solutions fell within in the range 0.89 - 0.98 with a likely equilibrium value of ~0.94 (data not shown). This study thus established that diclofenac was not strongly bound in donor solutions separated from dermis by a dialysis membrane.

3.4.3 Barrier membrane studies

The results for dialysis membrane permeability studies are shown in Figure 3.2 and Table 3.1. No significant difference was observed between the permeability coefficients or

dialysis membrane resistances for permeants tested with or without BSA in the receptor solutions. However, the amount of diclofenac permeated at 6 h with BSA in the receptor solution was significantly higher than that with PBS, suggesting that the decreased boundary layer resistance for the BSA solution did measurably impact transport. The average ratio of dialysis membrane resistances for DEET and diclofenac calculated from the values in Table 3.1, Column 2 (0.85), was very close to the inverse ratio of aqueous diffusivities calculated from the Wilke-Change relationship, Eq. 3.5 (0.83).

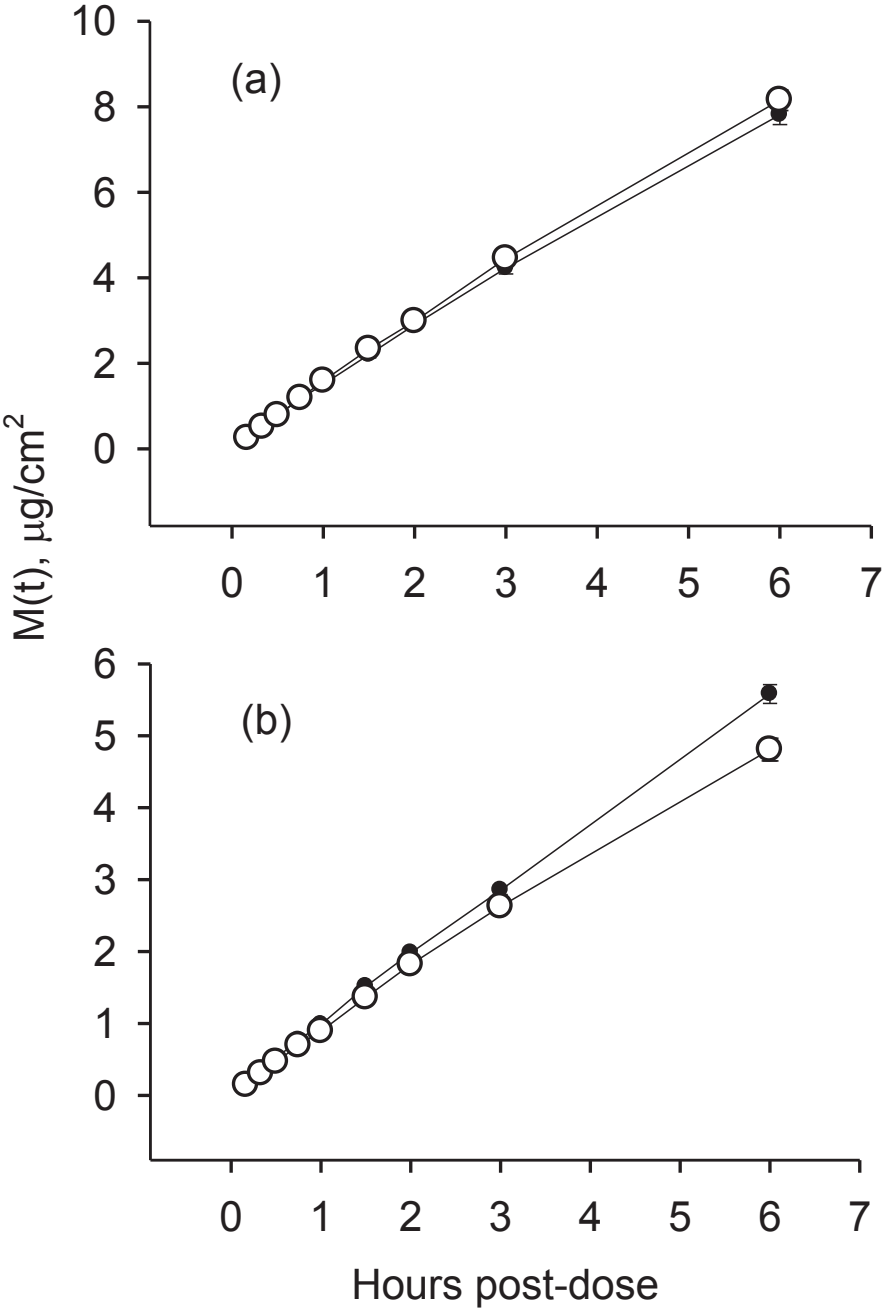

Figure 3.2 Permeation of (a) ^{14}C-DEET or (b) ^{14}C-diclofenac across dialysis membrane in the presence (●) and absence (○) of BSA in the receptor solutions. The data shown represent the mean ± SE of 13-19 replicates (DEET) and 4-5 replicates (diclofenac). Error bars are smaller than the size of the symbols.

Table 3.1 Transport Parameters (mean ± SE) for DEET and diclofenac in dialysis membrane obtained by analyzing the data shown in Figure 3.2.

	$k_p \times 10^5$ (cm/s)	$R_{Dial} \times 10^{-5}$ (s/cm)	T_L (h)
DEET			
PBS *n*=7(34)[a]	4.09 ± 0.09	0.203 ± 0.004	-0.06 ± 0.03
PBS + 2% BSA *n*=3(13)	4.00 ± 0.14	0.220 ± 0.009	-0.05 ± 0.03
Diclofenac			
PBS *n*=1(4)	3.35 ± 0.09	0.252 ± 0.008	-0.03 ± 0.01
PBS + 2% BSA *n*=1(5)	3.63 ± 0.08	0.247 ± 0.006	-0.02 ± 0.01

[a]Reported as *n* = No. of studies (Total no. of replicates)

This result is consistent with the expectation that diffusion through dialysis membrane occurs via aqueous channels. The average value R_{Dial} = 21,200 s/cm for DEET is within 3% of the value R_{Dial} = 21,740 s/cm obtained in the aqueous boundary layer study. These values are not significantly different. For the remainder of the analysis we used the average value obtained from the barrier membrane studies, R_{Dial} = 21,200 s/cm for DEET due to the higher number of replicates and R_{Dial} = 24,900 s/cm for diclofenac.

Results with PDMS membranes were not as consistent as those with dialysis membranes (data not shown). Although the permeability coefficient and associated diffusive resistance of PDMS membrane were comparable to dialysis membrane, the standard deviation of these values was higher and an additional time lag of approximately 0.4 h was introduced into the system. A plot of total diffusive resistance versus number of membranes for PDMS membranes placed in series was not as linear as that for dialysis

membranes (cf. Fig. 3.1b). We hypothesized that imperfect adhesion of the PDMS membranes to one another may have led to the variability. We tried to improve the results by coating the apposed PDMS surfaces with a thin layer of silicone grease; however, this approach was not effective. Consequently dialysis membrane was chosen as the barrier membrane for the dermis transport studies.

3.4.4 Dermis transport studies

The results of these studies are shown in Figures 3.3 and 3.4 and Tables 3.2 and 3.3. For DEET, the dialysis membrane and dermis functioned together as a barrier in an approximately additive manner. Flux across the diffusion cell (Figs. 3.3 and 3.4a) and tissue concentrations in the dermis (Table 3.2) were lowered by the presence of the dialysis membrane by an amount consistent with its diffusive resistance. Transport and partitioning parameters for DEET in dermis calculated from the data in the presence and absence of dialysis membrane, or in the presence and absence of BSA in the receptor solution, were not significantly different (Table 3.3). Diffusivities calculated from the time lag (Eq. 3.13) averaged 40-50% higher than those calculated from permeability data (Eq. 3.12). These differences were significant. Breast skin and abdominal skin samples had comparable permeability ($P_{de} = D_{de}K_{de}$) to DEET; however, breast skin had a lower diffusivity D_{de} (Eq. 3.12, $p = 0.11$; Eq. 3.13, $p < 0.01$) and a higher partition coefficient K_{de} ($p < 0.01$) relative to abdominal skin. DEET diffusivity in breast and abdominal skin, as calculated from Eq. 3.12, averaged 42% and 69%, respectively, of the calculated aqueous diffusivity $D_{aq}=8.54 \times 10^{-6}$ cm^2/s estimated from Eq. 3.5 at 37°C.

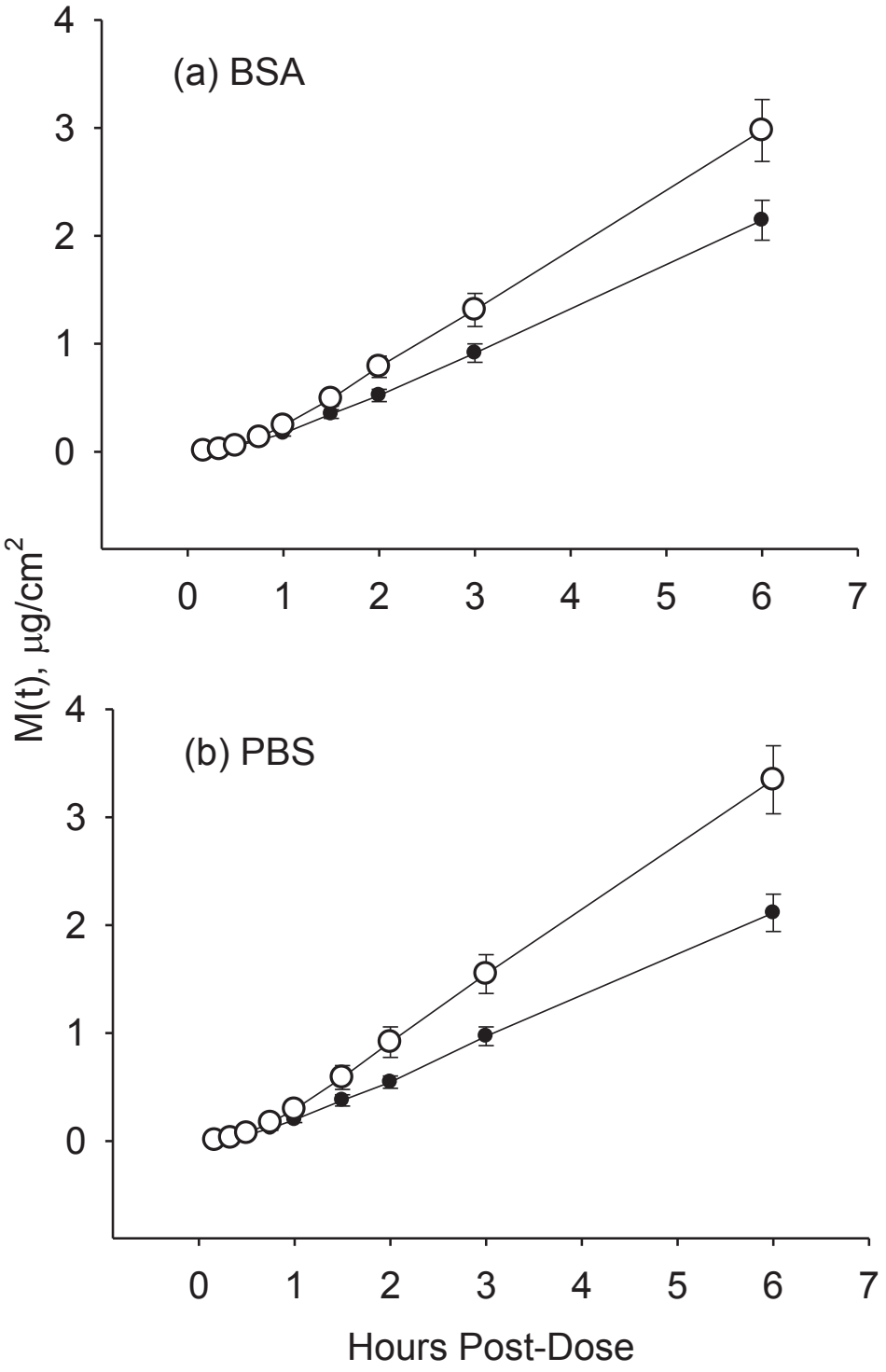

Figure 3.3 Results of breast skin dermis permeation studies with ^{14}C-DEET in the presence (•) and absence (o) of a dialysis membrane placed between the dermis and the donor solution. The donor solutions contained the permeants dissolved in PBS and the receptor solutions contained in either (a) PBS + 2% BSA or (b) PBS.

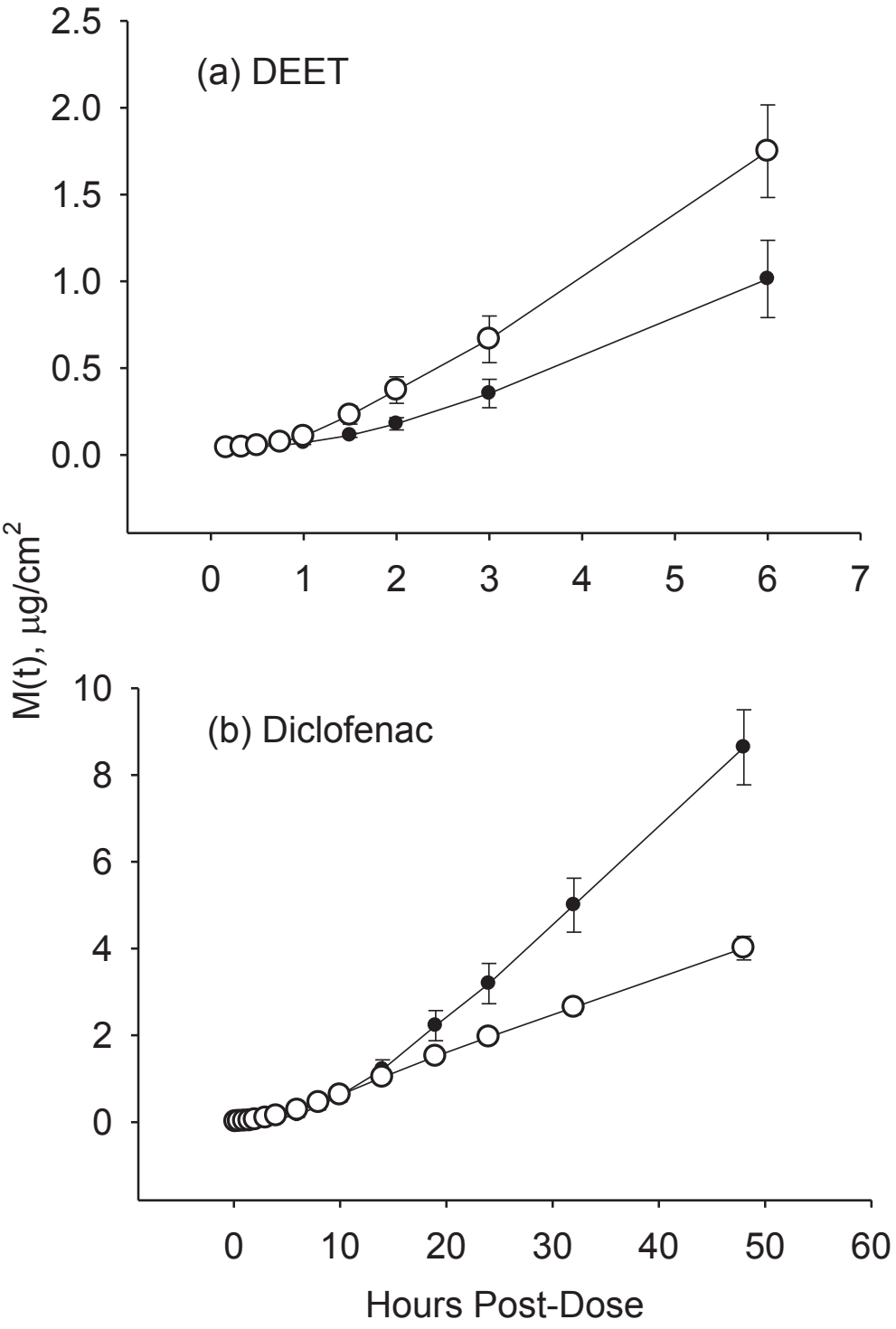

Figure 3.4 Results of abdominal skin dermis permeation studies in the presence (•) and absence (o) of a dialysis membrane placed between the dermis and the donor solution. The donor solutions contained the permeants dissolved in PBS and the receptor solutions contained PBS + 2% BSA.

Table 3.2 Thicknesses, permeability coefficients, time lags and tissue concentrations associated with the dermis transport experiments. Results are reported as mean ± SE.

Membrane	Receptor	n[a]	h_{de} (cm)	$k_p \times 10^5$ (cm/s)	T_L (h)	$\overline{C}_{de}$ (μg/cm^3)
DEET – breast skin						
Dialysis+Dermis	BSA	6(21)	0.246 ± 0.015	1.10 ± 0.09	0.68 ± 0.05	2.27 ± 0.20
	PBS	5(18)	0.205 ± 0.018	1.05 ± 0.09	0.50 ± 0.08	2.05 ± 0.29
Dermis Only	BSA	1(4)	0.250 ± 0.017	1.46 ± 0.14	0.53 ± 0.04	4.95 ± 0.16
	PBS	1(5)	0.254 ± 0.012	1.72 ± 0.16	0.53 ± 0.07	4.92 ± 0.24
DEET – abdominal skin						
Dialysis+Dermis	BSA	2(3)	0.508 ± 0.007	0.580 ± 0.124	1.10 ± 0.05	2.06 ± 0.19
	PBS	2(3)	0.499 ± 0.025	0.383 ± 0.042	1.70 ± 0.17	2.03 ± 0.52
Dermis Only	BSA	2(6)	0.462 ±0.029	0.993 ± 0.127	0.99 ± 0.11	3.15 ± 0.48
	PBS	2(4)	0.514 ± 0.019	0.588 ± 0.040	1.53 ± 0.70	3.12 ± 0.25
Diclofenac – abdominal skin						
Dialysis+Dermis	BSA	4(7)	0.379 ± 0.024	0.839 ± 0.081	9.07 ± 1.11	9.13 ± 1.62
Dermis Only	BSA	4(11)	0.386 ± 0.012	0.338 ± 0.023	-0.05 ± 2.20	3.42 ± 0.37

[a]No. of studies (Total no. of replicates)

Table 3.3. Transport and partitioning parameters (mean ± SE) obtained by analyzing the dermis transport and concentration data in Table 3.2.

Membrane	Receptor	$R_{de} \times 10^{-5}$ (s/cm)	$P_{de} \times 10^{6}$ (cm^2/s)	K_{de}	$D_{de} \times 10^{6}$ (cm^2/s)	
					Eq. 3.12	Eq. 3.13
DEET – breast skin						
Dialysis+Dermis	BSA	0.81 ± 0.02	4.16 ± 0.53	0.97 ± 0.08	4.63 ± 0.82	4.37 ± 0.44
	PBS	0.79 ± 0.09	3.45 ± 0.46	1.26 ± 0.22	3.17 ± 0.46	4.48 ± 0.74
Dermis Only	BSA	0.67 ± 0.06	3.77 ± 0.18	1.19 ± 0.04	3.03 ± 0.16	5.53 ± 0.52
	PBS	0.56 ± 0.05	4.66 ± 0.31	1.25 ± 0.03	3.49 ± 0.29	5.87 ± 0.59
Mean ± SE (All treatments)		0.71 ± 0.06	4.01 ± 0.26	1.17 ± 0.07	3.58 ± 0.36	5.06 ± 0.38
DEET – abdominal skin						
Dialysis+Dermis	BSA	1.60 ± 0.37	3.58 ± 0.90	0.54 ± 0.08	6.51 ± 1.00	10.0 ± 0.4
	PBS	2.38 ± 0.28	2.13 ± 0.15	0.55 ± 0.09	4.05 ± 0.54	7.03 ± 1.28
Dermis Only	BSA	1.10 ± 0.21	5.36 ± 0.76	0.70 ± 0.10	9.07 ± 1.96	11.7 ± 2.4
	PBS	1.69 ± 0.12	3.08 ± 0.20	0.76 ± 0.03	4.07 ± 0.34	8.13 ± 0.93
Mean ± SE (All treatments)		1.69 ± 0.26	3.54 ± 0.68	0.64 ± 0.05	5.93 ± 1.20	9.22 ± 1.03
Diclofenac – abdominal skin						
Dialysis+Dermis	BSA	1.02 ± 0.16	3.95 ± 0.31	7.56 ± 0.67	0.57 ± 0.06	0.72 ± 0.11
Dermis Only	BSA	3.18 ± 0.40	1.29 ± 0.09	1.21 ± 0.09	1.14 ± 0.08	NA[a]

[a]Not estimated due to lack of apparent time lag

The above results, in combination with literature reports involving skin and other biological membranes,(Sawada, Ho et al. 1994; Yamashita, Furubayashi et al. 2000; Cross, Anissimov et al. 2003) led us to focus further studies on combinations in which the receptor solutions were supplemented with BSA. These studies were confined to abdominal skin due to tissue supply. Based on the DEET results, the abdominal skin/BSA combination is suitable for study if adequate time is allowed for achievement of steady-state permeation. For the highly protein bound permeant, diclofenac, the study period was increased to 48 h.

Results for diclofenac were strikingly different from those for DEET. Flux across the diffusion cells was higher for the composite membrane (dialysis + dermis) compared to dermis alone (Fig. 3.4b). Average dermis tissue concentrations were 2.7-fold higher for the composite membrane (Table 3.2). All dermis transport and partition parameters calculated from these data were significantly different for the composite membrane and dermis only systems (Table 3.3). In general, the composite membrane system yielded higher dermis permeabilities P_{de}, with the major contributor to the difference being a higher dermis/donor solution partition coefficient K_{de}. Mean diffusivities for diclofenac in dermis estimated from the composite membrane data were 0.57×10^{-6} cm^2/s (Eq. 3.12) or 0.72×10^{-6} cm^2/s (Eq. 3.13). These values are 8% and 10%, respectively of the aqueous diffusivity $D_{aq} = 7.08 \times 10^{-6}$ cm^2/s estimated from Eq. 3.5.

3.4.5 Protein diffusion studies

Donor solution protein content following the mounting of human dermis in side-by-side cells are shown in Figure 3.5.

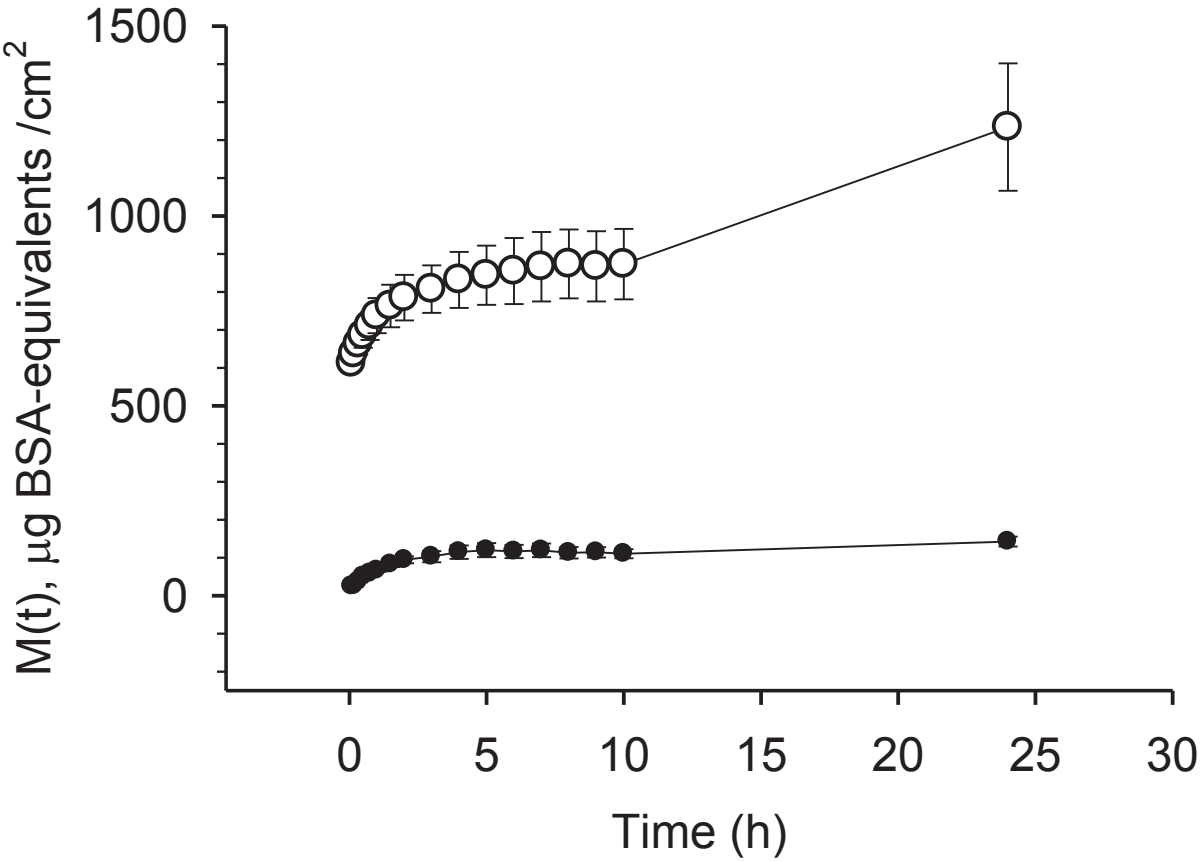

Figure 3.5 Results of protein assay studies in the presence (•) and absence (o) of a dialysis membrane (5000 Da cutoff) placed between the dermis and the donor solution. The donor solutions contained PBS and the receptor solutions contained PBS + 2% BSA. Data represent the mean ± SE of 10 determinations from one male donor.

In the absence of a dialysis membrane (5000 Da cutoff), protein concentrations in the donor solution 0.08 h (5 minutes) post-dose averaged 610 μg BSA-equivalents/cm^2. These values rose in a non linear pattern to approximately 870 μg BSA-equivalents/cm^2 at 10 h and 1230 μg BSA-equivalents/cm^2 at 24 h. The corresponding values for donor solution protein content in the presence of a dialysis membrane were 25, 110 and 140 μg BSA-equivalents/cm^2 at 0.08, 10 and 24 h. Thus, the total protein content in the donor

solution was reduced by the dialysis membrane by a factor ranging from 8 to 24. No significant differences were observed between studies employing 3500 Da and 5000 Da membranes (data not shown). Based on the stated cutoffs, it is likely the proteins in the donor solution for the cells containing a dialysis membrane were small peptides and protein fragments stemming from the dermis or the BSA solution. As described in the protein binding section, these fragments did not bind diclofenac to a significant extent.

3.5 DISCUSSION

Solute transport in dermis and the associated capillary and lymphatic clearance processes are key to the survival and health of skin tissue. Nutrients and oxygen delivered from the dermal capillaries diffuse into the dermis and overlying epidermis; waste products resulting from cellular metabolism are concurrently removed by the same capillaries. Larger cellular debris and serum proteins that have leaked into the tissue are removed by the skin lymphatics. These same mechanisms remove exogenous chemicals, beneficial or hazardous, that have permeated across the skin's outer defenses (i.e., the stratum corneum) following dermal exposure. Transient concentrations of these chemicals in the skin depend on the permeation and clearance rates and the partition coefficient of the chemical in the dermis tissue. In order to accurately predict these concentrations, the underlying transport and partition phenomena must be well understood.

This study addresses a question posed in a recent modeling study of transport and partitioning of solutes in dermis.(Kretsos, Miller et al. 2008) In that study the investigators noted that conventional in vitro permeation and partition measurements of solutes in dermis could be confounded by diffusion of soluble proteins from the tissue.

Strong binding of the solute to the diffusing protein would lead to inaccurate results. The present study confirms this to be the case for the highly protein bound drug, diclofenac (f_u = 0.04 in 2% BSA). Preventing the diffusion of large proteins, including albumin, into the donor solution in an in vitro permeation study involving human dermis resulted in a significantly higher permeability coefficient k_p (Table 3.2) and associated dermis permeability $P_{de} = D_{de}K_{de}$ (Table 3.3). The chief factor leading to this difference was the dermis/donor solution partition coefficient K_{de}. Blocking protein diffusion into the donor solution resulted in 2.7-fold higher tissue concentrations (Table 3.2) and a 6-fold higher calculated value of K_{de} for diclofenac (Table 3.3).

The same methodology applied to a moderately protein-bound solute, DEET (f_u = 0.19 in 2% BSA), did not reveal a significant difference between dermis transport or partition parameters determined in the presence and absence of a barrier membrane. The tests did, however, reveal significant differences between breast and abdominal skin samples with regard to DEET diffusivities and partition coefficients. Breast skin had lower values of D_{de} and higher values of K_{de}, but comparable permeability P_{de}, relative to abdominal skin. We suspect that these differences are related to the tissue thickness – abdominal samples were approximately twice as thick as breast samples. The 6-hour time frame of the DEET permeation experiments, which was adequate for the breast skin studies (Fig. 3.3), may not have been quite long enough to achieve a steady state in abdominal skin (Fig. 3.4a). Such an error would lead to parameter differences in the observed direction. However, alternative explanations involving variation in tissue structure with site or depth cannot be ruled out.

The 48-hour time frame of the diclofenac experiments was chosen to ensure achievement of a steady-state. It is evident from Fig. 3.4b that this goal was met. Accumulation of diclofenac in the receptor solution at 48 h exceeded the commonly accepted limit of 10% of the donor solution concentration; however, it may be seen from the figure that similar permeability coefficients and time lags would have been obtained had the experiment been terminated earlier. Any attempt to correct these data for non-sink conditions(Parry, Bunge et al. 1990) would only accentuate the difference between the dermis only and dermis + dialysis permeation profiles, as the latter would have the larger (positive) correction. We refrained from applying such a correction, since the uncorrected data already establish the case that the dialysis membrane is an essential component of the system. Were a correction to be made, the resulting time lags would be slightly longer, and the Eq. 3.13 diffusivities slightly lower, than those reported in Table 3.3. Permeabilities and Eq. 3.12 diffusivities would be slightly higher. Thus, agreement between diffusivities calculated from Eq. 3.12 and Eq. 3.13 would improve. In general, it is worth noting that, if the primary purpose of calculating a tissue diffusion coefficient is to estimate transport across the tissue, then the use of Eq. 3.12 (which directly invokes permeability) is a wiser choice than Eq. 3.13. The comparisons discussed below employ Eq. 3.12 diffusivities.

It is of interest to test the agreement of the data reported here with the model developed by Kretsos et al.(Kretsos, Miller et al. 2008), which represents the existing dermis permeability and partitioning database. For the case of delivery from a pH 7.4 donor solution into tissue at the same pH, Kretsos' formulas for diffusivity and partition coefficient can be summarized as follows:

$$K_{\mathrm{de/pH7.4}} = 0.6 \cdot \mathrm{BindingFactor} \tag{3.14}$$

$$D_{\mathrm{de}} = 10^{-4.15 - 0.655 \log \mathrm{MW}} / \mathrm{BindingFactor} \tag{3.15}$$

$$\mathrm{BindingFactor} = 0.68 + 0.32 / f_{\mathrm{u}} + 0.001 f_{\mathrm{non}} K_{\mathrm{oct}} \tag{3.16}$$

Here f_{non} is the fraction nonionized and K_{oct} is the octanol/water partition coefficient. Values for $K_{\mathrm{de/pH7.4}}$, D_{de} and P_{de} calculated from this model are shown in Table 3.4.

Table 3.4 Transport and partitioning parameters calculated from Eqs. 3.14-3.16.

Property	Units	DEET	Diclofenac
MW	Da	191.3	296.2
log K_{oct}	-	2.18[29]	4.51[29]
pK_{a}	-	-	4.0
f_{non} @ pH 7.4	-	1	3.98×10^{-4}
f_{u}	-	0.19	0.04
BindingFactor	-	2.52	8.69
$K_{\mathrm{de/pH7.4}}$	-	1.51	5.22
$D_{\mathrm{de}} \times 10^{6}$	cm^2/s	0.898	0.196
$P_{\mathrm{de}} \times 10^{6}$	cm^2/s	1.36	1.02

[a] $P_{\mathrm{de}} = K_{\mathrm{de/pH7.4}} D_{\mathrm{de}}$

For diclofenac a comparison with the Dialysis + dermis results in Table 3.3 shows that the model underestimates K_{de}, D_{de} and P_{de} by factors of 1.4, 2.9 and 3.9, respectively. For DEET comparison of these calculations with the averages of the values given for

breast skin in Table 3.3 shows that K_{de} is overestimated by a factor of 1.3, whereas D_{de} and P_{de} are underestimated by factors of 4.0 and 2.9, respectively. Agreement of the calculation with the abdominal skin parameters is comparable for P_{de} (2.6-fold underestimate) but less satisfactory for D_{de} and K_{de}. In any case, it is evident that Eqs. 3.14-3.16 underestimate dermis permeability P_{de} for both DEET and diclofenac by 3- to 4-fold when compared to the experiments reported here. It seems likely from the above analysis that a substantial portion of this error is incurred in the estimation of D_{de} according to Eq. 3.15. It should be noted that Eq. 3.15 is based on a diffusion model in which bound permeant is considered to be immobile.(Kretsos, Miller et al. 2008) Replacement of this approximation with a model in which both free and bound permeant diffuse through the tissue (cf. Eq. 3.8) may yield better agreement. Better characterization of the binding proteins and their mobility within the tissue is required in order to complete this task.

A recent study of the topical drugs pimecrolimus and tacrolimus highlights the complexity of protein binding in skin.(Weiss, Fresneau et al. 2008) These highly lipophilic macrolide anti-inflammatory drugs were found to bind extensively to skin and plasma proteins. Despite their lipophilic nature, the binding was largely to proteins (or, in blood, lipoproteins) other than albumin. In skin the strongest binding was to an unidentified ~16 kDa protein which may have been the 12 kDa tacrolimus binding protein Macrophilin-12. Although there are other compounds for which specific binding proteins in skin have been identified, e.g., retinoids and Vitamin A analogs, prediction of these highly specific interactions for the case of an arbitrary permeant is beyond our present capabilities. In the absence of detailed binding information, the use of 2%

albumin as a surrogate for the complex milieu of soluble proteins in skin seems a reasonable approach to studying transport in the lower skin layers.

3.6 CONCLUSION

Binding of lipophilic permeants to soluble proteins in the dermis plays an important role in determining their partition coefficient and effective diffusivity within the tissue. In the absence of a stratum corneum barrier, attention to diffusion of these proteins out of the tissue is necessary in order to obtain accurate values of these parameters from in vitro studies involving highly protein bound permeants. For permeation studies involving isolated dermis, this can be achieved by isolating the tissue from the donor solution with a dialysis membrane and supplementing the receptor solution with 2% BSA.

3.7 APPENDIX

3.7.1 Diffusion of a Reversibly Bound Permeant on a Mobile Substrate

Consider the case of a permeant diffusing in one dimension (x) across an aqueous membrane or layer containing a diffusing substrate, e.g., a macromolecule. The permeant is rapidly and reversibly bound to the substrate according to a linear isotherm; thus $C_{bound} = K\, C_{free}$, where K is the binding constant. The total permeant concentration C_{tot} is the sum of $C_{bound} + C_{free}$. The assumption of linearity restricts the present analysis to low permeant concentrations. The unbound fraction of permeant f_u is equal to $1/(1+K)$, and the partition coefficient of the medium relative to water is $1+K = 1 / f_u$. The flux of permeant at any point in the system, J, is equal to the sum of the free and bound fluxes. Assuming these fluxes to be governed by Fick's Law, one has

$$J = -D_{\text{free}} \frac{\partial C_{\text{free}}}{\partial x} - D_{\text{bound}} \frac{\partial C_{\text{bound}}}{\partial x} \tag{3A1-1}$$

Defining the effective diffusivity D_{eff} as the multiplier of the total concentration gradient that yields the observed flux, one has

$$\begin{aligned} D_{\text{eff}} \frac{\partial C_{\text{tot}}}{\partial x} &= D_{\text{free}} \frac{\partial C_{\text{free}}}{\partial x} + D_{\text{bound}} \frac{\partial C_{\text{bound}}}{\partial x} \\ &= (D_{\text{free}} + K D_{\text{bound}}) \frac{\partial C_{\text{free}}}{\partial x} \\ &= (D_{\text{free}} + K D_{\text{bound}}) \cdot f_{\text{u}} \frac{\partial C_{\text{tot}}}{\partial x} \end{aligned} \tag{3A1-2}$$

But $Kf_{\text{u}} = K/(1+K) = 1\text{-}f_{\text{u}}$, which is equivalent to the bound fraction f_{b}. Thus,

$$D_{\text{eff}} = f_{\text{u}} D_{\text{free}} + (1 - f_{\text{u}}) D_{\text{bound}} \tag{3A1-3}$$

which is the same as Eq. 3.8 in the text. The diffusive resistance of a layer of this medium is equal to its thickness divided by the product of effective diffusivity and partition coefficient relative to water. Identifying this resistance as R_2, the thickness as h_{ABL}, and recalling that the partition coefficient of the medium is $1 / f_{\text{u}}$ yields Eq. 3.7 in the text.

3.7.2: Calculation of K_{de} from Average Dermis Concentration

Assume the dermis is placed in series with a dialysis membrane in a side-by-side diffusion cell. Concentration C_{d} is maintained in the donor solution and sink conditions are maintained in the receptor solution. Unstirred aqueous boundary layers develop external to the composite membrane, as shown in Figure 3.6.

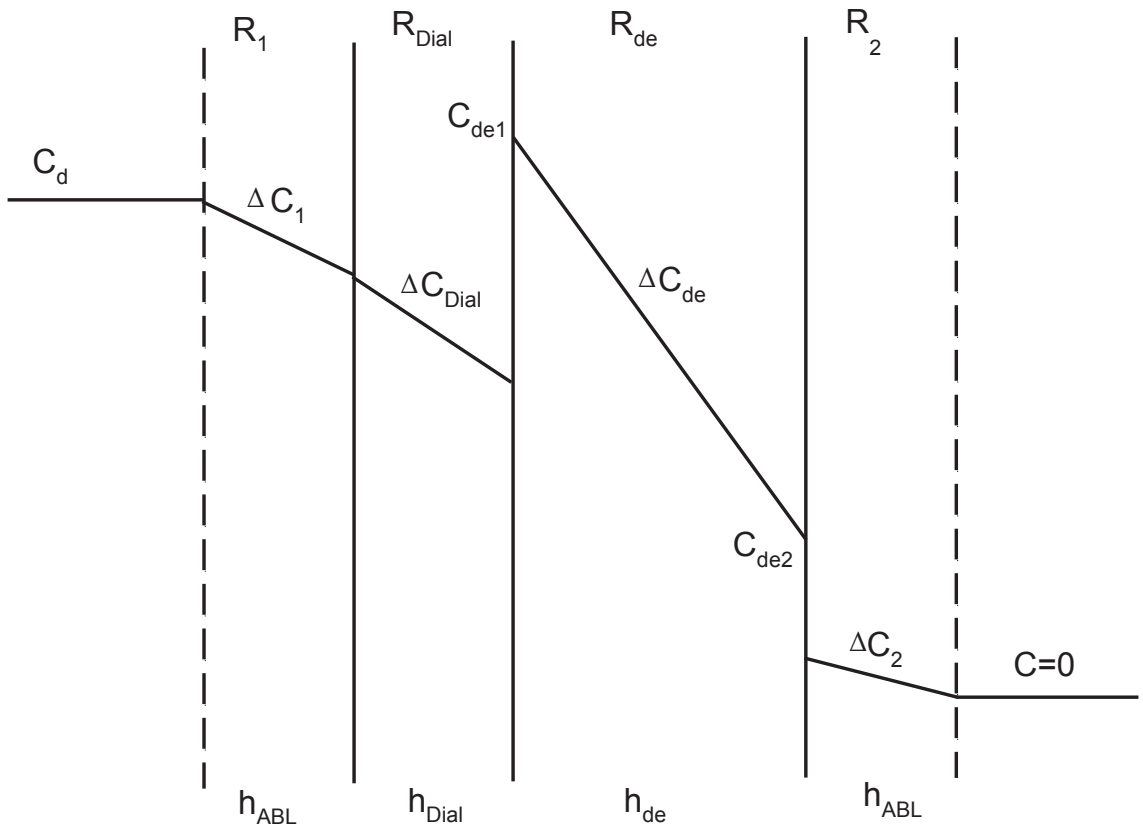

Figure 3.6. Steady-state concentration profiles for dermis + dialysis membrane system with aqueous boundary layers surrounding the composite membrane.

The steady-state the flux J_{ss} across this system is

$$J_{ss} = k_p(C_d - 0) = \frac{C_d}{R_{tot}} \tag{3A2-1}$$

where k_p is the permeability coefficient and $R_{tot} = R_{Dial} + R_{de} + R_1 + R_2$ is the total diffusive resistance. At steady-state, the flux across each layer is identical such that

$$\frac{C_d}{R_{tot}} = \frac{\Delta C_1}{R_1} = \frac{\Delta C_2}{R_2} = \frac{\Delta C_{Dial}}{R_{Dial}} = \frac{\Delta C_{de}}{R_{de}} \ . \tag{3A2-2}$$

Rearrangement of Eq. 3A2-2 yields

$$\Delta C_{\mathrm{de}} = \frac{R_{\mathrm{de}}}{R_{\mathrm{tot}}} C_{\mathrm{d}} = \frac{R_{\mathrm{de}} C_{\mathrm{d}}}{R_1 + R_{\mathrm{Dial}} + R_{\mathrm{de}} + R_2} \tag{3A2-3}$$

The sum of the concentration drops across each layer, normalized by partition coefficient, is equal to the donor concentration, i.e.,

$$C_{\mathrm{d}} = \Delta C_1 + \Delta C_{\mathrm{Dial}} + \Delta C_{\mathrm{de}} / K_{\mathrm{de}} + f_{\mathrm{u}} \Delta C_2 \tag{3A2-4}$$

Thus the average concentration in the dermis can be written as

$$\overline{C_{\mathrm{de}}} = \frac{C_{\mathrm{de1}} + C_{\mathrm{de2}}}{2} = \frac{K_{\mathrm{de}}\left(C_{\mathrm{d}} - \Delta C_1 - \Delta C_{\mathrm{Dial}}\right) + K_{\mathrm{de}} f_{\mathrm{u}} \Delta C_2}{2}$$

$$\begin{aligned} &= \frac{1}{2} K_{\mathrm{de}}\left(C_{\mathrm{d}} - \Delta C_1 - \Delta C_{\mathrm{Dial}} + f_{\mathrm{u}} \Delta C_2\right) \\ &= \frac{1}{2} K_{\mathrm{de}} C_{\mathrm{d}}\left(1 - \frac{R_1}{R_{\mathrm{tot}}} - \frac{R_{\mathrm{Dial}}}{R_{\mathrm{tot}}} + \frac{R_2}{R_{\mathrm{tot}}}\right) \\ &= \frac{1}{2} K_{\mathrm{de}} C_{\mathrm{d}}\left(\frac{R_{\mathrm{tot}} - R_1 - R_{\mathrm{Dial}} + R_2}{R_{\mathrm{tot}}}\right) \end{aligned} \tag{3A2-5}$$

Therefore the partition coefficient for the dermis relative to the donor solution is

$$K_{\mathrm{de}} = \frac{2\overline{C_{\mathrm{de}}}}{C_{\mathrm{d}}}\left(\frac{R_{\mathrm{tot}}}{R_{\mathrm{tot}} - R_1 - R_{\mathrm{Dial}} + R_2}\right) . \tag{3A2-6}$$

4. PARTITIONING AND DIFFUSION OF PARATHION IN HUMAN DERMIS

Ibrahim R, Kasting GB 2012. Partitioning and Diffusion of Parathion in Human Dermis. Int J Pharm: 435(1) 33-37 (Epub)

4.1 INTRODUCTION

The stratum corneum is the rate-limiting barrier to the permeation of polar and moderately lipophilic compounds, whereas, for highly lipophilic compounds this rate-limiting barrier may be dominated by the lower skin layers (Cleek and Bunge 1993). The binding of these often highly protein-bound solutes to extravascular albumin and other soluble proteins within the dermis is thought to contribute to their transport across this layer (Cross, Magnusson et al. 2003; Kretsos, Miller et al. 2008; Weiss, Fresneau et al. 2008). Soluble proteins present in the dermis can migrate slowly through the tissue. This potential movement necessitates a careful choice of the in vitro methodology employed in the measurement of dermis transport parameters of highly protein-bound solutes (Ibrahim and Kasting 2010). In particular, if soluble proteins migrate into the donor compartment of a side-by-side diffusion cell experiment, and the test permeant binds to these proteins, then an artificially low permeability would be obtained (Kretsos, Miller et al. 2008; Ibrahim and Kasting 2010). In a previous study we showed that exclusion of soluble proteins from the donor compartment of side-by-side diffusion cells had a significant effect on the measured transport parameters for a highly protein-bound solute, diclofenac. The study also showed that the diffusion of the soluble proteins into the donor compartment of the cells had no effect on the measured transport parameters for a moderately protein-bound compound, DEET. The objective of the present study is to

determine whether this phenomenon is important for parathion, which has a partition coefficient and protein binding affinity intermediate between DEET and diclofenac.

4.2 MATERIALS AND METHODS

4.2.1 Materials

Dialysis membrane (5000 Da cut-off) was purchased from Bel-Art Products (Pequannock, NJ). Unlabeled parathion (98.8%) was purchased from Sigma-Aldrich (Atlanta, GA). [Carbonyl-^{14}C]-parathion (0.8 mCi/mmol, radiochemical purity > 99%) was purchased from American Radiolabeled Chemicals (St. Louis, MO). Ultima Gold^{TM} XR scintillation cocktail and Solvable^{TM} were purchased from Perkin-Elmer (Boston, MA). Skin from abdominoplasty (3 donors) was obtained from Musculoskeletal Transplant Foundation (Edison, NJ). Phosphate-buffered saline (PBS), bovine serum albumin (BSA) and sodium azide were purchased from Sigma Chemicals.

4.2.2 Protein Binding

Binding of ^{14}C-parathion in a 2% w/v BSA solution in PBS was determined by equilibrium dialysis as previously described (Ibrahim and Kasting 2010). The 2% w/v level was chosen as it is the approximate average concentration of albumin in human dermis (Kretsos, Miller et al. 2008).

4.2.3 Dermis Transport Studies

Parathion transport studies in human dermis were conducted and analyzed as previously described (Ibrahim and Kasting 2010). Briefly, skin samples from abdominoplasties

were heat separated (Kligman and Christophers 1963) to isolate the dermis. The dermis was mounted in series with a dialysis membrane (donor side) in water-jacketed, side-by-side diffusion cells maintained at 37°C. The donor and receptor compartments were filled with PBS and 2% BSA-PBS solution respectively and allowed to equilibrate for 24 h. BSA was added to the receptor solution to maintain endogenous levels of albumin in the dermis (Kretsos, Miller et al. 2008) and to ensure sink conditions in the receptor solution for highly lipophilic solutes. Unlike the previously described studies (Ibrahim and Kasting 2010), both the donor and receptor compartments were then emptied and replenished with fresh solutions. The new donor solution contained 3.62 µg/mL and 0.1 µCi/mL of ^{14}C-parathion in PBS. This procedure was chosen due to inadequate mixing when ^{14}C-parathion was spiked directly into the donor compartment. Studies for Donor 1 were carried out for 6 h and Donor 2 and 3 studies were carried out for 32-48 h to ensure steady-state diffusion. The run time difference was due to the considerable difference in thickness of the samples. At the end of the experiment each dermis sample was dissolved in Solvable^{TM} (1mL) and analyzed by LSC. Additional studies were conducted using dermis samples mounted without dialysis membrane and the results were compared.

The cumulative amount of solute passing through unit area of membrane $M(t)$ was plotted versus time. The steady state flux J_{ss} was calculated as the slope of the linear portion of the graph, and the time lag T_L was calculated as the intercept of the regression line on the time axis. The permeability coefficient k_p and total diffusive resistance R_{tot} were calculated according to Eq. 4.1,

$$k_p = \frac{1}{R_{tot}} = \frac{J_{ss}}{\Delta C} \approx \frac{J_{ss}}{C_d} \tag{4.1}$$

where C_d is the donor solution concentration. The approximation $\Delta C \cong C_d$ was justified since the ratio of unbound permeant concentration in the receptor solution to that in the donor solution was always less than 7%.

The diffusive resistance of the dermis R_{de} to parathion was calculated according to Eq. 4.2,

$$R_{de} = R_{tot} - R_{Dial} - \left(R_1 + R_2\right) \tag{4.2}$$

where R_{Dial} is the resistance of the dialysis membrane and in the absence of the dialysis membrane was set equal to zero. R_1 and R_2 are the resistances of the aqueous boundary layers in the donor and receptor compartments, respectively,

$$R_1 = \frac{h_{ABL}}{D_{aq1}} \tag{4.3}$$

$$R_2 = f_u \frac{h_{ABL}}{D_{eff}} \tag{4.4}$$

In Eqs. 4.3 and 4.4 h_{ABL} is the thickness of the aqueous boundary layer (0.017 cm) (Ibrahim and Kasting 2010), D_{aq1} is the diffusivity of unbound parathion in water, f_u is the fraction unbound, and D_{eff} is the effective diffusivity of parathion in the receptor solution (Ibrahim and Kasting 2010),

$$D_{eff} = f_u D_{aq2} + (1 - f_u) D_{bound} \tag{4.5}$$

Here D_{bound} is the diffusivity of albumin in the boundary layer, taken to be equal to the diffusivity of BSA in water at 37°C, 9.29×10^{-7} $cm^2 s^{-1}$ (Fardet, Hoebler et al. 1998).

The value of D_{aqi} for parathion at 37°C was estimated according to the Wilke-Chang relationship (Poling, Prausnitz et al. 2001):

$$D_{aqi}\,(\mathrm{cm^2 s^{-1}}) = \frac{7.4\times10^{-8}(\phi M)^{1/2}T}{\eta_i V_A^{0.6}} \tag{4.6}$$

where ϕ = 2.26, M = 18.01 g·mol^{-1} and T = 310.15 K. The value of η_i was taken to be 0.6915 cP in the donor solution (Eq. 4.3, i = 1) and 0.7468 cP in the receptor solution (Eqs. 4.4 and 4.5, i = 2) based on viscosity estimates for albumin solutions discussed later. The values of ϕ and η_i represent slight improvements over those chosen by (Ibrahim and Kasting 2010), but they do not significantly change the earlier results. It is noteworthy that the value 2.26 for the association factor for water stems from work by (Hayduk and Laudie 1974) that is not incorporated in some modern references, e.g. (Poling, Prausnitz et al. 2001). The molar volume at the boiling point, V_A, was estimated using Schroeder's Method (Poling, Prausnitz et al. 2001) to be 279.5 cm^3/mol. Equation 4.6 then yielded D_{aqi} values of 7.23 × 10^{-6} cm^2/s and 6.69 × 10^{-6} cm^2/s for parathion in the donor and receptor solutions, respectively. The value R_{Dial} = 24700 s/cm for parathion was then estimated by interpolating between the values of R_{Dial} for DEET (21200 s/cm) and diclofenac (24900 s/cm) based on the assumption that $R_{Dial} \propto D_{aq1}{}^{-1}$ (Ibrahim and Kasting 2010). Here the donor solution value for D_{aq} was used since albumin is excluded from the membrane. In making this estimate we recalculated D_{aq1} for DEET (7.94 × 10^{-6} cm^2/s) and diclofenac (7.20 × 10^{-6} cm^2/s) using the updated values of ϕ and η_i. Insertion of these values into Eqs. 4.3-4.5 led to the result that R_1 = 2351 s/cm, R_2 = 1285 s/cm and D_{eff} = 1.77 × 10^{-6} cm^2/s.

The product of dermis diffusivity D_{de} and partition coefficient K_{de}, often termed permeability P_{de}, was calculated from R_{de} and the thickness h_{de} of each sample according to Eq. 4.7:

$$P_{de} = D_{de}K_{de} = \frac{h_{de}}{R_{de}} \tag{4.7}$$

The value of K_{de} was determined from the average concentration measured in the dermis tissue sample $\overline{C_{de}}$ after correction for series resistances; thus (Ibrahim and Kasting 2010)

$$K_{de} = \frac{2\overline{C_{de}}}{C_d}\left(\frac{R_{tot}}{R_{tot} - R_1 - R_{Dial} + R_2}\right) \tag{4.8}$$

The dermis diffusivity D_{de} was then calculated as

$$D_{de} = \frac{P_{de}}{K_{de}} \tag{4.9}$$

As a comparison, D_{de} was also estimated from the time lag T_L according Eq. 4.10**,** which assumes the time lag is dominated by the dermis.

$$D_{de} = \frac{h_{de}^2}{6T_L} \tag{4.10}$$

The validity of assuming symmetrical boundary layers in the donor and receptor solutions (Eqs. 4.3 and 4.4) and a time lag dominated by the dermis (Eq. 4.10) is discussed later.

4.3 STATISTICAL ANALYSIS

Results were calculated individually for each diffusion cell, and then averaged to obtain a mean and standard error. Transport and partitioning parameters were compared via two-way ANOVA using donor and presence or absence of a dialysis membrane as blocking variables. The pairwise comparison test used was Holm-Sidak; values of $p < 0.05$ were considered to be significant. For comparisons involving only two groups, a Student's *t*-test was employed. All tests were conducted using SigmaStat version 3.10 (SYSTAT, Chicago, IL).

4.4 RESULTS

Physical properties of parathion are shown in Table 4.1. The fraction unbound in 2% albumin solution was determined to be 0.134 ± 0.005 (n=5). The results for the dermis transport studies are shown in Table 4.2 and Figure 4.1. Data collected after 32 hours for Donors 2 and 3 (not shown) were found to depart from linearity and were therefore not included in the analysis. Transport and partitioning parameters calculated from the data in the presence and absence of dialysis membrane showed significant differences between the dermis diffusivity D_{de} ($p = 0.019$) and partition coefficient K_{de} ($p < 0.001$). A lower K_{de} and a higher D_{de} was observed in the absence of the dialysis membrane. Despite the lower K_{de} in the absence of the dialysis membrane, a higher permeation of parathion was observed (Figure 4.1). Diffusivities calculated from the time lag (Eq. 4.10) were generally higher than those calculated from the permeability data (Eq. 4.9).

Table 4.1 Physical properties of parathion

Property	Units	Value
MW	Da	291.26
V_A	cm^3/mol	279.5[a]
log K_{oct}	-	3.83[b]
S_w [c]	g/L	0.011[b]
f_u [d]	-	0.134 ± 0.005[e]

[a] Schroeder's Method (Poling, Prausnitz et al. 2001). A value of 20.5 cm^3/mol was used for phosphorus.
[b] (US_EPA, 2009)
[c] Water solubility at 20º C
[d] Fraction unbound in a 2% w/v BSA solution
[e] mean ± SE (n = 5)

Table 4.2 Transport and Partitioning Parameters and Data Associated With the Parathion Dermis Transport Studies (Mean ± SE).

Treatment	Donor (n)[a]	k_p x 10^5 (cm/s)	R_{tot} x 10^{-5} (s/cm)	$R_{de} \times 10^{-5}$ (s/cm)	$P_{de} \times 10^6$ (cm^2/s)	K_{de}	$D_{de} \times 10^6$ (cm^2/s) Eq. (4.9)	$D_{de} \times 10^6$ (cm^2/s) Eq. (4.10)	h (cm)	T_L (h)
Dialysis + Dermis	1 (12)	1.99 ± 0.10	0.52 ± 0.03	0.24 ± 0.03	7.55 ± 0.44	5.56 ± 0.27	1.17 ± 0.07	1.17 ± 0.08	0.17 ± 0.01	1.17 ± 0.11
	2 (7)	0.95 ± 0.08	1.11 ± 0.11	0.83 ± 0.11	3.68 ± 0.37	5.98 ± 0.64	0.66 ± 0.13	0.81 ± 0.07	0.28 ± 0.02	4.75 ± 0.49
	3 (7)	0.69 ± 0.08	1.62 ± 0.25	1.35 ± 0.25	2.63 ± 0.31	6.46 ± 0.71	0.45 ± 0.09	1.29 ± 0.18	0.31 ± 0.02	3.75 ± 0.41
Mean ± SE (All replicates)					5.18 ± 0.50	5.91 ± 0.28	0.83 ± 0.08	1.10 ± 0.07		
Dermis Only	1 (15)	4.26 ± 0.49	0.28 ± 0.03	0.24 ± 0.03	7.79 ± 0.70	2.88 ± 0.20	2.58 ± 0.42	4.21 ± 0.67	0.17 ± 0.01	0.42 ± 0.07
	2 (10)	1.17 ± 0.16	1.04 ± 0.18	1.00 ± 0.18	3.30 ± 0.39	5.26 ± 0.79	0.94 ± 0.30	2.19 ± 0.19	0.28 ± 0.01	1.73 ± 0.19
	3 (9)	1.07 ± 0.24	1.49 ± 0.34	1.45 ± 0.34	3.32 ± 0.60	3.14 ± 0.97	2.66 ± 0.94	3.52 ± 1.08	0.33 ± 0.02	2.08 ± 0.27
Mean ± SE (All replicates)					5.28 ± 0.53	3.65 ± 0.39 † ($p < 0.001$)	2.12 ± 0.34 † ($p \leq 0.05$)	3.43 ± 0.43 †		

[a]Donor (total no. of replicates).

†Statistical significance between treatments.

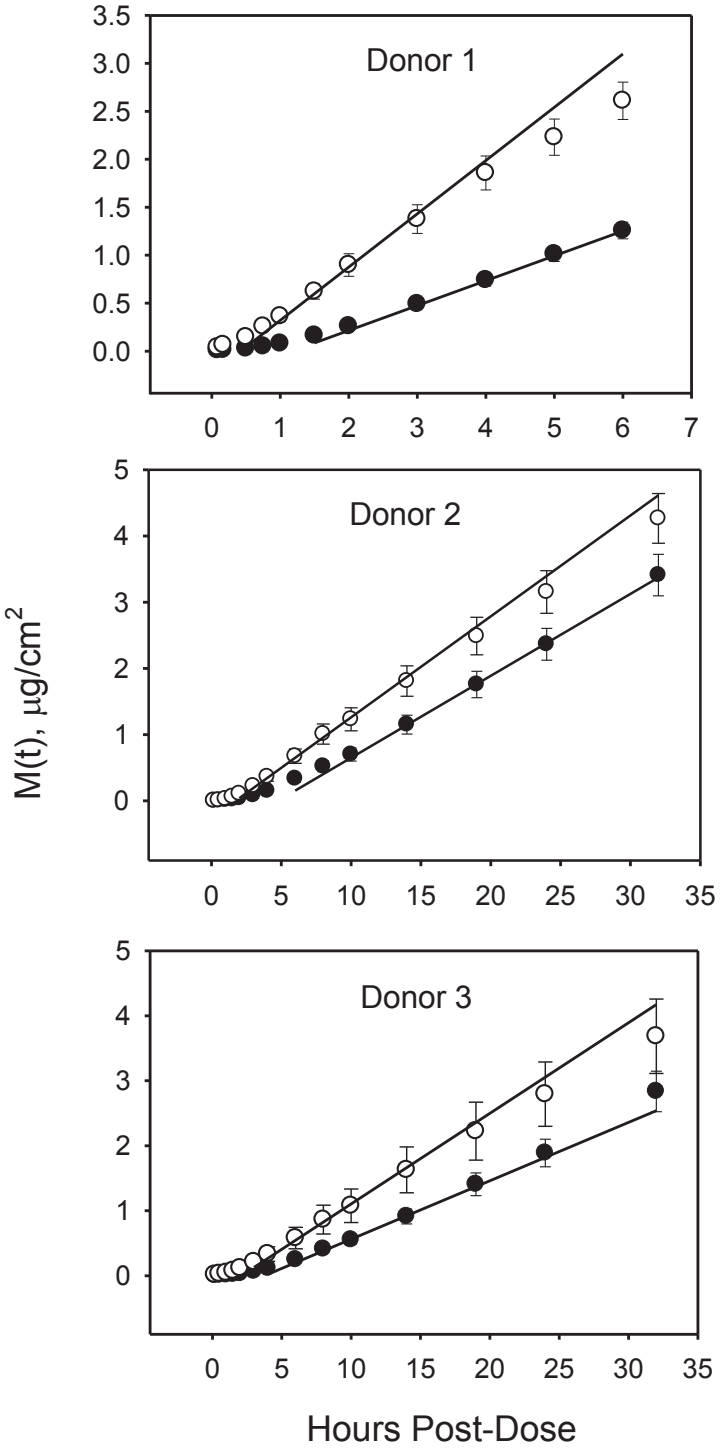

Figure 4.1 Results of skin dermis permeation studies for donors 1, 2 and 3 in the presence (●) and absence (○) of a dialysis membrane placed between the dermis and donor solution. The donor solutions contained ^{14}C-parathion dissolved in PBS and the receptor solutions contained PBS + 2% BSA. The solid lines were calculated as $M(t) = k_p C_d (t - T_L)$ using the average values of k_p and T_L in Table 2 and C_d = 3.62 μg/mL.

4.5 DISCUSSION

The analysis described by Eqs. 4.1–4.10 involves several assumptions that were briefly set forward in (Ibrahim and Kasting 2010) and are now discussed further. It is assumed that transport in the solutions bounding the membrane can be adequately described by film theory rather than the more elaborate boundary layer theory (Cussler 1997). This assumption has been found to be adequate for side-by-side diffusion cells of a similar design (Tojo, Masl et al. 1985). The widths of the aqueous boundary layers in the donor and receptor solutions, h_{ABL}, are assumed to be equal. This is reasonable since the cells are symmetrical and 2% BSA imparts little additional viscosity to the PBS solution. The effect may be estimated as follows: The intrinsic viscosity of BSA ($\lim_{c\to 0} \frac{\eta_{sp}}{c}$) is about 4 mL/g, where $\eta_{sp} = (\eta - \eta_0)/\eta_0$ is the fractional viscosity increase imparted by a concentration of c g/mL; furthermore the concentration dependence of BSA aqueous solution viscosity is linear for c up to 0.065 g/mL or 6.5% w/v (Friedli 1996). Thus addition of 2% w/v BSA to water increases its viscosity η by about 8%, i.e. $\eta_{sp} = 0.08$. Hence, the viscosity of a 2% w/v BSA solution at 37°C is about 0.75 cP, slightly higher than that of water (0.69 cP). Following the analysis of (Tojo, Masl et al. 1985), h_{ABL} scales as $\eta^{0.70}$; therefore an 8% increase in η would increase h_{ABL} by 5-6%. This change is well within the uncertainty of the analysis. Finally, Eq. 4.10 assumes the time lag (t_L) to be fully determined by diffusion in the dermis. Application of multilaminate time lag models (Ash, Barrer et al. 1965; Sinko 2011) to the data in Table 4.2 suggests this approximation cannot be justified. The dialysis membrane in particular is expected to contribute to the time lag since its diffusive resistance R_{Dial} is an appreciable fraction of

the dermis resistance and its effective partition coefficient K_{Dial} is very low. This effect may be estimated as follows: The thickness of this membrane was about 20 μm R_{Dial} was estimated above to be 24700 s/cm. Assuming an aqueous diffusivity within the pores of 7.23×10^{-6} cm^2/s yields an effective K_{Dial} value of 0.0112. Insertion of these values plus average values for the dermis (Table 4.2, Row 4) into the two-layer time lag formula given in Sinko (2011) leads to the prediction that the dialysis membrane should increase the time lag by 67% with respect to a dermis-only experiment. Examination of Table 4.2 shows that the actual impact of the dialysis membrane on the observed time lag is somewhat larger than this. However quantitative agreement between the time lags predicted from multilaminate slab models and those observed is poor. Hence, neither Eq. 4.10 nor multilaminate variations thereof can be recommended and diffusivity of the permeant in the dermis should be calculated from Eq. 4.9.

Kretsos et al. (2008) noted that the conventional in vitro permeation and partition measurements of solutes in the dermis could be confounded by diffusion of soluble proteins from the tissue. This hypothesis was confirmed in a previous study from this laboratory employing DEET and diclofenac (Ibrahim and Kasting 2010). Whereas results for DEET (f_u = 0.189 ± 0.004) were not affected by the insertion of a barrier membrane between the donor solution and dermis, results for diclofenac (f_u = 0.040 ± 0.005) were sensitive to this change. In the case of diclofenac, contrary to what one would expect, a higher permeation was observed in the absence of the dialysis membrane. This was attributed to the presence of soluble proteins in the donor compartment (Ibrahim and Kasting 2010). The objective of this study was to test the new methodology with parathion, a compound whose protein-binding affinity as expressed in

terms of fraction unbound (f_u = 0.134 ± 0.005) lies between DEET and diclofenac. . We had to modify the "control" methodology due to the low water solubility of parathion, which led to inadequate mixing when the donor solution was spiked with labeled solute immediately prior to the study as in the previous experiments. In the present study, following the equilibration period, the PBS solution was removed and replenished with a donor solution of radiolabeled parathion which had been agitated overnight. Thus, a substantial amount of the diffused soluble protein was removed. Yet, the results were still impacted by the presence or absence of dialysis membrane. Significant differences in D_{de} and K_{de} were obtained, although smaller than those observed for diclofenac. We conclude that compounds that are more than about 87% bound to soluble proteins in the dermis should be tested using the new methodology.

It is of interest to compare the results of these experiments with the predictions based on current models of dermis permeability. A limited comparison, using data and models generated by our research group, is shown in Table 4.3.

Table 4.3 Transport and Partitioning Parameters in Human Dermis for Selected Permeants (Mean ± SE)

Compound	$D_{de} \times 10^6$ (cm^2/s)	$K_{de/pH7.4}$	$P_{de} \times 10^6$ (cm^2/s)
DEET			
Observed[a,b]	4.59 ± 1.41	0.83 ± 0.35	3.33 ± 0.86
Kretsos et al. 2008	0.90	1.51	1.36
Dancik et al. 2012	0.96	1.51	1.44
Eqs. 4.11-4.14	1.41	1.51	2.13
Diclofenac			
Observed[a,b]	0.57 ± 0.06	7.56 ± 0.67	3.95 ± 0.31
Kretsos et al. 2008	0.196	5.22	1.02
Dancik et al. 2012	0.284	5.22	1.48
Eqs. 4.11-4.14	1.02	5.22	5.34

Parathion			
Observed[b,c]	0.83 ± 0.08	5.91 ± 0.28	5.18 ± 0.50
Kretsos et al. 2008	0.175	5.90	1.03
Dancik et al. 2012	0.196	5.90	1.16
Eqs. 4.11-4.14	0.372	5.90	2.20
Glucose			
Observed[d]	2.64 ± 0.42	0.65 ± 0.09	1.36 ± 0.22
Kretsos et al. 2008	2.36	0.61	1.41
Dancik et al. 2012	2.36	0.61	1.41
Eqs. 4.11-4.14	2.36	0.61	1.41

[a] (Ibrahim and Kasting 2010)
[b] Average of all dermis + dialysis measurements
[c] Table 4.2
[d] (Khalil, Kretsos et al. 2006)

The relationships employed in these calculations may be found in (Kretsos, Miller et al. 2008) or (Dancik, Miller et al. 2012) and the permeant physical properties may be found in the original references or in Table 4.1 (for parathion). The (Kretsos, Miller et al. 2008) model assumes permeant bound to albumin to be immobile. (Dancik, Miller et al. 2012) impute some mobility to bound permeant, assigning it a diffusivity $D_{\text{bound}}^{\text{tissue}}$ of 1×10^{-7} cm^2s^{-1} in the albumin-accessible region of the dermis only. The (Kretsos, Miller et al. 2008) calculation works effectively to predict K_{de}; consequently it has not been changed. It also gave a satisfactory prediction for D_{de} for glucose (which does not bind to proteins), but both (Kretsos, Miller et al. 2008) and (Dancik, Miller et al. 2012) substantially underestimate D_{de} for the other three permeants. Since $P_{\text{de}} = D_{\text{de}} K_{\text{de}}$, dermis permeability is also underestimated. In order to correct this we propose the following modification to the calculation scheme presented in (Dancik, Miller et al. 2012):

$$\text{BF} = 0.68 + 0.32 / f_{\text{u}} + 0.001 f_{\text{non}} K_{\text{oct}} \tag{4.11}$$

$$K_{\mathrm{de/pH7.4}} = 0.6 \times \mathrm{BF} \tag{4.12}$$

$$\log D_{\mathrm{free}} = -4.15 - 0.655 \log \mathrm{MW} \tag{4.13}$$

$$D_{\mathrm{de}} = \left[f_{\mathrm{u}} D_{\mathrm{free}} + (1 - f_{\mathrm{u}}) D_{\mathrm{bound}}^{\mathrm{tissue}} \right] / \left(f_{\mathrm{u}} \mathrm{BF} \right) \quad ; \quad D_{\mathrm{bound}}^{\mathrm{tissue}} = 3 \times 10^{-7}\ \mathrm{cm^2 s^{-1}} \tag{4.14}$$

In Eqs. 4.11-4.14, BF is a binding factor associated with permeant binding to mobile proteins as well as partitioning into immobile lipids, f_{u} is the unbound fraction, f_{non} is the fraction nonionized, K_{oct} is octanol/water partition coefficient and MW is molecular weight. K_{de} has been expressed relative to a pH 7.4 buffer to coincide with the experiments described herein. In order to calculate its value with respect to the nonionized concentration in water, the result from Eq. 4.12 should be divided by f_{non} (Kretsos, Miller et al. 2008). The value of $D_{\mathrm{bound}}^{\mathrm{tissue}}$ has been increased three-fold with respect to (Dancik, Miller et al. 2012), and it applies broadly across the tissue. The net change is a ten-fold larger contribution of bound permeant to D_{de}. In addition to providing a better match to the data in Table 4.12, a rationale for this change may be drawn from the work of Jain and coworkers (Nugent and Jain 1984; Chary and Jain 1989). Using two different optical methods, FITC-labeled albumin and an in vivo rabbit ear "sac" model, these workers measured albumin diffusivities in tissue ranging from 0.11×10^{-7} $\mathrm{cm^2 s^{-1}}$ to 5.8×10^{-7} $\mathrm{cm^2 s^{-1}}$. The former value was obtained with a relaxation method (Nugent and Jain 1984), the latter with Fluorescence Recovery After Photobleaching (Chary and Jain 1989). The investigators argued that the relaxation method measures diffusion in the gel phase of the dermis, whereas FRAP is sensitive to diffusion in the fluid phase. Notably FRAP diffusivity of FITC-albumin fell to 1.7×10^{-7}

cm^2s^{-1} in sacrificed rabbits. The investigators proposed that the fluid channels collapsed in the dead animals, leading to lower diffusivities. Considering these results it seems reasonable to propose the value $D_{\text{bound}}^{\text{tissue}} = 3 \times 10^{-7}$ cm^2s^{-1} in Eq. 4.14 for permeants in excised human dermis that primarily bind to albumin. It is furthermore possible that a larger value could apply to human dermis in vivo due to the presence of smaller binding proteins and (potentially) more open fluid channels.

The use of these values is as follows: Eqs. 4.11-4.14 summarize the results of a microscopic model for dermis partitioning and transport (Kretsos, Miller et al. 2008) that leads to a macroscopic value of the partition coefficient K_{de} and an effective diffusivity D_{de} that, when multiplied together, yield an estimate for dermis permeability P_{de} that may be used in a homogenized transport model in which each skin layer is represented as a uniform slab (Dancik, Miller et al. 2012). For ionizable solutes care must be taken to choose an appropriate reference state for K_{de} as described above.

5. DERMAL CLEARANCE MODEL FOR EPIDERMAL BIOAVAILABILITY CALCULATIONS

Ibrahim R, Nitsche JM, Kasting GB 2012. Dermal Clearance Model for Epidermal Bioavailability Calculations. J Pharm Sci. **101**: 2094-2108

5.1 INTRODUCTION

Knowledge of the rate and extent of permeation of topical applications on skin is of great importance in dermatology, transdermal drug delivery, cosmetic science and occupational safety. A quantitative description requires the understanding of not only the input rate of the permeant into the skin but also its output rate. A one-dimensional multilayer model allowing transient skin absorption calculations on a spreadsheet has been developed and described elsewhere.(Kasting, Miller et al. 2008; Dancik, Miller et al. 2012) A Java version of this program is available on the web.(Fedorowicz, Millller et al. 2011) This three-layer model represents the stratum corneum, viable epidermis and dermis as slabs with effective properties derived from underlying microscopic transport models. Capillary permeability was described by a simple relationship based on the Potts-Guy relationship to represent membrane permeability as in the Robinson model.(Wilschut, ten Berge et al. 1995) This relationship was adequate for small, moderately lipophilic permeants.(Kretsos, Miller et al. 2008) Here we present a clearance model more closely related to the capillary permeability literature and furthermore include lymphatic capillaries for the transport of large and highly protein-bound permeants. The primary purpose of the revised calculation is to make better predictions of skin concentrations of very hydrophilic and very lipophilic, low molecular weight skin permeants in the context

of the spreadsheet skin absorption model.(Kasting, Miller et al. 2008; Dancik, Miller et al. 2012) Since small lipophilic compounds are often highly bound to proteins it was important to include dermal clearance mechanisms for both small and large solutes into the model.

Capillary clearance has been widely studied for decades, yet the mechanisms involved in the transport of large solutes are still not fully understood. Several theories have been proposed, many tracing back to Renkin and coworkers.(Pappenheimer, Renkin et al. 1951; Renkin 1964; Renkin 1977; Renkin, Watson et al. 1977) The simplest of these is the pore/slit model.(Deen 1987; Curry 2005; Sugihara-Seki and Fu 2005) More elaborate theories are available, such as the fiber matrix theory,(Curry and Michel 1980; Sugihara-Seki and Fu 2005; Khakpour and Vafai 2008) the two-pore theory,(Rippe and Haraldsson 1994; Levick and Michel 2010) the three-pore theory(Rippe 1993; Rippe and Venturoli 2007) as well as complex 1D and 3D theories.(Weinbaum, Tsay et al. 1992; Zhang, Adamson et al. 2006) These models differ in complexity with regards to the physiologic microstructure of the blood capillaries. The most established routes of transport of solutes across blood capillaries are between the endothelial cells and through the endothelial membrane. Controversy surrounds other routes such as vesicles and large pores.(Rippe, Rosengren et al. 2002; Rosengren, Rippe et al. 2006; Sarin 2010) Furthermore, although it is widely accepted that the glycocalyx layer is the primary sieving element for large solutes and proteins, some investigators do not believe that there is enough evidence to support this claim.(Rippe 2008) These models, and all the open questions associated with them, pertain only to the clearance via blood capillaries, and do not address the competing mechanism of lymphatic clearance. Fewer studies have

been dedicated to lymphatic clearance, and to our knowledge no quantitative models have been developed. Published studies focus on determining the lymph flow rate by either cannulation of lymph ducts (Bill 1979; Bocci, Muscettola et al. 1986; Harake and Power 1986; Havas, Parviainen et al. 1997; Leu, MJW. et al. 2001) or by measuring the disappearance rate of large solutes from a specific site.(Hollander, Reilly et al. 1961; Ellis, Marks et al. 1970; Fernandez, Davies et al. 1983; Staberg, Klemp et al. 1983) Dermal capillary clearance was modeled by Kretsos et al.(Kretsos, Miller et al. 2008) as a uniform first order clearance through the blood capillaries into the systemic circulation. This simplified approach was adequate for the clearance of small permeants as well as moderately bound permeants. Here, we present a more general dermal clearance model based on a two-slit theory for blood capillary permeability which, when combined with a slow lymphatic clearance, is sufficiently flexible to describe the clearance of all diffusing species including macromolecules and protein-bound solutes. It should be noted that heterogeneous pore theory, slit theory and fiber matrix theory are equally efficient in describing the major features of capillary transport for small and large solutes and that there are no fundamental differences between these three concepts;(Rippe 2008) hence the selection of the two-slit theory for the present model is not essential, but rather is one of several nearly equivalent choices that could be made.

5.2 COMPUTATIONAL MODEL FRAMEWORK

5.2.1 Blood Capillary Clearance

Mass transport through capillary endothelia is often described by the Kedem-Katchalsky equations according to the principles of irreversible thermodynamics.(Kedem and

Katchalsky 1958; Curry 1983) Here these equations have been modified to include the effective exchange surface area *S*,(Rippe and Haraldsson 1994; Michel and Curry 1999) thus

$$J_s = P_{cap} S \cdot \Delta C + (1 - \sigma_f) J_v \overline{C} \tag{5.1}$$

$$J_v = L_p S(\Delta P - \sigma_d \Delta \pi) \tag{5.2}$$

where J_s is the solute flux per unit volume of tissue, J_v is the water flux per unit volume of tissue, P_{cap} is the total diffusive permeability to solutes, ΔC is the concentration difference across the membrane, σ_f is the solvent drag reflection coefficient (also known as the ultrafiltration coefficient) for the solute due to membrane restriction, $\overline{C}$ is the effective intramembrane solute concentration for convection, L_p is the hydraulic conductivity, ΔP is the difference between local capillary blood pressure and interstitial hydrostatic pressure, σ_d is the osmotic reflection coefficient which describes the selectivity of the membrane to solutes contributing to osmotic pressure and $\Delta\pi$ is the difference between colloid osmotic pressure in plasma and the interstitium. For ideal solutions containing a single solute σ_f is equal to σ_d and is represented by σ, the reflection coefficient.(Curry 1983; Michel and Curry 1999) For more complex solutions it is understood that the contributions of each solute must be summed to calculate the osmotic pressure; thus $\sigma_d \Delta\pi \rightarrow \sum_i \sigma_{d_i} \Delta\pi_i$. This formulation implicitly assumes that ΔC represents freely diffusing solute, equivalent to C_{free} in Ref (Kretsos, Miller et al. 2008). This distinction will become important later.

The permeability of the capillary wall is described in terms of flow through a water-filled cylindrical pore or rectangular slit, essentially the cleft between two adjacent endothelial cells. The representation of the interendothelial cleft as a slit is morphologically more defensible than a cylinder; hence the slit theory was chosen as our working model.(Rippe and Haraldsson 1994) The transport of macromolecules is a complex process that is riddled with controversy. We chose to use the framework of the two-pore theory presented by Rippe and Haraldsson,(Rippe and Haraldsson 1994) wherein small pores dominate the transport of smaller solutes and larger pores allow the transport of macromolecules. It should be noted that the purpose of the present model is to describe the clearance of a solute from the interstitial space into the blood and lymph, which are regarded as sinks. Hence, we focus on unidirectional transport, although consequences for the more general case in which bidirectional transport occurs are discussed. Because it is limited to the steady state the model in its present form will not be useful for studying swelling, inflammation or other pathophysiological conditions.(Rippe and Haraldsson 1994)

Following Rippe and Haraldsson,(Rippe and Haraldsson 1994) we assume there are two populations of slits; one has half-width $W_s/2$ (small), the other $W_L/2$ (large). The following equations apply to each population of slits.

The hydraulic conductivity L_p for a slit of width W in a capillary wall can be calculated from Poiseuille's Law (Michel and Curry 1999; Sugihara-Seki and Fu 2005)

$$L_p = \frac{LfW^3}{12\mu\Delta x} \tag{5.3}$$

where L is the total slit length per unit area of vessel wall, f is the fraction of the length of the slit open to the full width W, μ is the water viscosity at 37 °C, and Δx is the depth of the cleft from lumen to tissue.

The solute permeability within such a slit is (Michel and Curry 1999; Sugihara-Seki and Fu 2005)

$$P_{\text{slit}} = fWL \times D_{\text{slit}} \times \frac{\Phi}{\Delta x} \tag{5.4}$$

where D_{slit} is the solute diffusion coefficient within the slit, and Φ is the solute partition coefficient. In Eqs. (5.3-5.4) the product of fWL is defined as the slit area per unit membrane area and can be denoted as A_o and the slit area per unit cleft depth as $A_o/\Delta x$.(Fernandez, Davies et al. 1983; Sugihara-Seki and Fu 2005) The diffusion coefficient contains a hindrance factor $H(\lambda)$ that depends on the ratio λ of solute radius r_s to slit half-width $W/2$. We choose a form that has been recommended for calculations involving a wide range of solute sizes, thus(Dechadilok and Deen 2006)

$$H(\lambda) = 1 + \frac{9}{16}\lambda \ln\lambda - 1.19358\lambda + 0.4285\lambda^3 - 0.3192\lambda^4 + 0.08428\lambda^5 \tag{5.5}$$

$$D_{\text{slit}} = D_{\text{aq}} \bullet H(\lambda) \tag{5.6}$$

$$\lambda = \frac{r_s}{(W/2)} \tag{5.7}$$

The solute radius r_s is generally chosen to be the hydrodynamic radius, i.e. one associated with an appropriate diffusion equation.(Renkin 1977) Given that

$$r_s = \left(\frac{3V_A}{4N_A \pi} \right)^{1/3} \tag{5.8}$$

for a spherical solute of molar volume V_A, we can relate r_s and λ to an appropriately chosen molar volume. Here division by Avogadro's number (N_A) converts from molar to molecular properties. Because the values of r_s and V_A are essential to the theory and furthermore are not readily available for most solutes, their estimation will be carefully described later.

The solute partition coefficient for a slit is (Deen 1987)

$$\Phi = (1 - \lambda) \tag{5.9}$$

and the reflection coefficient σ may reasonably be chosen as (Anderson 1981)

$$\sigma = 1 - \frac{3}{2}\Phi + \frac{1}{2}\Phi^3 \tag{5.10}$$

The aqueous diffusivity of a solute can be calculated as follows:

$$D_{aq} = \frac{7.4 \times 10^{-10} T (\mathrm{MW}_{water} \cdot \theta_{water})^{1/2}}{\mu V_A^{0.6}} \qquad r_s \leq 0.56 \text{ nm} \tag{5.11a}$$

$$= \frac{kT}{6\pi\mu r_s} \qquad r_s > 0.56 \text{ nm} \tag{5.11b}$$

In Eq. (5.11a) T is the temperature in K; θ_{water} is the solvent association parameter for water; μ is the viscosity of water in poise, V_A is calculated at the normal boiling point,(Poling, Prausnitz et al. 2001) and k is Boltzmann's constant (1.38×10^{-16}

dyne·cm·K^{-1}). Equation (5.11a), the Wilke-Chang relationship,(Cussler 1997; Poling, Prausnitz et al. 2001) is used to calculate D_{aq} for solutes with a radius r_s smaller than about 0.56 nm. For solutes with a larger r_s, the Stokes-Einstein relationship (Eq. 5.11b) is used, which works better than Eq. (5.11a) for macromolecules diffusing in a dilute solution.(Cussler 1997; Poling, Prausnitz et al. 2001) The transition is made at 0.56 nm because the two calculations give very nearly the same result at this value of r_s (which corresponds to V_A = 443 cm^3/mol).

The integration of Eq. (5.1) between the boundary conditions C_p (unbound concentration in the plasma) and C_{free} (unbound concentration in the dermis) yields (Rippe and Haraldsson 1994)

$$J_s = P_{cap} S \cdot \Delta C + \sum_i J_{v_i} (1 - \sigma_i) \frac{C_p - C_{free} e^{-Pe_i}}{1 - e^{-Pe_i}} \tag{5.12}$$

where i represents the population of slit (s=small, L=large), and Pe a modified Peclet number. The equations presented by Rippe and Haraldsson (Rippe and Haraldsson 1994) describe solute/tracer flux from blood to tissue, hence C_{free} = 0 and the solute flux described in terms of clearance can be written as

$$(PS)_{eff} = \frac{J_s}{C_p} = \left[P_{cap} S + \sum J_{v_i} (1 - \sigma_i) \frac{1}{1 - e^{-Pe_i}} \right] \tag{5.13}$$

Our model was developed to describe solute/tracer flux from tissue to blood; in this case C_{free} is finite and C_p =0 and Eq. (5.12) can be expressed as

$$(PS)_{\text{eff}} = \frac{J_s}{C_{\text{free}}} = \left[P_{\text{cap}} S + \sum J_{v_i} (1 - \sigma_i) \frac{-e^{-\text{Pe}_i}}{1 - e^{-\text{Pe}_i}} \right] \tag{5.14}$$

Following Rippe and Haraldsson,(Rippe and Haraldsson 1994) Pe is calculated as

$$\text{Pe}_i = \frac{J_{v_i} (1 - \sigma_i)}{P_{\text{slit}_i} S}. \tag{5.15}$$

The right-most term within the brackets in Eq. (5.14) has the limit $\sum J_{v_i} (1 - \sigma_i)$ for large Peclet numbers and $\sum P_{\text{slit}_i} S$ as Pe $\rightarrow$ 0.(Rippe and Haraldsson 1994) Thus this contribution to $(PS)_{\text{eff}}$ is dominated by the diffusive portion, $P_{\text{slit}}S$, for low values of Pe and by the convective portion, $J_v(1-\sigma)$, for high values of Pe.

J_v^{tot} is the total fluid volume flux per unit area of tissue across both slits; thus (Rippe and Haraldsson 1994)

$$J_v^{\text{tot}} = J_{vs} + J_{vL} \tag{5.16}$$

The components of Eq. (5.16) are represented by (Rippe and Haraldsson 1994)

$$J_{vs} = \alpha_s L_p^{\text{tot}} S (\Delta P - \sigma_s \Delta \pi) \tag{5.17}$$

$$J_{vL} = \alpha_L L_p^{\text{tot}} S (\Delta P - \sigma_L \Delta \pi) \tag{5.18}$$

or, alternatively, by (Rippe and Haraldsson 1994)

$$J_{vs} = -\alpha_L (1 - \alpha_L) L_p^{\text{tot}} S (\sigma_s - \sigma_L) \Delta \pi + \alpha_s J_v^{\text{tot}} \tag{5.19}$$

$$J_{vL} = \alpha_L (1-\alpha_L) L_p^{tot} S(\sigma_s - \sigma_L)\Delta\pi + \alpha_L J_v^{tot} \tag{5.20}$$

Here α_L is the fraction of hydraulic conductivity attributed to the large slit and $\alpha_s = 1 - \alpha_L$ that of the small slit. Their ratio is given by (Rippe and Haraldsson 1994)

$$\frac{\alpha_L}{\alpha_s} = \frac{n_L}{n_s}\left(\frac{W_L}{W_s}\right)^3 = \frac{A_L}{A_s}\left(\frac{W_L}{W_s}\right)^2 \tag{5.21}$$

where n_s is the number of small slits, n_L is the number of large slits, A_s is the small pore area and A_L the large pore area. Note that Eq. (5.21) differs from the corresponding formula in Ref. (Rippe and Haraldsson 1994) because the hydraulic conductivity of slits is proportional to W^3 (cf. Eq. (5.3)) whereas that of cylindrical pores varies as r^4. The slit length per unit area of vessel wall for each slit population is calculated as

$$L_s = L \cdot n_s ; L_L = L \cdot n_L \tag{5.22}$$

The osmotic pressure difference $\Delta\pi$ develops largely through the size-selective leakage of serum proteins from the blood capillaries into the tissue. In our formulation of the problem we simplify this picture by assuming representative values of ΔP and $\Delta\pi$ taken from the literature, then calculating J_{vs} and J_{vL} based on the properties of albumin. Thus σ_s and σ_L are reflection coefficients related to albumin. The hydraulic conductivity L_p^{tot} is chosen so that the total water flux into the tissue, J_v^{tot}, is equal to the lymph flow (discussed later). The albumin balance between blood and tissue, C_p/C_i, can then be determined by simultaneously solving Eq. (5.12) and Eqs. (5.16-5.18) for a solute having the properties of albumin.

At this point we return to Eqs. (5.12-5.14) and consider also the permeability of the endothelial cell membrane lining the blood capillaries, P_{cap}. This term must be included in order to properly calculate the clearance of membrane-permeable solutes. P_{cap} consists of a membrane permeability P_{mem} in series with an aqueous boundary layer having permeability P_{aq}; thus (Xiang and Anderson 1994)

$$\frac{1}{P_{cap}} = \frac{1}{P_{mem}} + \frac{1}{P_{aq}} \tag{5.23}$$

Permeability across the endothelial wall P_{mem} is described in terms of a regression model based on phospholipid bilayer membrane data assembled from the literature (JMN, unpublished data). This is the primary route for the diffusion of highly diffusible lipid-soluble solutes.(Michel and Curry 1999) An analysis of these data to be discussed separately yielded

$$\log P_{mem} = 1.64 \log K_{oct} - 1.37\,\mathrm{MW}^{1/3} + 2.82 \tag{5.24}$$

$n = 37$; $s = 0.71$; $r^2 = 0.8951$

Equation (5.24) was developed primarily from data on the permeability of egg lecithin and DOPC bilayers, as well as DMPC bilayers, to low molecular weight solutes under the constraint that solute lipophilicity be characterized by K_{oct}. It factors in a correction to 37°C, an assumed cholesterol mole fraction of 0.30 and the fact that the solute must pass through two such membranes to traverse the capillary endothelial cell. A more precise analysis of the phospholipid data is possible using 1,9-decadiene/water partition coefficient to describe lipophilicity (Xiang and Anderson 1994) and accounting explicitly

for the free surface area of the phospholipid bilayer.(Xiang and Anderson 1995; Xiang and Anderson 1997) However as neither approximation has been compared directly with endothelial cell membrane permeability and $K_{\text{decadiene/water}}$ values are not readily available we choose Eq. (5.24) to represent P_{mem}. Because of additional limits imposed by aqueous boundary layers, slit permeability, and blood and lymph flow (discussed below), total dermal clearance is not highly sensitive to P_{mem} so long as its value is chosen reasonably.

In Eq. (5.23) P_{aq} is the permeability coefficient across the aqueous boundary layer adjacent to the membrane. Inclusion of the P_{aq} term limits the permeability of small highly lipophilic solutes, which are otherwise overestimated.(Xiang and Anderson 1994)

$$P_{\text{aq}} = \frac{D_{\text{aq}}}{h_{\text{aq}}} \tag{5.25}$$

where h_{aq} is the thickness of the boundary layer and for small solutes is estimated to be about 1×10^{-8} cm.

To connect Eq. (5.14) with the clearance model described in Ref. (Kretsos, Miller et al. 2008), we now consider the limitation of blood flow, Q^{blood}, on clearance; thus, the microscopic blood capillary clearance constant of unbound solute $k_{\text{free}}^{\text{blood}}$ is given by (Kretsos, Miller et al. 2008)

$$k_{\text{free}}^{\text{blood}} = \left(\frac{1}{(PS)_{\text{eff}}} + \frac{1}{Q^{\text{blood}}} \right)^{-1} \tag{5.26}$$

The corresponding microscopic clearance constant for bound solute $k_{\text{bound}}^{\text{blood}}$ follows directly from Eq. (5.26). For a low molecular weight solute one simply replaces $(PS)_{\text{eff}}$

with the appropriate value for the binding protein. Thus, for a small solute bound to albumin one has

$$k_{\text{bound}}^{\text{blood}} = \left(\frac{1}{(PS)_{\text{eff}}^{\text{albumin}}} + \frac{1}{Q^{\text{blood}}} \right)^{-1} \tag{5.27}$$

For a large solute bound to a protein one must recalculate the properties of the complex, but this limit is not of much interest. If Q^{blood} is given in (cm^3 of blood)/[(cm^3 of tissue)·s], then the units of $k_{\text{free}}^{\text{blood}}$ and $k_{\text{bound}}^{\text{blood}}$ are s^{-1}. Other clearance constants discussed below share these units.

5.2.2 Lymphatic Capillary Clearance

The blood capillaries are poorly permeable to large hydrophilic macromolecules; as a result, these larger molecules are primarily transported via the lymphatics. Supersaxo et al. (Supersaxo, Hein et al. 1990) studied the effect of molecular weight on lymphatic absorption following subcutaneous injection. A linear relationship was found between the molecular weight and the proportion of dose lymphatically absorbed, such that for compounds with a molecular weight of 16,000 Da and above, more than 50% of the administered dose was found to be transported via the lymphatics.

The lymphatic capillaries are extremely permeable, admitting cellular debris as well as small molecules and proteins. Hence it is reasonable to assume that lymphatic clearance is flow-limited and $k_{\text{free}}^{\text{lymph}} = k_{\text{bound}}^{\text{lymph}} = Q^{\text{lymph}}$, where Q^{lymph} is the volume flow of lymph per unit volume of tissue ($\text{cm}^3/\text{cm}^3\cdot\text{s} = \text{s}^{-1}$).

5.2.3 Macroscopic Clearance Constants

In order to link the microscopic dermal clearance constants to a first-order clearance constant in a homogenized tissue model (Kasting, Miller et al. 2008; Kretsos, Miller et al. 2008; Dancik, Miller et al. 2012) a relationship must be established between the concentration of solute in each dermis compartment and the average bulk tissue concentration C_{de}. This relationship is developed in the Appendix. The result for clearance from the tissue into the body is

$$k_{de}^{blood} = \frac{1}{f_u \mathrm{CF}} \left[f_u k_{free}^{blood} + (1 - f_u) k_{bound}^{blood} \right] \tag{5.28a}$$

$$k_{de}^{lymph} = \frac{k^{lymph}}{f_u \mathrm{CF}} \tag{5.28b}$$

$$k_{de}^{total} = k_{de}^{blood} + k_{de}^{lymph} \tag{5.28c}$$

In Eq. (5.28) f_u is the unbound fraction of the solute and CF is a proportionality constant defined such that $C_{de} = \mathrm{CF} \cdot C_{free}$. It is calculated to be

$$\mathrm{CF} = \emptyset_{aq} \left(0.68 + \frac{0.32}{f_u} \right) + \emptyset_{lip} f_{non} K_{lip/w} \tag{5.29}$$

where ϕ_{aq} and ϕ_{lip} are the volume fractions of the aqueous and lipid compartments, respectively, and f_{non} is the nonionized fraction of solute in the aqueous compartment. The percentage of permeant cleared by the lymphatics is

$$\%\ \mathrm{lymph} = \left(\frac{k_{de}^{lymph}}{k_{de}^{blood} + k_{de}^{lymph}} \right) \times 100\% \tag{5.30}$$

The use of Eq. (5.28) is such that solute flux per unit area out of the tissue in a homogenized, spatially-dependent model such as the one discussed in Refs. (Kasting, Miller et al. 2008) and (Kretsos, Miller et al. 2008) is

$$J_s^{tot} = \int k_{de}^{tot} C_{de}(z)dz + (\text{loss into underlying tissue}) \quad (5.31)$$

Here the integral extends over the entire thickness of perfused dermis and the loss into underlying tissue is calculated as the Fickian flux into the fat layer. It is understood that an extension of this scheme to allow blood and lymphatic capillary density and/or flow to vary with depth in the tissue (e.g., by varying S or Q^{blood}) would cause k_{de}^{tot} to become spatially dependent. Such an elaboration might better represent the capillary loop structure of the reticular dermis, which is more highly perfused than the papillary dermis (Kretsos and Kasting 2005) or even the lymphatic network, which has been depicted as confined to the papillary dermis.(Kretsos and Kasting 2005) If blood clearance starts very close to the dermal-epidermal junction and lymphatic clearance is restricted to the papillary dermis, then the percentage of a topically applied permeant cleared via the lymph will be lower than that predicted by Eq. (5.30). We note that the product Area × Depth × k_{de}^{tot} plays a role analogous to clearance (Cl) in a compartmental model, but it is not expressed this way because of the spatial variation in C and (potentially) of k_{de}^{tot}.

For blood-to-tissue clearance relationships analogous to Eqs. (5.28) and (5.29) apply, but the lymphatic clearance term is not relevant and the concentration factor CF is calculated more simply. If solute concentration is expressed with respect to plasma volume, then Eq. (5.29) is replaced by

$$\mathrm{CF} = \frac{1}{f_{\mathrm{u}}^{\mathrm{plasma}}} \tag{5.32}$$

where $f_{\mathrm{u}}^{\mathrm{plasma}}$ is the fraction of unbound solute in plasma. It should be noted that binding of small solutes in the present model is assumed to involve only albumin.(Kretsos, Miller et al. 2008) We realize that this is a simplification of the binding processes occurring in the dermis, considering that solutes may bind to a wide variety of soluble proteins.(Weiss, Fresneau et al. 2008) It is possible to later relax this restriction once more information is known regarding the binding of a specific solute.

5.3 SELECTION OF PARAMETER VALUES

The parameters appearing in the outlined theory are assembled in Table 5.1. The clearance data we considered most relevant to the analysis (in addition to those described in Ref. (Kretsos, Miller et al. 2008)), are listed in Tables 5.2 and 5.3. Column 6 of Table 5.2 gives blood capillary permeabilities inferred from experiments on hydrophilic solutes diffusing from blood to tissue, P_{eff}(observed).

Table 5.1 Parameter values used for dermal clearance calculations

Nomenclature	Definition	Value	Units	Reference
	Model Parameters			
W	Width of slit	10×10^{-7}(small) 50×10^{-7} (large)	cm	(Rippe and Venturoli 2007)
f	Fraction of length of slit open to width W	0.05(small slit) 0.025 (large slit)	-	(Michel and Curry 1999)
μ	Viscosity of water at experimental temperature	0.0069	dyne·s/cm^2	(Zhang, Adamson et al. 2006)
Δx	Depth of cleft from lumen to tissue	4×10^{-5}	cm	(Weinbaum, Tsay et al. 1992)
L	Total slit length per unit area of vessel wall	1000	cm/cm^2	(Adamson 1993) (Bundgaard and Frokjaer-Jensen 1982) (Zhang, Adamson et al. 2006)
α_L	Fraction of total L_pS for large slit	0.05		(Rippe and Haraldsson 1994; Rippe and Venturoli 2007)
S	Effective exchange surface area	70	cm^2/cm^3	(Renkin 1977)
Q^{lymph}	Lymph flow rate in the dermis	8×10^{-6}	s^{-1}	Table 3

Q^{blood}	Blood flow rate in the dermis	22×10^{-4}	s^{-1}	(Kretsos, Miller et al. 2008)
ΔP	Difference between local capillary blood pressure and interstitial hydrostatic pressure	21600	$dyne/cm^2$ (Typical value under basal conditions)	(Levick and Michel 2010)
$\Delta\pi$	Difference between colloid osmotic pressure in plasma and underside of glycocalyx	18700	$dyne/cm^2$	(Rippe and Haraldsson 1994)
MW_{water}	Molecular weight of water	18.01	Da	
θ_{water}	Solvent association parameter	2.26	-	(Hayduk and Laudie 1974; Cussler 1997)
T	Temperature	310.15	K	
ΔC	Concentration difference between plasma C_p and tissue C_{de}		mg/cm^3	(Rippe and Haraldsson 1994)
$\overline{C}$	Effective intramembrane solute concentration		mg/cm^3	(Rippe and Haraldsson 1994)
h_{aq}	Thickness of the aqueous boundary layer adjacent to endothelial membrane	1×10^{-8}	cm	
L_p^{tot}	Total hydraulic conductivity	1.01×10^{-11}	$cm^3/dyne \cdot s$	(Curry and Michel 1980; Weinbaum, Tsay et al. 1992; Rippe and Haraldsson 1994)
ϕ_{fiber}	Fiber volume fraction in dermis	0.30		(Kretsos, Miller et al. 2008)
ϕ_{aq}	Aqueous volume fraction in dermis	0.70		(Kretsos, Miller et al. 2008)
ϕ_{lip}	Lipid volume fraction in dermis	0.0007		(Kretsos, Miller et al. 2008)

Derived Values				
$(PS)_{eff}$	Total solute clearance		s^{-1}	(Rippe and Haraldsson 1994)
n_i	Number of slits			
P_{cap}	Solute permeability	-	cm/s	(Michel and Curry 1999)
D_{slit}	Solute diffusion coefficient within slit	-	cm^2/s	(Happel and Brenner 1973)
Φ	Solute partition coefficient into a slit.	-	-	(Happel and Brenner 1973) (Michel and Curry 1999)
λ	Ratio of radius of solute to half-width of slit	-	-	(Happel and Brenner 1973) (Michel and Curry 1999)
J_s^{tot}	Total solute flux from tissue to blood	-	s^{-1}	(Staverman 1951) (Kedem and Katchalsky 1958)
A_L	Large pore fractional area	0.0021		
L_s	Slit length per unit area of vessel wall attributed to small slit	0.42		
L_L	Slit length per unit area of vessel wall attributed to large slit	999.58		
σ_f	Solvent drag reflection coefficient	-	-	(Michel and Curry 1999)
J_{vs}	Solvent flux from blood to tissue or tissue to blood in small slit		s^{-1}	(Staverman 1951) (Kedem and Katchalsky 1958)

J_{vL}	Solvent flux from blood to tissue in large slit		s^{-1}	
Pe	Modified Peclet number			
$\sigma_{s(albumin)}$	Reflection coefficient for albumin in small slit	0.577		
$\sigma_{L(albumin)}$	Reflection coefficient for albumin in large slit	0.029		
r_s	Solute radius	-	cm	(Happel and Brenner 1973) (Michel and Curry 1999)
V_A	Molar volume of solute (hydrodynamic value)	-	cm^3/mol	
CF	Concentration factor relating C_{de} to C_{free}	-		
C_p/C_{free}	Ratio of albumin concentration in blood and dermis	1.847		

Table 5.2 Model calculations for blood capillary permeability compared to observed values. P_{eff} was calculated using Eqs. (5.13) and (5.14) to obtain $(PS)_{eff}$, then dividing the result by S as in Ref. (Renkin 1977).

Solute	MW	log K_{oct}	r_s,[a] nm	$D_{aq} \times 10^5$, cm^2/s	Observed[b]	$P_{eff} \times 10^6$, cm/s	
						Blood to tissue Eq. (5.13)	Tissue to blood Eq. (5.14)
Urea	60.06	–2.11	0.285	1.85	28[c], 26[d]	19.29	19.17
Glucose [c]	180.16	–3.24	0.424	0.90	13.1[c], 10.7[d]	8.15	8.04
Sucrose	342.30	–3.70	0.489	0.70	8.6[c], 6.1[d]	6.03	5.91
Raffinose	504.44	–6.76	0.542	0.58	5.4[c], 5.3[d]	4.83	4.72
Inulin	5500	-	1.5	0.22	0.9[c], 1.2[d]	0.92	0.81
Myoglobin	16.7 K	-	1.9	0.17	0.3[d]	0.53	0.44
Albumin	69 K	-	3.55	0.092	0.047[e], 0.01[d]	0.071	0.017
Transferrin	90 K	-	4.3	0.076	0.063[e]	0.032	3.2×10^{-4}
Haptoglobin	100 K	-	4.6	0.072	0.031[e]	0.023	1.5×10^{-6}
Immunoglobulin	160 K	-	5.6	0.059	0.033[e]	0.010	8.5×10^{-16}
Fibrinogen	340 K		10.8	0.031	0.016[e]	0.0081	2.2×10^{-53}
α_2-Macroglobulin	820 K	-	9.1	0.037	0.007[f]	0.0088	1.9×10^{-36}

[a] Hydrodynamic radius. Associated molar volumes are shown in Table 5.4.
[b] Data from Ref. (Renkin 1977)
[c] Human forearm
[d] Mammalian skeletal muscle (cat leg)
[e] Mammalian skeletal muscle (dog paw)
f Dog intestine

Table 5.3 Lymphatic flow data calculated from the disappearance of ^{131}I-albumin from the injected site.

Injection	Site	$Q \times 10^6$, s^{-1} [a]	Reference
Intradermal	Cheek	5.76	(Ellis, Marks et al. 1970)
Intradermal	Leg	6.62	(Staberg, Klemp et al. 1983)
Subcutaneous	Forearm	8.33	(Hollander, Reilly et al. 1961)
Subcutaneous	Leg	5.75-5.89	(Hollander, Reilly et al. 1961; Fernandez, Davies et al. 1983)

[a] Resting limb

Table 5.3 gives lymphatic flow rates in humans estimated from disappearance of ^{131}I-albumin. Additional data on dermal physiology were assembled in a recent review.(Kretsos and Kasting 2005) In selecting these data from many others the following points were recognized: (1) Blood capillary permeability to lipophilic solutes is much higher than that for hydrophilic solutes and has not, to our knowledge, been measured in vivo. It must be inferred from other sources. (2) Blood capillary permeability to highly lipophilic solutes is likely to be limited by diffusion across an aqueous layer, as it is in phospholipid membranes.(Xiang and Anderson 1994) (3) Lymphatic flow is highly dependent on body site, physical activity, heat and venous pressure.(Olszewski, Engeset et al. 1977; Schmid-Schonbein 1990) Blood flow also depends on site and activity and is strongly connected to body temperature as a consequence of thermoregulation. Only representative values can be suggested. Given these inherent restrictions on obtaining a solution that represents any more than an

"average" condition, the process used to select parameter values is outlined in the following section.

5.3.1 Blood Capillary Clearance

The observed width of the interendothelial cleft is about 20 nm;(Weinbaum, Tsay et al. 1992; Sugihara-Seki and Fu 2005; Weinbaum, Tarbell et al. 2007) however, due to the absence of the glycocalyx layer and the simplicity of the theory, the width is usually chosen to be no larger than 10 nm in order to provide reasonable hindrance to the transport of macromolecules.(Curry and Michel 1980; Rippe and Haraldsson 1994; Michel and Curry 1999; Rippe 2008) Based on the work of other investigators (Rippe and Venturoli 2007) and fits of the model parameters to the data in Tables 5.2 and 5.3, the widths of the small and large slits were chosen to be 10 nm and 50 nm, respectively (Table 5.1). The presence of the junction strands within the cleft can be roughly modeled by restricting the open fraction of the length of the slit to lie between 0.025 and 0.10.(Michel and Curry 1999) Based on fits to the data in Table 5.2, we chose 0.05 and 0.025 for small and large slits, respectively. Additionally, according to the two-pore theory of Rippe and Haraldsson,(Rippe and Haraldsson 1994) the ratio of the contribution of small and large pores to the hydraulic conductance L_p^{tot} is 95:5. Yet, in the three-pore theory,(Rippe and Venturoli 2007) which includes a contribution from aquaporins, the ratio (small pores:large pores:aquaporins) is 90:7:3. Considering these values, along with the literature data for blood capillary permeability and lymphatic clearance, we selected the two-pore model ratio (α_s:α_L) of 95:5. It follows then from Eq. (5.21) and the chosen slit widths that the number ratio n_L:n_s of large slits to small slits is 4.21×10^{-4}. The

cylindrical pore literature states that large pores constitute only 1 part per 10,000-30,000 of the total population which corresponds to number ratios from $3.33 \times 10^{-5} - 1 \times 10^{-4}$.(Rippe and Haraldsson 1994; Michel and Curry 1999) The present ratio is somewhat higher since the hydraulic conductance of slits varies as W^3 whereas that of cylindrical pores varies as r^4.

Selection of the values $\Delta P = 21{,}600$ dyne/cm^2 and $\Delta\pi = 18{,}700$ dyne/cm^2 was based upon the literature. Levick (Levick and Michel 2010) reported 21560 dyne/cm^2 (22 cm H_2O) to be a typical value for ΔP under basal conditions. This value takes into account both small and large pore filtration and is furthermore associated with normal (not inflamed) blood capillaries. Rippe and Haraldsson (Rippe and Haraldsson 1994) employed the value $\Delta\pi = 18745$ dyne/cm^2 (14.06 mmHg) in their two-pore model calculations. Based on a colloid osmotic pressure calculation from Landis and Pappenheimer (Landis and Pappenheimer 1963) they state that this value corresponds to a ratio $C_i/C_p = 0.5$ for total protein (albumin) concentration at a plasma protein concentration of 6.5 g/dL. (*Note*: The published value of 6.5 g/L(Rippe and Haraldsson 1994) is clearly a misprint.) Their interstitial concentration C_i is equivalent to C_{free} in Eq. (5.12). A constant $\Delta\pi$ is expected during tracer experiments in which the changes in solute concentration in blood and tissue are negligible.

Reported values for the blood capillary hydraulic conductance L_p of varying species/sites are within the range of $1.3 \times 10^{-8} - 3.0 \times 10^{-13}$ cm^3/dyne·s.(Renkin 1977) The upper and lower limits of L_p represent fenestrated capillaries and tight junctions found in the brain, respectively. The reported L_p values for non-fenestrated capillaries, which are typically

found in the skin,(Imayama 1981) are between 2.5×10^{-11} and 5×10^{-10} $cm^3/dyne \cdot s$.(Renkin, Watson et al. 1977) Investigators proposing single pore theories (Curry and Michel 1980; Weinbaum, Tsay et al. 1992) utilized L_p values on the order of 10^{-10} $cm^3/dyne.s$ for the model calculations. In the two (Rippe and Haraldsson 1994) and three-pore(Rippe 1993) theories estimates of L_p on the order of 10^{-10} $cm^3/dyne.s$ were employed. The present value $L_p^{tot} = 1.01 \times 10^{-11}$ $cm^3/dyne \cdot s$ was chosen to match the volume flux of water into the tissue, J_v^{tot}, to the lymphatic flow rate, Q^{lymph}, described later. This choice leads to a steady-state water balance in the interstitial tissue, a condition representing healthy physiology. It should be noted that a higher value of L_p^{tot} would be required if a lower value of $\Delta\pi$ was selected as discussed by Levick and Michel.(Levick and Michel 2010)

The values of additional parameters used in this theory and their literature sources are shown in Table 5.1.

5.3.2 Lymphatic Capillary Clearance

Although the lymphatics have not been extensively investigated as blood capillaries, several studies dedicated to the measurement of lymph flow rate can be found. Careful consideration was given to the methodologies employed in these studies, the species, site and state of subject, specifically muscle activity. It was determined that the most applicable studies for our purposes were those involving the intradermal and subcutaneous injection of radiolabeled albumin into resting the limbs, forearm and cheek of human subjects.

Values for the lymph flow rate, Q^{lymph}, calculated from the disappearance of ^{131}I-albumin from subcutaneous and intradermal injection sites in human subjects are shown in Table 5.3. The disappearance was measured using a Geiger counter and Q^{lymph} was calculated from the half –life. The selected value of $Q^{lymph} = 8 \times 10^{-6}\ s^{-1}$ lies toward the upper end of the range reported in the literature. It should be noted that values for Q^{lymph} for the fingers and hands (Ellis, Marks et al. 1970; Pain, Barber et al. 2003) are much higher; thus application of the model to body sites other than limbs or broad body surfaces may require adjustments to this value.

5.3.3 Molecular parameters

At various points in the calculation three different measures of molecular size are required – molecular weight (MW), hydrodynamic solute radius (r_s) and associated hydrodynamic molar volume (V_A). MW is generally available. V_A and r_s were always related by Eq. (5.8), but they were obtained in different ways depending on the size of the molecule and available information.

Small solutes (MW ≤ 1000 Da): If aqueous diffusion data were available, V_A was calculated from D_{aq} by rearranging Eq. (5.11a). If they were not, V_A was calculated from Schroeder's Method.(Poling, Prausnitz et al. 2001) Eq. (5.8) was then used to calculate r_s. This procedure yielded solute radii slightly different from those calculated by Renkin (Renkin 1977) or other workers from that period (Beck and Schultz 1972), who employed other modifications to the Stokes-Einstein relationship that are now less accepted than the Wilke-Chang relationship. To evaluate Eq. (5.11a) we used the modified association constant ($\theta_{water} = 2.26$) suggested by Hayduk and Laudie, (Hayduk and Laudie 1974) a

temperature of 310.15 K and a viscosity of 0.0069 poise. In order to plot graphs for arbitrary solutes as a function of molecular weight we developed a relationship for V_A from a regression on MW using the database of Schroeder V_A values reported by Wang et al.(Wang, Kasting et al. 2007) These data are shown in Figure 5.1.

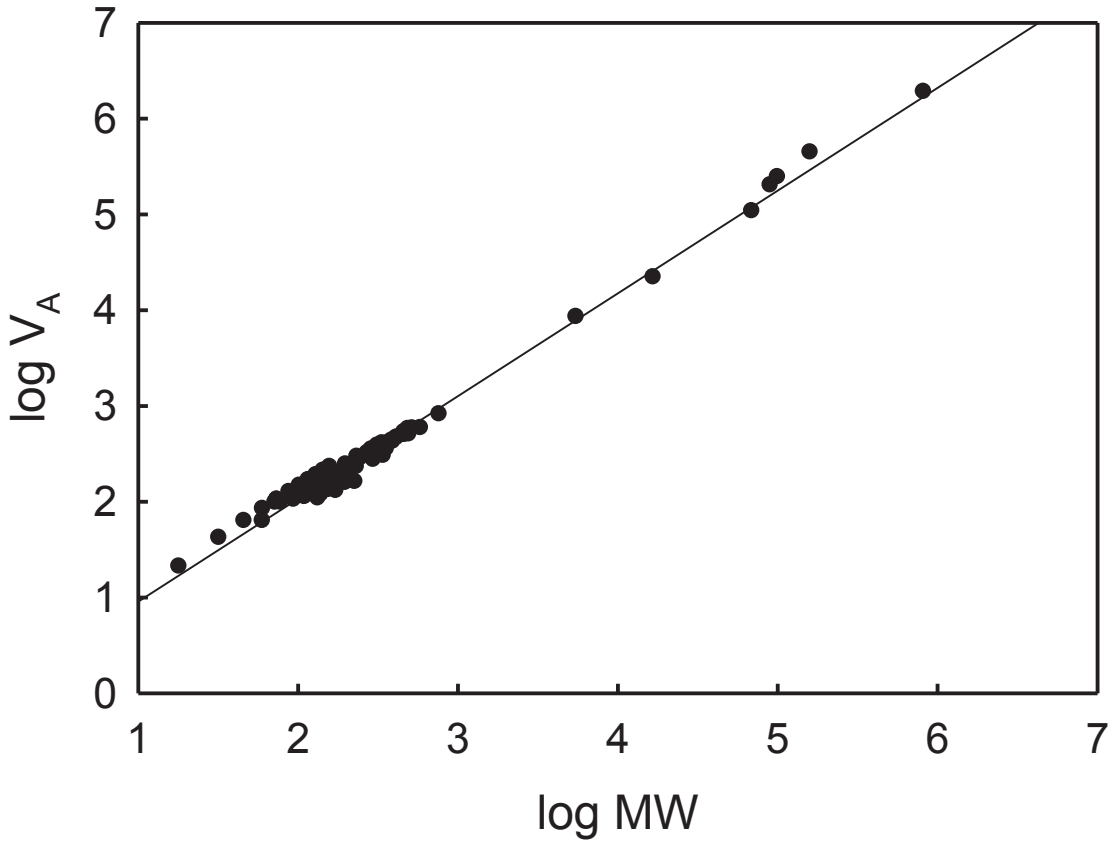

Figure 5.1 Relationship of molar volume (V_A, cm^3/mol) to molecular weight (MW, Da) for a variety of solutes. V_A values for small molecules (MW < 1000) were taken from supplemental material for Wang et al.(Wang, Kasting et al. 2007) and represent molar volume at the normal boiling point calculated from Schroeder's Method.(Poling, Prausnitz et al. 2001) V_A values for large molecules (MW > 1000) were those in Table 5.4. The solid line represents Eqs. (5.33a) and (5.33b).

The resulting regression equation was

$$\log V_A = 0.9365 \log \mathrm{MW} + 0.1890 \qquad 10 < \mathrm{MW} \le 1000 \tag{5.33a}$$

$n = 98$; $s = 0.062$; $r^2 = 0.9528$

Large solutes (MW > 1000 Da): For the solutes studied by Renkin (Renkin 1977) we used the r_s values reported therein. These are hydrodynamic values obtained from aqueous diffusivities by means of the Stokes-Einstein equation, Eq. (5.11b). For other solutes and to draw the graphs we used V_A values calculated from Eq. (5.33b). This relationship was obtained by first calculating V_A for the Renkin solutes from Eq. 5.(8), then regressing these values against MW with the constraint that the result match Eq. (5.33a) at MW 1000.

$$\log V_A = 1.1565 \log MW - 0.4710 \qquad MW > 1000 \tag{5.33b}$$

$n = 7$; $s = 0.086$; $r^2 = 0.9988$

These data and the regression line are also plotted in Figure 5.1.

Octanol/water partition coefficient ($\log K_{oct}$) was obtained from the experimental values in the EpiSuite database,(US_EPA 2009) when such values were available; otherwise it was obtained from the estimated values in this database. For hydrophilic macromolecules not contained in the database we set $\log K_{oct} = -1$. This choice was suitable because the membrane permeability to these molecules (Eq. (5.24)) is negligible compared to that of large and small slits.

Protein binding data (f_u) were either taken from the literature or estimated according to the method of Yamazaki and Kanaoka.(Yamazaki and Kanaoka 2004) The latter method has been employed before to provide estimates where no experimental data are available.(Kretsos, Miller et al. 2008) This is essentially a hydrophobic binding model that provides guidance for the binding of lipophilic compounds to albumin. It should be considered a rough estimate only for f_u; for greater accuracy experimental data or more sophisticated calculations (Kratochwil, Huber et al. 2002) are required. For hydrophilic macromolecules for which the arbitrary value $\log K_{oct} = -1$ was assigned, f_u was set equal to 1, as these molecules are not expected to undergo binding in aqueous solutions.

5.3.4 Albumin plasma/tissue ratio

Based on the model parameters already selected and the requirement of albumin balance, a unique ratio of plasma-to-tissue albumin concentration, C_p/C_{free}, can be calculated from Eq. (5.12). The albumin balance is achieved by equating the leakage rate into the tissue calculated from Eq. (5.12) with the lymphatic clearance, $Q^{lymph} \cdot C_{free}$. For the present choice of parameters, the result is $C_p/C_{free} = 1.847$. Thus if the plasma concentration of albumin is 40 mg/mL, then the predicted tissue concentration is 40/1.847 = 21.7 mg/mL. This value is close to the average value of 20 mg/mL determined by analysis of human dermis post-mortem as discussed in Ref. (Kretsos, Miller et al. 2008). Application of van't Hoff's Law to this concentration difference yields an osmotic pressure contribution from albumin of 9015 dyne/cm^2, or 48% of the $\Delta\pi$ value listed in Table 5.1.

5.4 RESULTS

The results of dermal clearance calculations using the developed model are shown in Tables 5.2 and 5.4 and Figures 5.2-5.5.

Table 5.4 Model calculations for total dermal clearance k_{de}^{total} (Eq. (5.28c)) and the percentage of solute recovered in the lymph (Eq. (5.30)).

Solute	MW	V_A, cm^3/mol	log K_{oct}	f_u	CF	$k_{de}^{total} \times 10^6$, s^{-1}	% Lymph (calc)[a]	% Lymph (observed)[b]
Urea	60.06	58.4[c]	–2.11		0.70	1206	0.95	
Glucose	180.16	192.8[c]	–3.24		0.70	651	1.8	
Methoxsalen	216.19	203.0[d]	2.00	0.09[e]	3.03	755	3.9	
Didanosine	236.23	224.0	–1.24	0.95[f]	0.71	590	2.0	
FUDR	246.2	206.5[d]	–1.16		0.70	627	1.8	4.0 ± 1.5
Sucrose	342.30	295.4[c]	–3.70		0.70	509	2.2	
Piroxicam	331.35	322.0[d]	3.06	0.02[g]	11.7	227	15.1	
Desoximetasone	376.47	416.5[d]	2.35	0.15[h]	2.13	1012	2.5	
Econazole	381.68	360.5[d]	5.61	0.02[i]	297	8.96	15.0	
Raffinose	504.44	400.6[c]	–6.76		0.70	422	2.7	
Inulin	5500[j]	8511[c]	-		0.70	90.8	12.6	21 ± 7.1
Cytochrome C	12.3 K	19.2 K[k]	-		0.70	50.4	22.7	38.6 ± 6.7
Myoglobin	16.7 K	17.3 K[c]	-		0.70	54.7	20.9	
rIFN alpha-2a	19 K	31.4 K[k]	-		0.70	33.9	33.7	59.5 ± 7.7
Albumin	69 K	113 K[c]	-		0.70	13.2	86.9	
Transferrin	90 K	200 K[c]	-		0.70	11.5	99.7	
Haptoglobin	100 K	245 K[c]	-		0.70	11.4	100.0	

Immunoglobulin	160 K	443 K[c]	-	0.70	11.4	100.0
Fibrinogen	340 K	822 K[c]		0.70	11.4	100.0
α_2-macroglobulin	820 K	1900 K[c]	-	0.70	11.4	100.0

[a] Eq. (5.30); [b] Supersaxo et al. 1990(Supersaxo, Hein et al. 1990); [c] Calculated from r_s (Table 5.2) using Eq. (5.8); [d] Schroeder's Method; [e] Obach 1999(Obach 1999); [f] Hardman et al. 2001(Hardman, Limbird et al. 2001) ; [g] Richardson et al. 1987(Richardson, Blocka et al. 1987); also f_{non} = 0.0124 @ pH 7.4 since pK_a = 5.5; [h] Yamazaki & Kanoka 2004(Yamazaki and Kanaoka 2004); [i] DoubleCheckMD(Enhanced_Medical_Decisions 2009); [j] Supersaxo et al.(Supersaxo, Hein et al. 1990) reported the MW as 5200;[k] Eq. (5.33b).

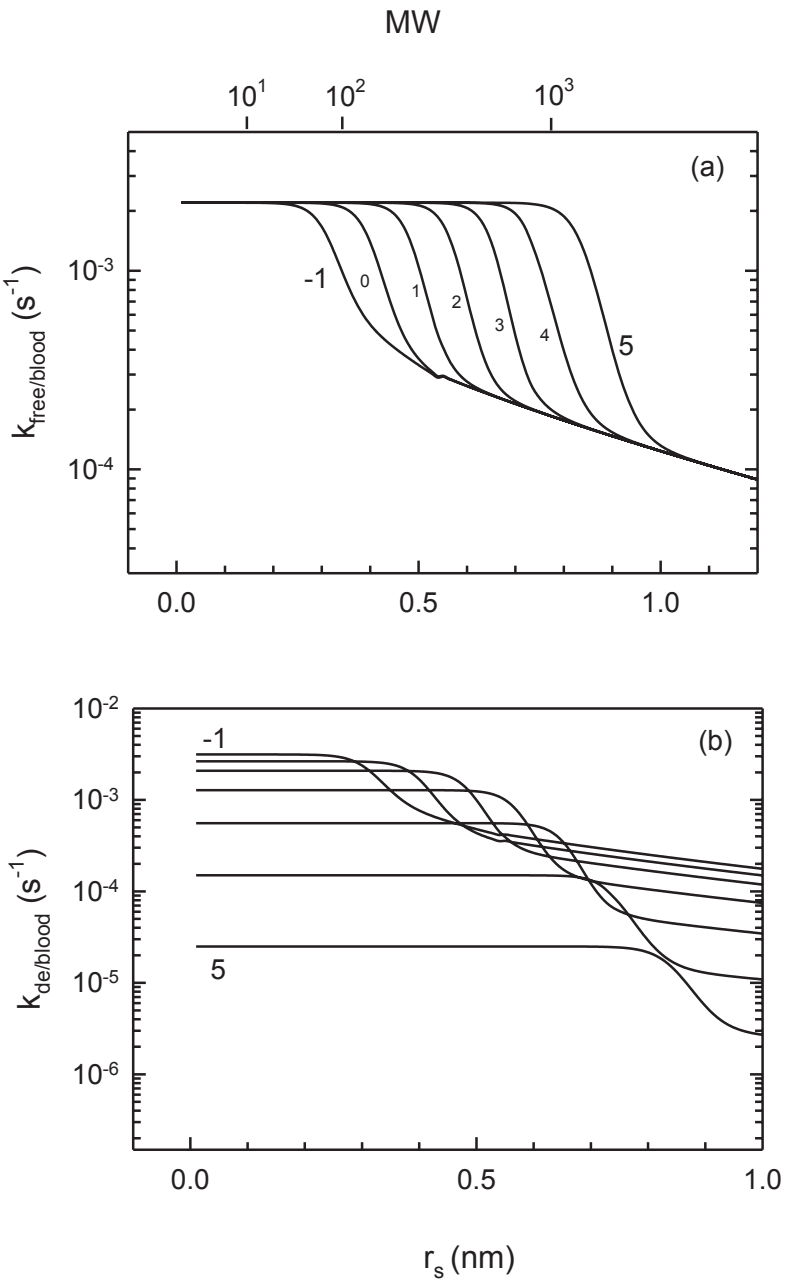

Figure 5.2 Calculated tissue-to-blood clearance constants for solutes having varying radii and log K_{oct} (−1, 0, 1, 2, 3, 4, 5). The corresponding f_u values were (1, 0.63, 0.39, 0.19, 0.08, 0.03, 0.01).(Yamazaki and Kanaoka 2004) (a) Microscopic clearance constant for

unbound solute calculated using Eq. (5.26). (b) Total tissue-to-blood clearance constant calculated using Eq. (5.28a).

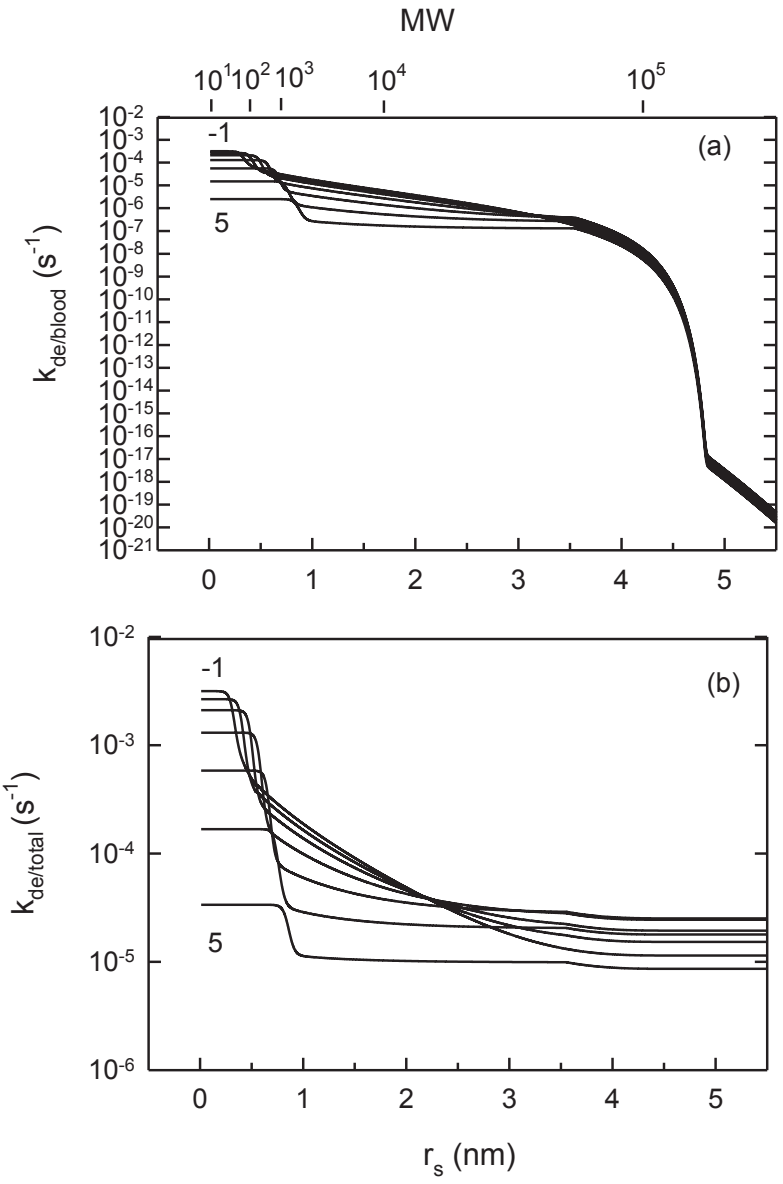

Figure 5.3 (a) Total tissue-to-blood clearance constant for larger solutes calculated as in Figure 5.2b. (b) Total dermal clearance constant calculated using Eq. (5.28c). This

relationship includes lymphatic clearance, which dominates the blood clearance for larger solutes.

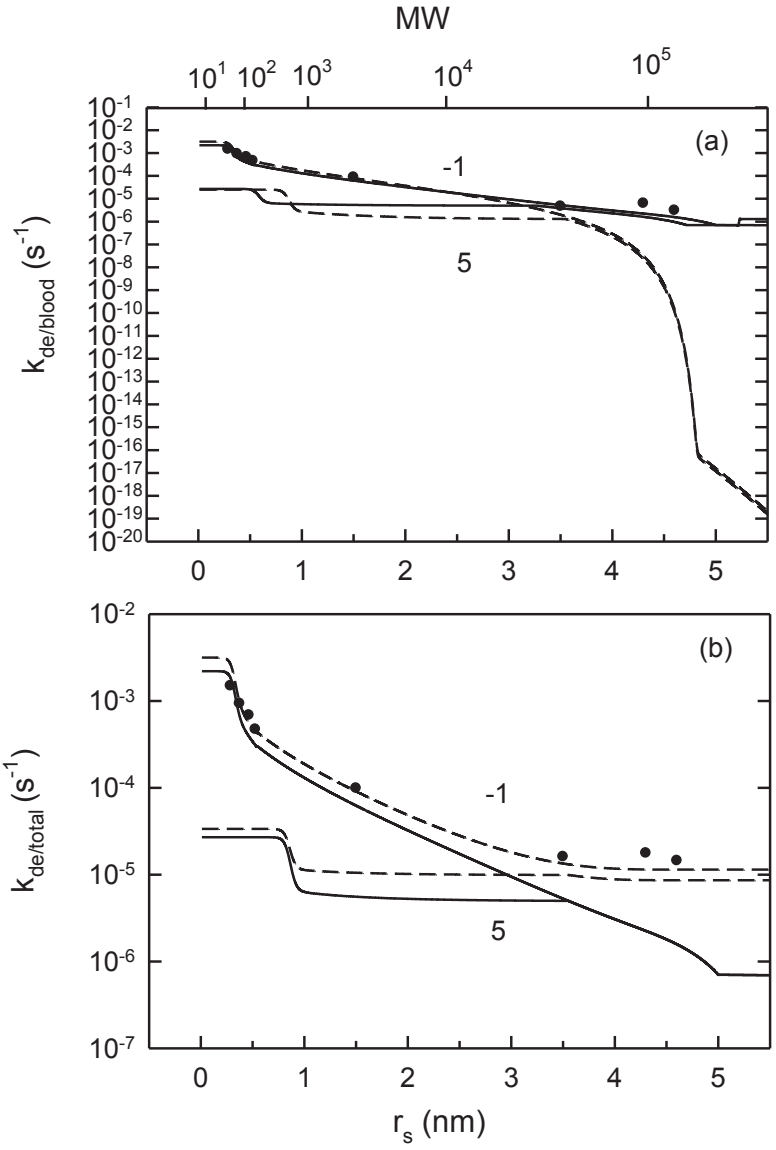

Figure 5.4 Calculated blood-to-tissue (solid line) and tissue-to-blood (dashed line) clearance constants for varying radii and log K_{oct} (–1, 5). The symbols represent the

experimental data in Column 6 of Table 5.2. The points were calculated by substituting the P_{eff} (observed) value from the table for P_{cap} in Eq. (5.13), then calculating k_{free}^{blood} from Eq. (5.26). For these hydrophilic solutes $f_u = 1$.

The general features of the model will first be noted, followed by a comparison of these results with experimental clearance data. To understand the smooth curves that are reported it should be noted that a specific relationship between octanol-water partition coefficient K_{oct}, and binding to albumin (f_u) has been employed.(Yamazaki and Kanaoka 2004) This is not a requirement for solutes for which these values are obtained independently, or which bind to proteins other than albumin. The curves are thus illustrative of model properties, but lack the specificity that detailed information on solute properties could ultimately provide.

5.4.1 Capillary Clearance – Tissue-to-Blood

Figure 5.2 shows the impact of lipophilicity/protein binding on tissue-to-blood capillary clearance for solutes with radii less than 1 nm, corresponding to molecular weights less than about 2000 Da. Panel (a) shows the microscopic clearance coefficient for freely diffusing solutes (Eq. (5.26)), whereas Panel (b) reflects clearance with respect to total solute concentration in the dermis (Eq. (5.28c)). Both curves illustrate the selectivity of the capillary membrane to solute molecular weight and lipophilicity according to Eq. (5.24). The plateau for small solutes reflects blood flow limitations as exemplified in Eq. (5.26). The convergence to a single value of k_{free}^{blood} for solutes with radii > 1.0 nm reflects clearance through the aqueous slits. The solutes are differentiated in this region

when lipophilicity/protein binding is taken into account (k_{de}^{blood}, Fig. 5.2b). Highly bound solutes are cleared more slowly by blood capillaries than free solutes because the diffusion of small solutes bound to macromolecules is hindered within the slits (cf. Eqs. (5.4-5.14)).

Figure 5.3a shows the continuation of Fig. 5.2b for solutes up to and exceeding molecular weights of 10^5 Da. The impact of the two-slit structure may be clearly seen as clearance drops sharply when the small slits are unable to accommodate the solute. However, this behavior is completely masked when lymphatic clearance is added, as shown in Figure 5.3b.

5.4.2 Capillary Clearance – Blood-to-Tissue

In order to compare the model predictions with the experimental results summarized by Renkin (Renkin 1977) it was necessary to compute the effective permeability in the blood-to-tissue direction (Eq. (5.13)), rather than tissue-to-blood (Eq. (5.14)). This is because the experiments were conducted by measuring depletion of solutes in venous blood versus arterial blood after circulation through the tissue. The results of these calculations are shown in Table 5.2 and Figure 5.4. For small solutes there is little difference between effective permeabilities in both directions because transport is primarily diffusive. However, this pattern changes for solutes the size of inulin (r_s = 1.5 nm) and above. For these compounds blood capillary transport is primarily mediated by convection within the slits. Since the volume flow of water (J_v) in the steady-state model is always from blood to tissue, the corresponding values of blood capillary permeability and clearance for large solutes are much higher in this direction. Good agreement

between the model predictions and capillary permeability in human forearm or cat leg (Table 5.2, Rows 1-5) may be seen. For the larger solutes, for which permeability was measured in either dog or cat limbs, the model underpredicts some of the experimental values by as much as a factor of 3.3. However it should be noted, as discussed by Renkin,(Renkin 1977) the experimental values "…are diffusion permeabilities, calculated on the basis that diffusion or vesicular exchange is the dominant mode of transport in this size range. To the extent that convective transport is involved, they are *overestimates* of the true permeabilities." The present calculation is consistent with this statement.

5.4.3 Lymphatic Clearance

Lymphatic clearance calculations and experimental data for selected molecules are shown in Figure 5.5 and Table 5.4.

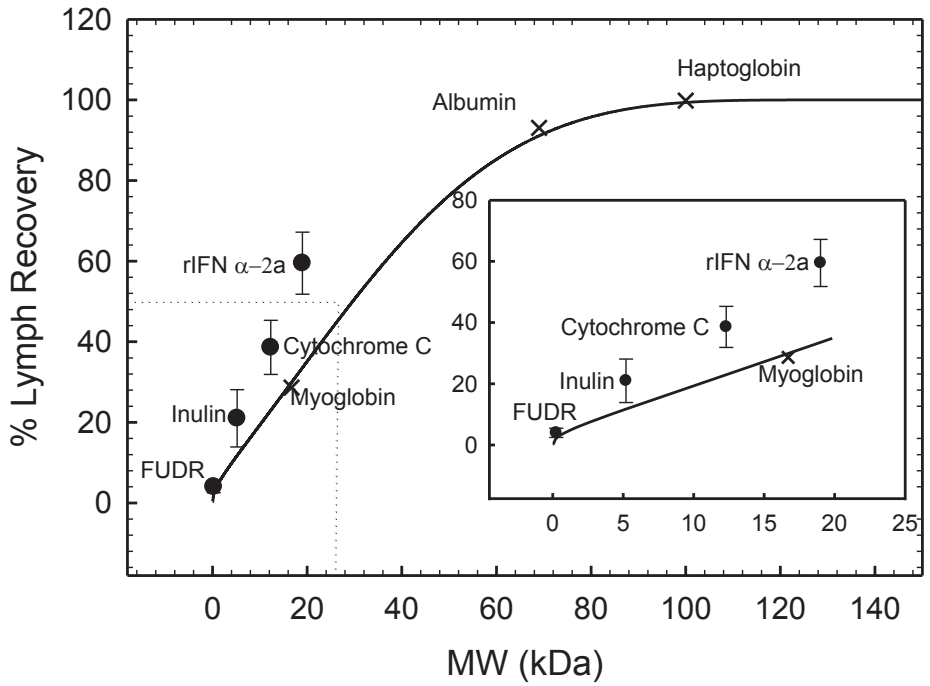

Figure 5.5 Model predictions for percentage of solute cleared by the lymphatic capillaries for solutes log K_{oct}= –1 and f_u = 1. The dotted line represents the crossover point at which lymphatic clearance begins to dominate the overall clearance in the dermis. The inset represents a subset of the data at lower MW. The symbols are the values from sheep hind limb(Supersaxo, Hein et al. 1990) listed in Column 9 of Table 5.4.

For hydrophilic solutes that do not themselves bind to larger molecules, lymphatic uptake in the present model is simply a function of size. A linear increase in lymphatic uptake with increasing molecular weight is predicted for solutes up to approximately 40 kDa, corresponding to a lymphatic recovery of 67%. For larger solutes the curve gradually approaches the 100% plateau. The crossover point at which lymphatic uptake equals 50% occurs at 29 kDa. Highly protein-bound molecules show an entirely different pattern, as the bound fraction moves with albumin, which is 87% cleared through the lymph (Table 5.4). Hence a small, lipophilic compound like econazole, reported to be >98% bound in plasma,(Enhanced_Medical_Decisions 2009) has a calculated lymphatic recovery of 15% based on the assumption f_u = 0.02 in tissue, with the binding confined to albumin. It may be seen from an examination of Figure 5.5 that solutes binding to smaller proteins would have lower clearance through the lymphatics for an equivalent binding affinity.

Figure 5.5 and Table 5.4 show also the experimental percentage lymphatic recovery of hydrophilic, radiolabeled compounds following injection into cannulated hind legs of sheep.(Supersaxo, Hein et al. 1990) These data follow the linear trend with molecular weight exhibited by the model; however lymphatic recovery is significantly higher than the model predictions, with the crossover point from blood to lymph occurring at 16 kDa. We found we could not match these values and still maintain consistency with Renkin (Figure 5.4) as well as a plausible resting lymph flow. It is worth noting that hind leg cannulation is an invasive procedure that may have increased the lymph flow in sheep.(Supersaxo, Hein et al. 1990) Were this the case the experimental data may be no more accurate than the model for predicting lymphatic recovery in humans. Hence we chose to accept this difference in favor of a good match to blood capillary permeability.(Renkin 1977)

5.5 DISCUSSION

Dermal capillary clearance was modeled by Kretsos et al.(Kretsos, Miller et al. 2008) as a uniform first order clearance of permeant through the blood capillaries into the systemic circulation. This simplified approach was adequate for the clearance of small permeants and moderately protein-bound permeants. However, for plasma proteins, macromolecules and highly protein-bound permeants, the contribution of the lymphatic capillaries to the overall clearance cannot be ignored.

The transport of solutes across the blood capillaries, especially macromolecules, is not completely understood; nevertheless, it has been extensively described at several levels of complexity. The slit/pore theory and its variants are among the simplest of the theories.

These models do not account for the complex physiology of the interendothelial cleft, specifically the presence of the glycocalyx which is believed to be the primary sieve for macromolecules, as well as the junction strands present within the cleft that restrict the transport of solutes by narrowing the width of the available cleft region. Although these models are unable to successfully explain the whole body of available experimental data, they do provide a good starting point to understanding and being able to evaluate the permeability properties of the blood capillary wall.(Sugihara-Seki and Fu 2005) The present analysis shows that a two-pore model combined with a constant lymphatic clearance term is adequate for simultaneously describing certain blood capillary permeability data (Renkin 1977) and lymphatic clearance data (Supersaxo, Hein et al. 1990) available in the literature. Because both blood and lymph flow vary substantially with body site and physical activity of the subject, and because of the limited calibration dataset, quantitative predictions arising from the present model should be treated cautiously. However certain qualitative features emerge within a framework that lends itself to improved calibration for specific exposure scenarios as more experimental data become available.

For very highly protein-bound solutes and macromolecules, the dominating clearance mechanism is via the lymphatic capillaries. The permeability of these capillaries is very high; hence, the rate of clearance is flow-limited. The selected value for this flow (Q^{lymph}) for subjects at rest was 8×10^{-6} s^{-1}. This value does not take into consideration data obtained from studies involving the fingers and hands.(Ellis, Marks et al. 1970; Pain, Barber et al. 2003) Clearance at these specific sites is very high due to physiological differences from other body sites. Use of the model to describe uptake of chemicals from

hands should judiciously reflect increased lymphatic flow, as well as other physiological differences including the structure and permeability of palmar stratum corneum. The present model parameters are considered to be useful for estimating uptake from limbs and other broad body surfaces. This restriction is consistent with other approximations incorporated in our present three-layer skin model.(Kasting, Miller et al. 2008; Dancik, Miller et al. 2012) In particular, stratum corneum permeability in the full-thickness model also derives from experiments involving broad body surfaces. These limitations should be kept in mind when analyzing different exposure scenarios.

Other key factors that must be considered when attempting to quantitatively explain the uptake of small molecules from skin are the details of the binding processes occurring within the dermis, especially those involving soluble proteins. The strength and reversibility of the binding as well as the molecular weight of the substrate(s) all play a role in clearance. Highly bound solutes will be predominately cleared in a pattern dictated by the substrate. Consequently detailed information on protein binding in the skin is of considerable value in assessing the fate of topically applied permeants. In the current model, it is assumed that these compounds primarily bind to albumin. This is an oversimplification as there are other proteins to which these solutes may bind. For example the highly lipophilic macrolides pimecrolimus and tacrolimus have been found to bind to a variety of soluble skin proteins with the most clearly identified substrate an approximately 15 kD protein postulated to be macrophilin 12.(Weiss, Fresneau et al. 2008) Examination of Figure 5.5 suggests that the size of the binding proteins will have a strong effect on the lymph/blood clearance ratio. It is readily shown that lipophilicity, molecular weight and protein binding affinity of the solute all play a role in determining

this ratio. Consequently we encourage those who would use this model to make predictions for hazardous compounds to develop reliable protein binding data before attaching too much meaning to the results. This is especially the case for topically-applied compounds whose systemic toxicity is considered to be related to the mode of uptake within the skin. Great care must be exercised to avoid drawing inappropriate conclusions by using an oversimplified model.

5.6 CONCLUSION

The mechanism of dermal clearance for both small and large solutes can be adequately modeled using a two-slit theory model for the blood capillary component and a constant clearance for the lymphatic component. We have shown that the current model makes adequate predictions for both large and small solutes when compared to literature data.

5.7 APPENDIX.

5.7.1 Clearance of free and bound solute

Consider the dermis to be a porous matrix composed of three compartments – collagen and elastin fibers, aqueous/GAG milieu, and embedded lipids – with volume fractions ϕ_{fiber}, ϕ_{aq}, and ϕ_{lip}, respectively. These volume fractions sum to one. Solutes are excluded from the fibrous region; their average concentrations in the other regions are C_{aq} and C_{lip}. Following Kretsos et al.(Kretsos, Miller et al. 2008) the aqueous region has an albumin-inaccessible region (68%) and an albumin-accessible region (32%). The latter contains free and bound solute in the ratio $f_u/(1-f_u)$; thus $C_{\text{aq}} = 0.68C_{\text{free}} + 0.32(C_{\text{free}} + C_{\text{bound}}) = (0.68 + 0.32/f_u)C_{\text{free}}$ since $C_{\text{bound}} = [(1-f_u)/f_u]\ C_{\text{free}}$. C_{lip} is related to the nonionized

component of C_{free} by an equilibrium partition coefficient $K_{lip/w}$; thus $C_{lip} = K_{lip/w} f_{non} C_{free}$. In the present simplified picture all bound solute is bound to albumin and $K_{lip/w}$ is represented by the octanol/water partition coefficient K_{oct}. These definitions vary slightly from those presented in Ref. (Kretsos, Miller et al. 2008), where ϕ_{lip} was considered to be a subcompartment of ϕ_{aq}.

Mass balance on a unit volume of dermis requires that

$$C_{de} = \emptyset_{aq} C_{aq} + \emptyset_{lip} C_{lip}$$

$$= \left[\emptyset_{aq} \left(0.68 + \frac{0.32}{f_u} \right) + \emptyset_{lip} K_{lip/w} f_{non} \right] C_{free} \qquad \text{(5A-1)}$$

$$= CF \cdot C_{free}.$$

Here the concentration factor CF is defined as the proportionality constant between the freely diffusing unbound solute concentration C_{free} and the average concentration in the bulk tissue C_{de}. This distinction is useful in linking the microscopic clearance constants to the effective clearance parameter k_{de} in a homogenized tissue model.(Kasting, Miller et al. 2008) CF is closely related to the binding factor introduced by Kretsos et al.(Kretsos, Miller et al. 2008) except that it explicitly contains ϕ_{aq}. The relevant phase volumes are approximately $\phi_{fiber} = 0.3$, $\phi_{aq} = 0.7$ and $\phi_{lip} = (0.7)(0.001) = 0.0007$.(Kretsos, Miller et al. 2008)

The total flux of solute out of the tissue is the sum of the fluxes of free and bound forms into the blood and the lymph. Thus

$$J_s^{tot} = J_s^{blood}(\text{free}) + J_s^{blood}(\text{bound}) + J_s^{lymph}(\text{free}) + J_s^{lymph}(\text{bound}) \tag{5A-2}$$

Rewriting Eq. (5A-2) in terms of clearance one has

$$J_s^{tot} = k_{de}^{total} C_{de} = k_{free}^{blood} C_{free} + k_{bound}^{blood} C_{bound} + k_{free}^{lymph} C_{free} + k_{bound}^{lymph} C_{bound} \tag{5A-3}$$

Substituting Eq. (5A-1) for C_{de} and rewriting C_{bound} in terms of C_{free}, then dividing the result by C_{free} yields

$$\begin{aligned} k_{de}^{total} &= \frac{k_{free}^{blood}}{CF} + k_{bound}^{blood}\left(\frac{1-f_u}{f_u CF}\right) + \frac{k_{free}^{lymph}}{CF} + \left(\frac{1-f_u}{f_u CF}\right) k_{bound}^{lymph} \\ &= \frac{1}{f_u CF}\left[f_u k_{free}^{blood} + (1-f_u) k_{bound}^{blood} + k^{lymph}\right] \end{aligned} \tag{5A-4}$$

since free and bound solutes are cleared at the same rate in lymph. The effective blood and lymphatic capillary clearances are

$$k_{de}^{blood} = \frac{1}{f_u CF}\left[f_u k_{free}^{blood} + (1-f_u) k_{bound}^{blood}\right] \tag{5A-5}$$

$$k_{de}^{lymph} = \frac{k^{lymph}}{f_u CF} \tag{5A-6}$$

6. ANALYSIS OF EX VIVO SKIN CONCENTRATION USING A TRANSIENT DIFFUSION MODEL WITH DISTRIBUTED DERMAL CLEARANCE

6.1 INTRODUCTION

The ability to calculate in vivo skin concentrations of topically-applied compounds and estimate their epidermal bioavailability relies on the knowledge of both the input and output rate from the tissue. The former is dominated by the barrier properties of the stratum corneum, whereas the latter is dominated by capillary clearance unless the compound degrades extensively in the skin. Both blood capillaries and lymphatic capillaries contribute to clearance; however, their contribution varies widely depending on the physicochemical properties of the solute. Small permeants are largely cleared through the bloodstream unless they are highly protein-bound. High molecular weight permeants (>16 kDa) are largely cleared through the lymph.(Supersaxo, Hein et al. 1990) The availability of in vivo data in the literature is scarce. Additionally, the performance of such studies today poses serious ethical concerns. Hence, the ability to predict skin concentrations in vivo of topically-applied permeants would be invaluable. The organization of the blood and lymphatic capillary network within the dermis varies with depth, body site, age, skin condition and ultimately the individual. This complexity makes the accurate depiction of such networks with mathematical models extremely difficult.

It is believed that the subepidermal layer for most human skin contains non-fenestrated or continuous capillaries.(Imayama 1981) These capillaries have a high permeability to smaller permeants and a much lower permeability to larger solutes. The transport or

diffusion of solutes across these blood capillaries is primarily through the interendothelial cleft found between two adjacent endothelial cells and across the endothelial cell membrane.(Michel and Curry 1999; Curry 2005; Sugihara-Seki and Fu 2005; Sarin 2010) Other routes of transport, e.g. vesicular transport, which some consider the main route for macromolecules and proteins, are controversial.(Rippe, Rosengren et al. 2002; Rosengren, Rippe et al. 2006; Sarin 2010) The interendothelial cleft is about 20 nm wide,(Michel and Curry 1999; Curry 2005; Sugihara-Seki and Fu 2005; Sarin 2010) however, in the absence of explicitly representing the glycocalyx layer, which is believed by some to be the primary molecular sieve for macromolecules and has a gap length of 7 nm between fibers,(Berg, Nieuwdorp et al. 2006; Flessner 2008; Rippe 2008) the cleft can be considered to have a width of 8-10 nm.(Michel and Curry 1999; Sugihara-Seki and Fu 2005; Rippe and Venturoli 2007) The controversy surrounding vesicular transport as a route of transport for macromolecules has led some investigators to propose that the presence of clefts with a width far larger than 20 nm, about 500 nm, is responsible for macromolecular transport.(Renkin and Curry 1982; Rippe 1993; Rippe and Haraldsson 1994; Michel and Curry 1999; Rippe, Rosengren et al. 2002; Rippe and Venturoli 2007) This theory is not without some controversy.(Michel and Curry 1999; Sarin 2010)

The microstructure of the lymphatic capillaries is not as crucial as that of the blood capillaries due to the fact that the former have a high permeability to macromolecules and hence, are flow-limited. Supersaxo et al. (1990) showed that for solutes larger than 16 kDa, more than 60% of the clearance is attributable to by the lymphatic capillaries.(Supersaxo, Hein et al. 1990) Additional literature reports of clearance

following dermal and subcutaneous injections of ^{131}I-albumin at various body sites in humans were utilized to derive the lymphatic component of the model.(Hollander, Reilly et al. 1961; Ellis, Marks et al. 1970; Fernandez, Davies et al. 1983; Staberg, Klemp et al. 1983)

Using our current dermal clearance model combined with existing models for stratum corneum permeability and appropriate measures of protein binding; the goal of this present work is to analyze in vivo concentration data from the literature and compare it to predictions made by the current mathematical model. (Dancick et al, 2012)

6.2. DIFFUSION MODEL

A transient one-dimensional diffusion model implemented as an Excel spreadsheet was used for all calculations. This multilayer model has been described in considerable detail elsewhere.(Miller, Bhatt et al. 2006; Nitsche, Wang et al. 2006; Wang, Kasting et al. 2006; Wang, Kasting et al. 2007; Kasting, Miller et al. 2008; kasting, Miller et al. 2008; Kretsos, Miller et al. 2008; Nitsche and Kasting 2008) Briefly, the model is a transient 1-dimensional 3 layer diffusion model where predictions can be made for both finite and infinite doses. The stratum corneum is represented by a brick and mortar model (Nitsche, Wang et al. 2006; Wang, Kasting et al. 2006; Wang, Kasting et al. 2007), the viable epidermis is represented as unperfused dermis, and the dermis is represented as a homogenous layer with a distributed capillary clearance.(Kretsos, Kasting et al. 2004; Kretsos, Miller et al. 2008) Within the dermis component of the model is the dermal clearance component, which consists of both the blood and lymphatic capillary clearance mechanisms. The dermal clearance model has been described in detail elsewhere in

Chapter 5. Briefly, the dermal capillary clearance is represented by a two-slit theory with a contribution of lymphatic clearance for highly protein-bound solutes and macromolecules. The slit represents the interendothelial cleft between two adjacent endothelial cells. The small slit is 10 nm wide and is the primary route for small solutes, the large slit is 50 nm wide and is the primary route for macromolecules. The ratio of small slits to large slits is 95:5. Furthermore, solutes may diffuse through the endothelial cell wall. This contribution to the total capillary permeability is based on a model of phospholipid permeability summarized in Chapter 5 and described in detail elsewhere (JMN, GBK, J Pharm Sci, submitted).

Lymphatic capillaries are abundant in the dermis. They have been reported to start in the sub-papillary layer, specifically under the capillary loops and microvascular meshwork.(Schmid-Schonbein 1990) Joory (Joory 2004) measured lymphatic vessel depth and distribution in the human forearm and reported that the highest lymphatic vessel density occurred within 250 μm of the dermal-epidermal junction. Considering that the reported value represents the highest lymphatic vessel density, a distance of 200 μm from the dermal-epidermal junction was chosen as the starting point for lymphatic clearance in the model. The model value for lymphatic clearance value was derived from data involving the disappearance of ^{131}I-albumin from subcutaneous and intradermal injection sites.(Hollander, Reilly et al. 1961; Ellis, Marks et al. 1970; Fernandez, Davies et al. 1983; Staberg, Klemp et al. 1983); this development in described in Chapter 5.

6.3 EX VIVO SKIN CONCENTRATION DATA

The physical properties for each permeant are listed in Tables 6.1 and 6.2. The in vivo skin concentration data are summarized in Table 6.3. Many of the data listed in Table 6.3 have previously been analyzed using a simpler model for partitioning, diffusivity and clearance in dermis.(Kretsos, Miller et al. 2008) The objective was to describe the skin concentration profiles using the modified mathematical model. The experimental in vivo data are shown in Figures 6.1 and 6.2. A regression analysis was preformed on the experimental data (not shown), such that the slope E, also referred to as the decay parameter, was used to calculate the clearance constant k_{de} while assuming a 1st order clearance (Kretsos, Miller et al. 2008).

$$E = \sqrt{\frac{k_{de}^{total}}{D_{de}}} \tag{6.1}$$

All equations used for this analysis can be found in explicit detail in Chapter 5.

6.3.1 Methoxsalen (Kammerau et al.)

The data from the patient exposed to the wool-wax alcohol ointment was used for this analysis. The authors assumed a thickness of 20μm for the stratum corneum, 160 μm for the epidermis and 1050μm for the dermis. Urinary excretion data was available for this patient.

6.3.2 Triamcinolone Acetonide

Patients with both healthy/uninvolved skin concentrations and urinary excretion data available were used in this analysis. Although urinary excretion data was available, it was

not used due to the fact that the permeant was applied to both healthy and psoriatic skin and too many assumptions would have been made in order to extrapolate data that could have been used in this analysis.

6.3.3 Flurbiprofen and Ketoprofen

The current model represents physiological parameters for both human and mouse species. Hence for this data, the mouse species model was utilized to analyze the rat data which assumes that mouse skin is three times more permeable than human skin. For this analysis optimum values for D_{sc} were fit to four types of data: the total tissue concentration in the viable epidermis, the total dermis concentration, the absolute bioavailability (taken to be the amount absorbed) and amounts remaining in the patch. Additionally a different value for the diffusivity of bound solute D_b was used than the 3 x 10^{-7} cm/s^2 used for human data; a detailed description of this parameter can be found in Ibrahim, Kasting 2012. The solubility of the solutes in the vehicle was unknown, hence two conditions were tested, negligible solubility and 10% solubility (100g/L). Furthermore, two assumptions were built into the analysis, complete removal of the solute from the surface of the skin after patch removal was assumed, and that the absorption amounts reported were taken at 12 hours. This latter assumption works well for fluorbiprofen but not ketoprofen.

6.3.4 Econazole

The concentration profile data for patient #2 was utilized for analysis. Urinary excretion data was available from another patient whose skin concentration profiles had not been

measured. However, the data were not used because the amounts absorbed at 1.5 hours in the dermis were very similar to the amounts absorbed at 48 hours, which seemed highly unlikely.

6.3.5 Piroxicam

Urine concentrations were not measured here, however, the authors reported a mass balance from which amounts absorbed were deduced. The experiments were conducted in pigs, because of the similarity in skin permeability to human, the human species model was used to generate predictions. Concentration profiles from both cranial and caudal sites were utilized for analyses.

6.3.6 Hydrocortisone and Testosterone (Huber)

The experiments were conducted in hairless rats, however due to the lack of a rat model, the mouse model parameters were used for analysis. Both compounds were tritium-labelled. The concentration profiles for normal skin after 6 hours post-treatment were used for our analysis.

6.3.7 Methoxsalen and Desoximetasone (Schaeffer)

Concentration profiles for normal/healthy skin were utilized for analyses. Urinary excretion data was not available for either these solutes.

6.3.8 Retinoic Acid

The radioactive solute was tested in two different fat-like ointments, however, it is unclear in the concentration profiles shown which ointment was being observed. Only one concentration profile was shown for uncompromised skin; this profile was used for analyses. It should be noted that excretion data were presented, however, they corresponded to patients with compromised skin and so were not used for analyses purposes.

6.3.9 Didanoisne (Gao and Gupta)

Both experiments utilized Fisher rats, that is, rats with high follicular density. Plasma concentration profiles were available for both studies, however, they were not used because systemic pharmacokinetic parameters for didansosine in rat were not available. Assumptions regarding the rate of blood-flow and flux would furthermore have been required.

6.3.10 Hydrocortisone (Schaeffer)

During the initial analysis of this data set, it was the opinion of the investigators that the skin concentrations reported by the authors were unrealistically high for such a solute as hydrocortisone. In order to better comprehend the data, the investigators communicated with the author (Schaeffer), who stated that he believed that the radiolabelled compound had been unstable, leading to measurement of both the solute and a radiolabeled exchange product, thus exaggerating the actual solute concentrations in skin.

6.4 DATA ANALYSIS

Two types of analyses were employed, the choice depending on the published data for each permeant. All data were analyzed using the modified mathematical model (Chapter 5); however, for permeants with reported absorption data, a curve-fitting spreadsheet was also used which took into account both skin concentration profiles and absorption profiles in urine. It should be noted that the current model makes predictions for only two species, human and mouse. Hence, for the data listed in Table 6.3, the mouse model was used to represent the rat data and the human model was used for the porcine data.

With regards to the curve-fitting spreadsheet used for solutes with absorption data, the diffusivity of the stratum corneum (D_{sc}) was overridden such that optimum values of D_{sc} and a first order irreversible viable tissue binding rate constant ($k_{vt/bind}$) were simultaneously fit to three data value types: the total tissue concentration in the viable epidermis, the total dermis concentration and the total urinary excretion (taken to be the amount absorbed). Concentration profile data were not fit, only the total concentration in each of the two viable tissue layers. Solutes analyzed by this method are shown in Figure 6.1. Figure 6.2 shows concentration profile predictions for solutes that did not have absorption data reported. In such analyses, the curve-fitting program was not utilized and fitting was controlled solely by adjusting D_{sc}. Additionally, D_b values of 3×10^{-7} cm/s^2 was used for human data and 3×10^{-8} cm/s^2 for rat data.

6.5 RESULTS

The skin concentration profiles from the literature and our model predictions as shown in Figures 6.1 and 6.2. Figure 6.1 represents solutes where both the model and curve-fitting spreadsheet program were used due to the availability of urine excretion data. Figure 6.2 is representative of the solutes where only the computational model was used to generate the concentration profiles. The parameters calculated by the model for each solute can be found in Tables 6.2 and 6.3. It should be noted that for the literature data calculations, only the regression constant E was deduced from the actual data. The clearance parameters were based on assumptions incorporated into the model and actual values from the model. For permeants that had not attained steady-state conditions, the semi-experimental clearance constants were not calculated.

6.5.1 Methoxsalen (Kammerau et al.)

The concentration profile was well fitted with D_{sc} being the only parameter that was adjusted. The concentrations in the epidermis were under predicted by the model. A regression analysis of the data indicated that steady-state had not been attained.

6.5.2 Triamcinolone Acetonide

Figure 6.2 shows that the model was unable to accurately predict total concentrations in the tissue layers. It should be noted that the results of a regression analysis on the experimental data indicated that steady-state had not been reached.

6.5.3 Flurbiprofen and Ketoprofen

The model significantly under predicted the concentration profiles for both solutes. The predictions were significantly improved when the diffusivity of the stratum corneum was increased by about 50 times, except for flurbiprofen when the solubility in the vehicle was assumed to be 10%. This resulted in a D_{sc} value 500 times larger than the model prediction, which seems highly unrealistic. It should be noted that for ketoprofen, the 4 and 8 hr profiles were considered to be at steady-state, whereas the other concentration profiles were significantly lower than the maximum concentration achieved; hence, they were not considered to be at steady-state. With regards to flurbiprofen, the 2 and 4 hour profiles were considered to be at steady-state.

6.5.4 Econazole

Figure 6.2 shows that the concentration profile was accurately predicted in the epidermis and even more so in the dermis without any need to adjust the diffusivity of the stratum corneum or any other model parameters.

6.5.5 Piroxicam

The model under predicted the concentration profiles; the fit shown could only be achieved with a D_{sc} value 50 times higher than the *a priori* value. At depths approximately greater than 1440 μm, the model predicted a steeper decline in the concentration with depth than shown by the experimental data.

6.5.6 Hydrocortisone and Testosterone (Huber)

The model under predicted the concentration profile for hydrocortisone; the optimum fit was achieved by multiplying D_{sc} by a factor of 30. For testosterone the model under predicted concentrations at depths less than 163 μm, yet at increasing depths, the model was able to make adequate predictions as seen in Figure 6.2. The model also predicted a steeper decline in concentration at depths below 800 μm than shown in the experimental profile. The value of D_{sc} was multiplied by a factor of 3 for the fit shown. It should be noted that the investigators state that a significant variability in skin concentrations were observed between rats.

6.5.7 Methoxsalen (Schaeffer)

D_{sc} was multiplied by a factor of 100 in order to fit the experimental data. Although, the adjusted model slightly overestimated the concentration, it provided an adequate fit. One cannot ignore that D_{sc} was increased significantly. The difference is difficult to understand. It should also be noted that a regression analysis on the experimental data indicated that steady-state had not been attained. It has also been found that other methoxsalen datasets have much lower skin concentrations and do not require a substantial increase in D_{sc} to be consistent with the diffusion model (M. A. Miller, personal communication). This difference could possibly be attributed to the fact that in this experiment, methoxsalen was applied to a site that was to be surgically excised for the presence of tumors.

6.5.8 Desoximetasone

D_{sc} was multiplied by a factor of 20, yet despite this, the model significantly under predicted the concentration profile. Increasing the diffusivity of the stratum corneum depleted the concentration at 100 minutes, which was the experimental time interval; hence the value of D_{sc} was not further increased because doing so did not improve the fit. Furthermore, desoximetasone was applied to a site that was to be surgically excised for the presence of tumors.

6.5.9 Retinoic Acid

D_{sc} was multiplied by a factor of 15. The adjusted model prediction falls within the experimental time points. It should be noted that the fraction unbound calculated by the model using the Yamazaki and Kazaka method was approximately 0.006 which is barely above the minimum allowed by the current model. Additionally, steady-state had not been attained at the experimental time interval according to model calculations. It should be noted that the authors stated that there was evidence of the degradation of the formulation on the surface of the skin, hence it was unknown whether the label measured in the skin corresponded to retinoic acid or a degraded by-product.

6.5.10 Didanosine (Gao and Gupta)

The model under predicted the concentration profile for the Gupta data, yet the slopes of both profiles are in adequate agreement. With respect to the Gao data, the model adequately predicted the concentration profiles. It should be noted that the optimum D_{sc} was 2000 times and 3500 higher than the *a priori* value of the stratum corneum

diffusivity for the Gupta and Gao data, respectively. This optimum D_{sc} indicates that the stratum corneum barrier was almost completely removed in the model in order to achieve the respective concentration profiles. This finding raises the question as to whether the barrier was intact during the in vivo study.

6.5.11 Hydrocortisone (Schaeffer)

Although D_{sc} was multiplied by a factor of 100, the model continued to significantly under predict the solute concentration in the lower skin layers. This was understandable in light of the opinions of Dr. Schaeffer mentioned above. Despite the under predictions of the model, it can be seen that the slopes of both curves are in good agreement with one another.

6.6 DISCUSSION

The number of studies dedicated to permeant transport in the dermis in vivo are limited. Despite this limited availability, such in vivo data are invaluable in determining the efficacy of mathematical models in making adequate predictions for solute skin concentration profiles. Here we analyzed the skin concentration profiles of in vivo data from the literature and compared them to our model predictions as shown in Figures 6.1 and 6.2. Assuming a 1^{st} order clearance in the dermis and the model calculation of k_{de}, k_{free}, D_{de}, the model generates an expected concentration profile based on the physicochemical properties of the permeant. Furthermore experimental conditions for each solute were incorporated into the model, such as concentration of the solute applied,

hydration state of the skin, dermis and epidermis thickness and complete removal of the solute from the surface of the skin at the end of the exposure period.

For most permeants the model predicts a steeper slope and hence a quicker decrease in the skin concentration with depth than the observed data. This is most probably due to the simple assumption built into the model, that clearance is uniformly distributed within the dermis. We recognize that this assumption is oversimplified and that in fact, it does not accurately depict the capillary network distribution physiologically. In Table 6.3, the semi-experimental values for k_{de}^{total} and k_{free}^{blood} are calculated from the slopes of the experimental profiles and assumptions built in the current clearance model. A comparison between the semi-experimental values for k_{de}^{total} and the model predictions indicates that for compounds such as piroxicam, testosterone, flubriprofen and didanosine (Gupta), the values are in good agreement and this can be further observed in the graphical representations shown in Figures 6.1 and 6.2 for these solutes. The values for k_{free}^{blood} also seem to be within adequate agreement except for flurbiprofen, where the semi-experimental value is much higher.

There are several identifiable factors that may be contributing to the overall picture portrayed here. There is no question that the current model is an oversimplification of the actual skin processes occurring during the transdermal delivery of permeants across the skin. Specifically, the lack of shunt pathways, follicular pathways, the oversimplification of the stratum corneum, the lack of data available to construct models to better represent the rat and mouse species, the depiction of the epidermis as unperfused dermis, the over simplification of the complex microcirculatory network found physiologically in the skin and finally the lack of microstructures and proteins present in the dermis that contribute

to the binding of permeants in the dermis. These limitations are not easily addressed due to the complexity of the skin structure and the fact that not all of these processes are completely understood today. Additionally, questions arise regarding the actual experimental concentration profiles. The instability of ^{3}H-hydrocortisone raises the question as to whether this issue applies to other tritiated corticosteroids. Also, the fact that several of the profiles had not attained steady-state raises the question whether the model would have made better predictions had steady-state been achieved. This conjecture can be justified by the fact that in some instances, the model was able to accurately predict the total concentrations achieved in the lower layers of the skin, however, the variation with depth was poorly predicted.

Table 6.1. Physical properties of permeants required by mathematical model.

Permeant	MW	Log K_{oct}[a]	fu	$S_w \times 10^2$ (32°C)[b] (mg/L)	P_{vp} (32°C)[a] torr
Methoxsalen	216.19	2.00	0.09[c]	49.8	5.99E-06
Econazole	381.68	4.48[d]	0.02[e]	124[f]	2.33E-9
Desoximetasone	376.47	2.35	0.15[e]	42.1	9.71E-12
Piroxicam	331.35	3.06	0.02[g]	29.0	8.71E-14
Didanosine	236.23	-1.24	0.95[e]	1.60	6.03 E-10
Testosterone	288.43	3.32	0.30	2.75	5.79E-08
Hydrocortisone	362.47	1.62	0.25	37.6	5.92E-13
Retinoic Acid	300.44	6.30	0.01	0.013	3.09E-07
Triamcinolone Acetonide	434.51	2.53	0.125	2.60[h]	5.90E-14
Flurbiprofen	244.26	4.16	0.01[j]	1.01	9.70E-06
Ketoprofen	254.29	3.12	0.05[j]	6.42	4.08E-06

[a]Experimentally measured values obtained from EPISUITE, Version 4.1, U.S. EPA, 2011 (2011) unless otherwise noted.
[b]Experimentally measured values obtained from EPISUITE, Version 4.1, U.S. EPA, 2011 (2011) and temperature corrected by Jain and Yalkowski's equation (Jain and Yalkowsky 2001) unless otherwise noted.
[c] Obach, 1999
[d]Calculated values obtained from PhysChem Suite 12.0, 2010, Advanced Chemistry Development (2010).
[e] Calculated by the method of Yamazaki and Kanaoka(Yamazaki and Kanaoka 2004), neutral/basic category
[f] Regression on 23, 37˚C experimental values from Cogswell et al., 2006(Cogswell, Berger et al. 2006)
[g] Richardson et al. 1987(Richardson, Blocka et al. 1987)
[h] Regression on 23-50˚C experimental values from the Aquasol database, (Yalkowski 1993)
[j]Kratochwil et al., 2002(Kratochwil, Huber et al. 2002)

Table 6.2 Model calculations for diffusivity of stratum corneum D_{sc}, partition coefficient of stratum corneum K_{sc}, solubility of solute in the stratum corneum C_{sat}, and the amount of solute it takes to saturate the deposition zone in the stratum corneum M_{sat}.

Permeant	Model	$D_{sc} \times 10^{10}$ cm^2/s (fitted)	K_{sc}	C_{sat} mg/cm^3	M_{sat} $\mu g/cm^2$
Methoxsalen Schaffer	Human	23.1	16.09	0.80	0.04
Methoxsalen Kammerau	Human	1.0	16.09	0.80	0.04
Econazole	Human	3.85	82.71	10.24	1.11
Desoximetasone	Human	0.56	21.05	1.58	0.05
Piroxicam (caudal)	Human	5.47	39.59	1.15	0.04
Piroxicam (cranial)		6.43			
Didanosine Gao	Mouse	57.3	1.42	4.24	0.85
Didanosine Gupta	Mouse	6.83	2.24	6.68	5.35
Testosterone	Mouse	11.6	51.87	1.83	0.18
Hydrocortisone	Mouse	0.95	12.20	4.41	0.44
	Human	1.41	12.20	4.41	0.15
Retinoic Acid	Human	3.63	5274.77	0.08	0.01
Triamcinolone Acetonide	Human	0.04	24.40	0.65	0.02
Flurbiprofen	Mouse	314	51	0.52	0.05
Ketoprofen	Mouse	118	15	0.97	0.10

Table 6.3 *In vivo* studies of dermal skin concentrations of topically applied permeants

Permeant	Species	Time[a] min	E cm^{-1}	$D_{de} \times 10^7$ cm^2/s	$k_{de}^{total} \times 10^4$ s^{-1} Semi-experimental	$k_{free}^{blood} \times 10^4$ s^{-1} Semi-experimental	$k_{de}^{total} \times 10^4$ s^{-1} Model	$k_{free}^{blood} \times 10^4$ s^{-1} Model	Ref.
Methoxsalen	Human	100	-	-	-	-	7.56	21.90	[b]
Methoxsalen	Human	300	-	-	-	-	7.56	21.90	[c]
Econazole	Human	90	-	-	-	-	0.79	22.00	[d]
Desoximetasone	Human	1000	7.39	16.95	0.93	1.39	9.93	20.90	[b]
Hydrocortisone	Human	1000	44.05	17.19	33.35	46.30	10.19	13.90	[e]
Retinoic Acid	Human	100	-	-	-	-	0.96	22.00	[e]
Triamcinolone Acetonide	Human	30	-	-	-	-	8.16	20.40	[f]
Piroxicam	Pig (caudal)	720	8.06	13.95	1.15	27.82	2.28	22.00	[g]
	Pig (cranial)		14.11	13.95	2.78	8.78	2.28	22.00	
Didanosine	Rat	360	22.90	27.79	14.69	10.35	5.90	4.11	[h]
Didanosine	Rat	360	10.16	27.79	2.87	1.95	5.90	4.11	[i]
Hydrocortisone	Rat	360	143.11	11.30	231.52	324.78	10.19	13.90	[j]
Testosterone	Rat	360	43.14	6.72	12.50	33.21	8.31	22.00	[j]
Flurbiprofen	Rat	1440	-	-	-	-	1.36	22.00	[k]
		960	-	-	-	-			
		840	-	-	-	-			
		720	-	-	-	-			
		480	-	-	-	-			
		240	41.45	2.14	3.68	75.01			
		120	50.78	2.14	5.53	172.22			
		60	-	-	-	-			
Ketoprofen	Rat	1440	-	-	-	-	4.81	22.00	[k]
		960	-	-	-	-			
		840	-	-	-	-			
		720	-	-	-	-			

480	36.35	4.95	6.54	30.56
240	47.53	4.95	11.19	53.54
120	-	-	-	-

The concentration data is shown in Figs. 6.1 and 6.2. Regression constant E represents the slope (regression not shown in Figs 6.1 and 6.2). D_{de} was derived from Equations found in Chapter 5 and k_{de}^{total} (Semi-experimental) was calculated from the slope E, using Eq. (6.1). k_{free}^{blood} (Semi-Experimental) was calculated from k_{de}^{total} using Equations from Chapter 5. k_{de}^{total} (model) and k_{free}^{blood} (model) were calculated the same Equations found in Chapter 5. .

[a] Time of tissue collection post-dose application
[b] (Schaefer, Stuttgen et al. 1978)
[c] (Kammerau, Zesch et al. 1975)
[d] (Schaefer and Stuttgen 1976)
[e] (Zesch and Schaefer 1975)
[e] (Schaefer and Zesch 1975)
[f] (Schaefer, Zesch et al. 1977)
[g] (Monteiro-Riviere, Inman et al. 1993)
[h] (Gao, Wientjes et al. 1995)
[i] (Gupta, Wientjes et al. 1995)
[j] (Hueber, Wepierre et al. 1992)
[k] (Goi, Morishita et al. 2010)

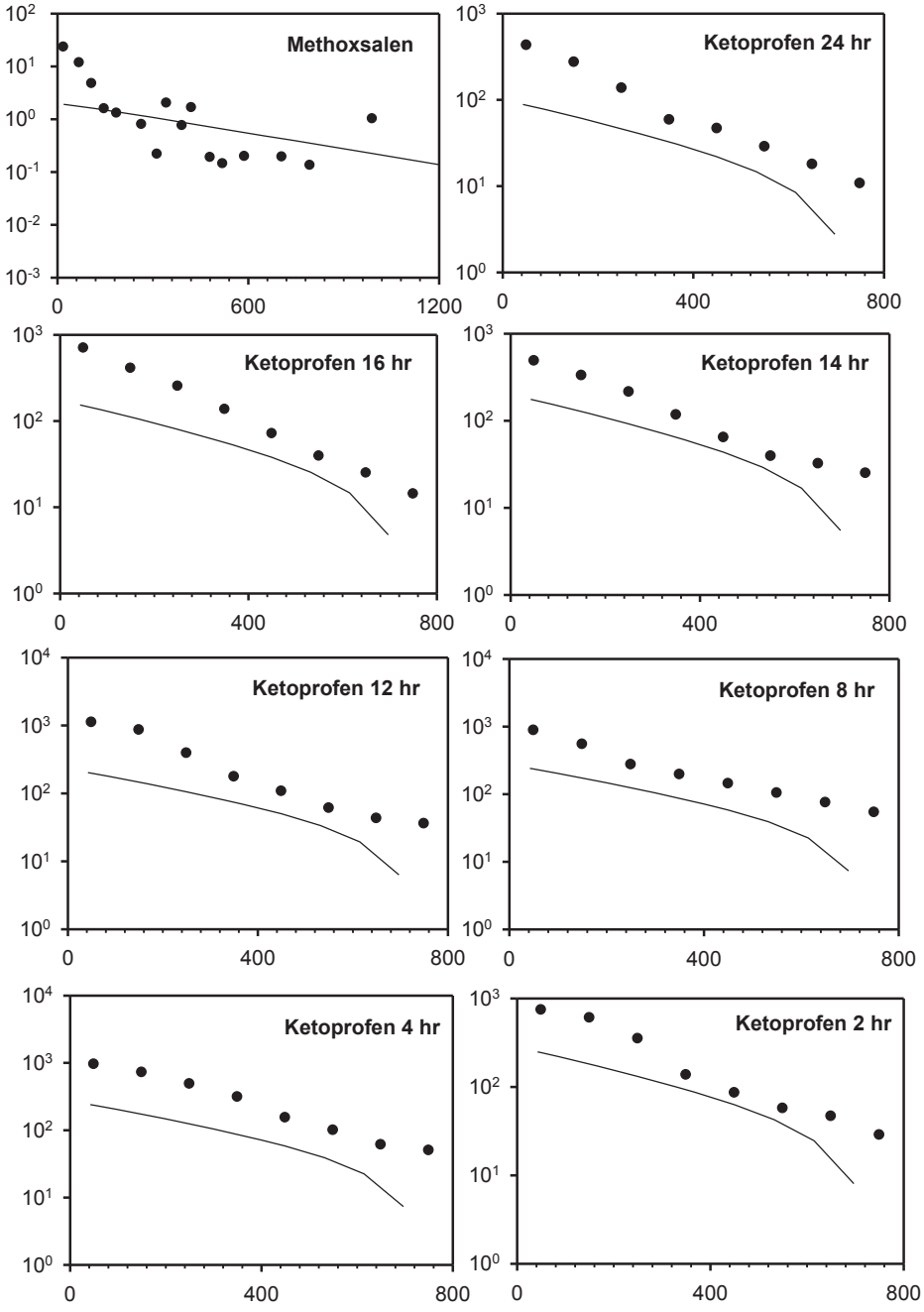
Methoxsalen
Ketoprofen 24 hr
Ketoprofen 16 hr
Ketoprofen 14 hr
Ketoprofen 12 hr
Ketoprofen 8 hr
Ketoprofen 4 hr
Ketoprofen 2 hr

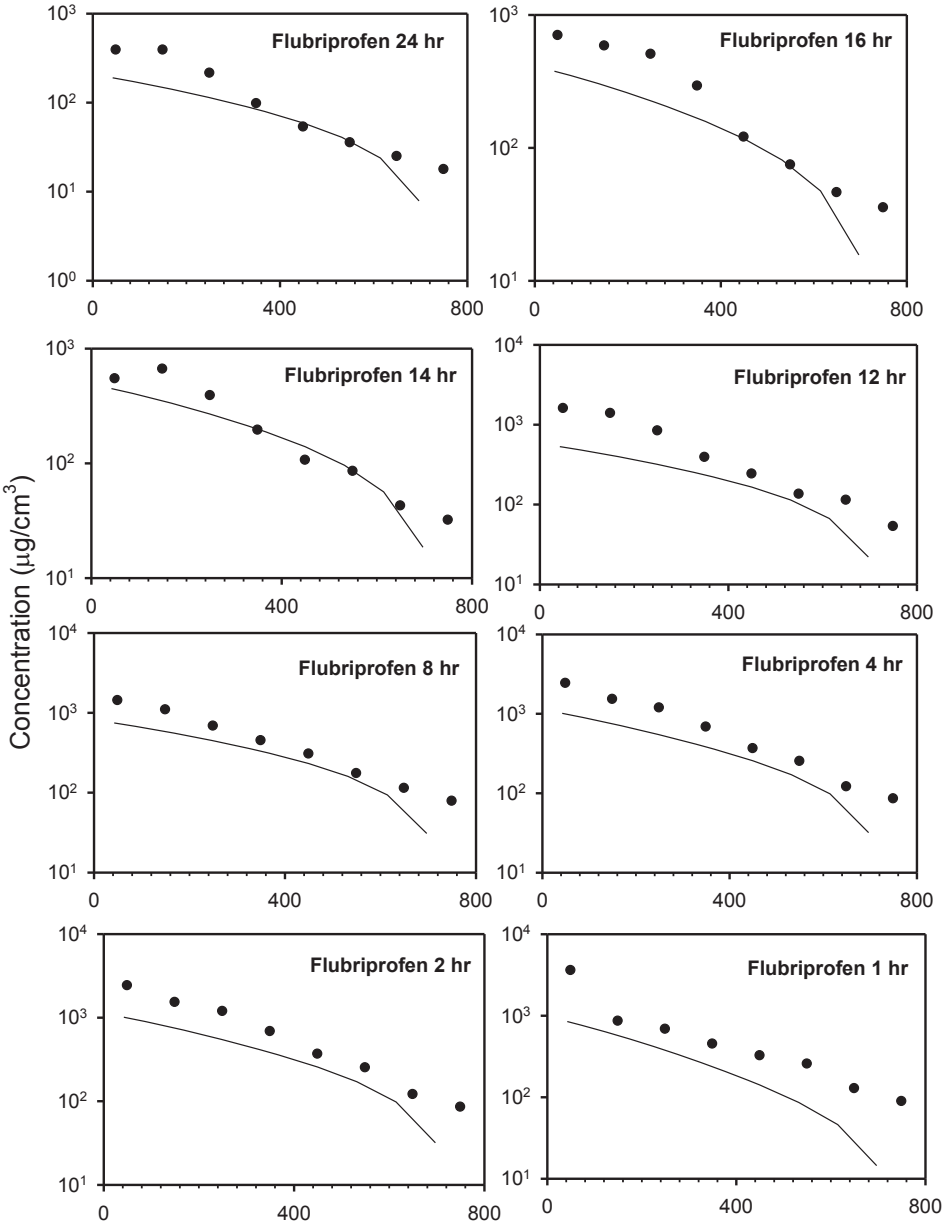
Flubriprofen 24 hr
Flubriprofen 16 hr
Flubriprofen 14 hr
Flubriprofen 12 hr
Flubriprofen 8 hr
Flubriprofen 4 hr
Flubriprofen 2 hr
Flubriprofen 1 hr
Concentration (μg/cm3)
0
400
800

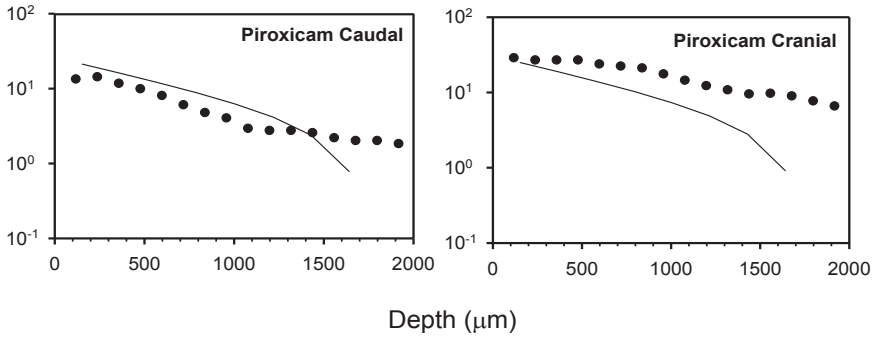

Figure 6.1. *In vivo* skin concentration profiles for permeants with skin concentration profiles and urinary excretion data (not shown) listed in Table 6.3. The scatter plot represents the experimental data and the solid line represents the model prediction at the experimental time interval.

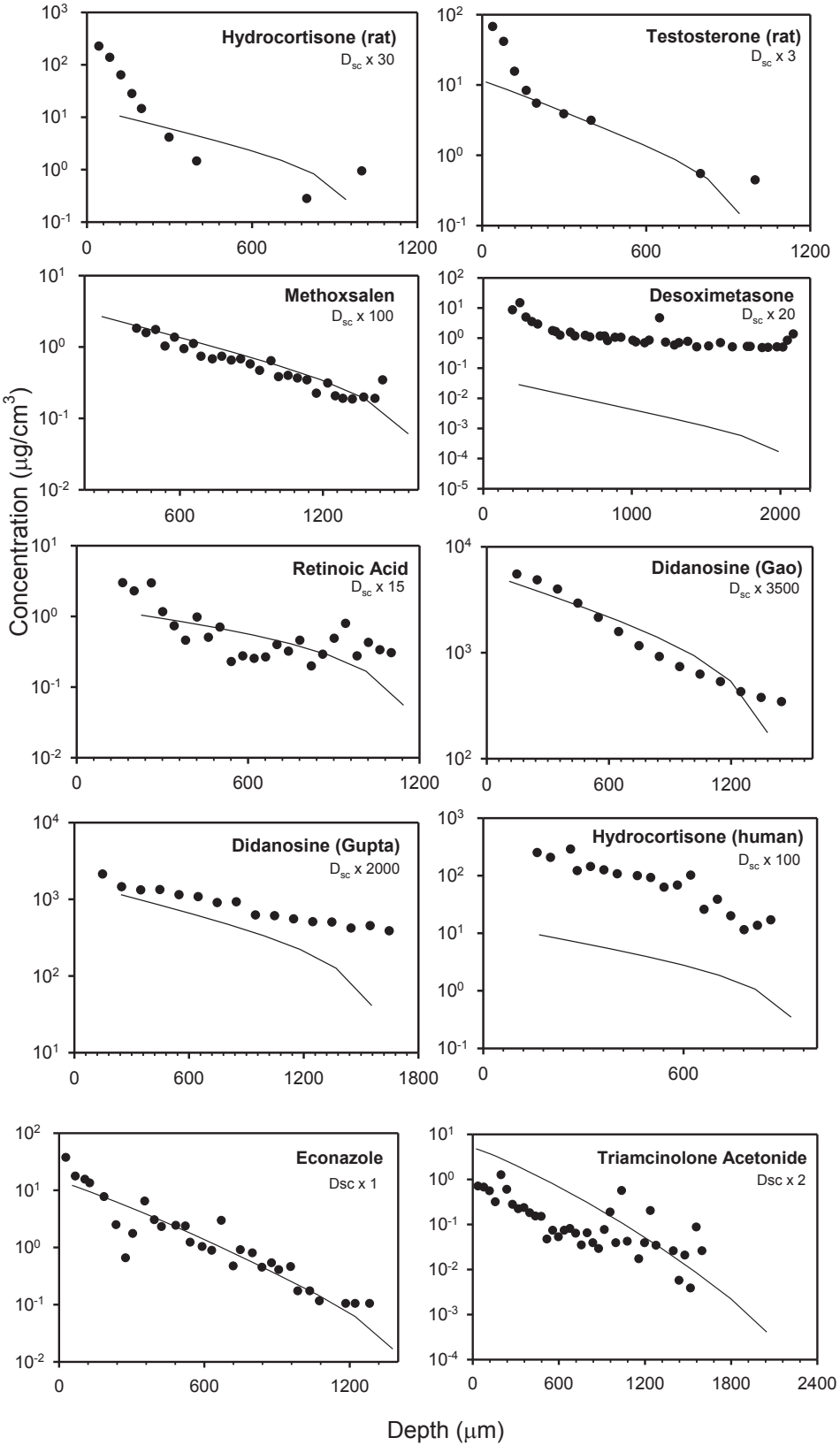
Hydrocortisone (rat)
D_{sc} x 30
Testosterone (rat)
D_{sc} x 3
Methoxsalen
D_{sc} x 100
Desoximetasone
D_{sc} x 20
Retinoic Acid
D_{sc} x 15
Didanosine (Gao)
D_{sc} x 3500
Didanosine (Gupta)
D_{sc} x 2000
Hydrocortisone (human)
D_{sc} x 100
Econazole
Dsc x 1
Triamcinolone Acetonide
Dsc x 2
Concentration (μg/cm^3)
Depth (μm)

Figure 6.2. *In vivo* skin concentration profiles for permeants with no urinary excretion data listed in Table 6.3. The scatter plot represents the experimental data and the solid line represents the model prediction at the experimental time interval.

7. CONCLUSIONS AND RECOMMENDATIONS

The use of predictive models in the field of dermal risk assessment for topically applied solutes is of great importance in several industries. The development of these models stems from both experimental data and theory. Experimental data are used to calibrate the models; hence, the quality of the data used is of high importance. The objective of this investigation was to improve upon the experimental procedures used to study the transport of solutes across the dermis and also improve the theory as implemented in the dermis portion of the current three-layer skin diffusion model.

With regards to in vitro methods, our hypothesis was that the traditional experimental techniques were inadequate for highly protein bound solutes. We postulated that the transport parameters calculated for such solutes would be incorrect if soluble proteins present in the dermis tissue were allowed to diffuse out the tissue and into the donor compartments of side-by-side diffusion cells. The binding of the test solute to these soluble proteins would lead to lower available concentration. Three solutes with varying lipophilicities were studied -- DEET, diclofenac and parathion. A new experimental technique utilizing a dialysis membrane placed in series with the dermis tissue was compared to the traditional technique where the dermis tissue is placed between both compartments. The results of the study showed that for a moderately lipophilic compound such as DEET, the presence of the dialysis membrane had no significant effect on the measured values of the transport parameters. However, for the highly protein bound solutes diclofenac and parathion, significant differences in both diffusivity D_{de} and partition coefficient K_{de} were observed in the presence and absence of the dialysis membrane. The differences observed were more pronounced for diclofenac, and were in a

direction such that the calculated values of D_{de} and K_{de} were significantly higher in the presence of the membrane. For parathion, D_{de} was significantly higher and K_{de} was significantly lower in the presence of the membrane. Additionally, we further established the hypothesis of soluble proteins diffusing from the dermis tissue into the diffusion cell donor compartments by conducting protein assay studies in the donor solutions of cells containing excised human dermis. The results showed that the total amount of protein present in the donor compartment in the presence of the dialysis membrane was lowered by a factor ranging from 8 to 24 compared to values without dialysis membrane. We conclude that, for solutes that are more than 87% bound to soluble proteins, a dialysis membrane should be utilized in transport studies.

In the second part of this investigation, the dermal clearance calculation within the three-layer skin diffusion model was revised to make better predictions of skin concentrations of very hydrophilic and very lipophilic, low molecular weight skin permeants. Previously, capillary permeability was described by a simple relationship based on the Potts-Guy equation to represent membrane permeability. This relationship was adequate for small, moderately lipophilic permeants. Since small lipophilic compounds are often highly bound to proteins it was important to include dermal clearance mechanisms for both small and large solutes into the model.

The blood capillary component employed a two-slit theory with contributions from both small (10 nm) and large (50 nm) slits. The lymphatic component was based on previously reported clearance measurements of dermal and subcutaneous injections of ^{131}I-albumin in humans. Model parameters were fit to both blood capillary permeability data and lymphatic clearance data. Small molecules were cleared largely by the blood and

large molecules by the lymph. Implementation of the revised clearance model showed a crossover behavior at approximately 29 kDa, which was in acceptable agreement with the reported value of 16 kDa. Furthermore, the clearance of small hydrophilic solutes with low binding affinities to proteins was adequately described by the model when compared to the blood capillary clearance data reported by Renkin. The clearance of these solutes is predominately controlled by the size of the permeant. In conclusion, the mechanism of dermal clearance for both small and large solutes was adequately modeled using a two-slit theory model for the blood capillary component and a constant clearance for the lymphatic component. A comparison with literature data shows that the revised model makes adequate predictions for both large and small solutes.

Finally, the revised computational model was utilized to make predictions for *in vivo* skin concentration data reported in the literature. Two types of analyses were employed based upon the available reported data. All data were analyzed using the revised computational model, however, for solutes for which absorption data were reported, an additional a curve-fitting spreadsheet which took into account both skin concentration profiles and absorption profiles in urine was employed. For most permeants the model predicted a steeper slope and hence a more rapid decrease in the skin concentration with depth than the observed data. This was most probably due to the simple assumption built into the model, that clearance is uniformly distributed within the dermis. For most permeants, diffusivity within the stratum corneum D_{sc} was adjusted by upward in order to match the experimental data. The complexity of comparing the model predictions to the *in vivo* data is thought to arise from several identifiable contributing factors including the reliability of the experimental data and the lack of follicular and polar diffusion pathways in the

model. Other contributing factors may be the oversimplification of the stratum corneum portion of the model, the depiction of the epidermis as unperfused dermis, the over simplification of the complex microcirculatory network and finally the lack of microstructures and proteins present in the dermis that contribute to the binding of permeants in the dermis. These limitations are not easily addressed due to the complexity of the skin structure and the fact that not all of these processes are completely understood today. This conjecture can be justified by the fact that in some instances the model predicted the concentration profile accurately, in others it was able to accurately predict the total concentrations achieved in the lower layers of the skin, but the variation with depth was poorly predicted.

Further improvement of the predictive abilities of the revised computational model should be achievable by addressing some of the limitations described above. Developing a more realistic representation of the distribution of the microcirculatory network would potentially improve the ability to make better predictions of skin concentration with depth. Also, improving the quantification of binding in the dermis would enhance the predictive capabilities of the model, especially in instances where the current model underpredicts the amount of solute present in the dermis. The current model assumes that most binding occurs to albumin, an assumption which published literature shows is not completely accurate. The incorporation of binding substrates such as collagen and other proteins would improve this aspect of the model. A less simplified representation of the stratum corneum would also play a big role in the improvement of the current computational model. The development of these predictive models is still progressing.

The introduction of polar pathways, shunt pathways and follicular pathways would present a more complete picture of transport across the stratum corneum and hence improve the predictive ability of the model.

The importance of adequate predictive models to describe the transport of topically applied permeants continues to be a pressing need in the field of dermal risk assessment. The objective of this work was to gain a step closer in attaining a more realistic depiction of the model as well as develop better methods for determining parameters that are ultimately used to calibrate such models. This work, clearly demonstrated that the current experimental methodologies used in the determination of transport parameters for highly protein bound solutes are inaccurate. In turn we have provided an improved in vitro methodology which reduces this inaccuracy. Furthermore, to our knowledge there are no models describing the clearance of macromolecules and highly protein bound solutes. We have introduced a model that is more closely related to the physiology of blood capillaries, as well as a lymphatic clearance portion that contributes and at times dominates the clearance of macromolecules and highly protein bound solutes. The significance of this work is the presentation of a predictive model that can describe the clearance of a wider spectrum of solutes and can be applied within its current limitations to the field of dermal risk assessment.

As we better understand the skin and the complex processes involved in transport of topically applied solutes and as more data become available, the predictive power of these models will increase.

8. REFERENCES

(2010). ACD PhysChem Suite. Toronto, Ontario, Canada, Advanced Chemistry Development**:** Estimation Programs Interface Suite™ for Microsoft® Windows.

(2011). Estimation Programs Interface Suite™ Washington, DC, USA, U.S. Environmental Protection Agency**:** for Microsoft® Windows.

Adamson, R. H. (1993). "Microvascular endothelial cell shape and size in situ." Microvasc Res **46**: 77-88.

Albery, W. J. and J. Hadgraft (1979). "Percutaneous absorption: theoretical description." J Pharm Pharmacol **31**: 129-139.

Altshuler, G., M. Smirnov, et al. (2005). "Lattice of optical islets: a novel treatment modality in photomedicine " J Phys D: Appl Phys **38**: 2732-2747.

Anderson, J. L. (1981). "Configurational effect on the reflection coefficient for rigid solutes in capillary pores." J Theor Biol **90**: 405-426.

Ash, R., R. M. Barrer, et al. (1965). "Diffusion in multiple laminates." British Journal of Applied Physics **16**: 873-884.

Audus, K. L. and R. T. Borchardt (1991). "Transport of macromolecules across the capillary endothelium." Handbook Exp Pharmacol **100**: 2842-2848.

Bach, C. and G. P. Lewis (1973). "Lymph flow and lymph protein concentration in the skin and muscle of the rabbit hind limb." J Physiol **235**: 477-492.

Basketter, D. A., C. Pease, et al. (2007). "Skin sensitisation and epidermal disposition. The relevance of epidermal bioavilability for sensitisation hazard indetification/risk assessment." ATLA **35**: 137-154.

Beck, R. E. and J. S. Schultz (1972). "Hindrance of solute diffusion within membranes as measured with microporous membranes of known pore geometry." Biochimica Biophysica Acta **255**: 273-303.

Berg, B. M., M. Nieuwdorp, et al. (2006). "Glycocalyx and Endothelial (dys) Function from Mice to Men." Pharmacological reports **58**: 75-80.

Berner, B. and E. R. Cooper (1987). Models of skin permeability. Boca Raton, FL, CRC Press.

Bert, J., J. M. Mathieson, et al. (1982). "The exclusion of human serum albumin by human dermal collagenous fibres and within huma dermis." Biochem J **201**: 395-403.

Bert, J., R. H. Pearce, et al. (1986). "Concentration of plasma albumin in its accessible space in postmortem human dermis." Microvasc Res **32**: 211-223.

Bill, A. (1979). "Regional lymph flow in unanesthetized rabbits." Upsala J Med Sci **84**: 129-136.

Blancato, J. N. and N. Chiu (1994). Use of pharmacokinetic models of estimate internal dose exposure. Water contamination and health integration of exposure assessment =, toxicology and risk assessment. R. M. Wang. New York, Marcel Dekker Inc.

Bocci, V., M. Muscettola, et al. (1986). "The lymphatic route-II. Pharmacokinetics of human recombinant interferon-alpha$_2$ injected with albumin as a retarder in rabbits." Gen Pharmacol **17**: 93-96.

Braverman, I. M. and A. Yen (1977). "Ultrastructure of the humand dermal microcirculation. II. The capillary loops of the dermal papillae." J Invest Dermatol **68**: 44-52.

Brown, H. S. and D. Hattis (1989). "The role of skin absorption as a route of exposure to volatile organic compounds in household tap water: a simulated kinetic approach." J Am Coll Toxicol **8**: 839-851.

Bundgaard, M. and J. Frokjaer-Jensen (1982). "Functional aspects of the ultrastructure of terminal blood vessels: a qualitative study on consecutive segments of the frog mesenteric microvasculature." Microvasc Res **23**: 1-30.

Bunge, A. L., R. L. Cleek, et al. (1995). "A new method for estimating dermal absorption from chemical exposure.3. Compared with steady-state methods for prediction and data analysis." Pharmaceutical Research **12**: 972-982.

Bunge, A. L., G. L. Flynn, et al. (1994). "Predictive model for dermal exposure assessment."

Chambers, R. and B. W. Zweifach (1947). "Intercellular cement and capillary permeability." Physiol Rev **27**(3): 436-463.

Chary, S. R. and R. K. Jain (1989). "Direct measurement of interstitial convection and diffusion of albumin in normal and neoplastic tissues by fluorescence photobleaching." Proceedings of the National Academy of Sciences, USA **86**: 5385-5389.

Chinery, R. L. and A. K. Gleason (1993). "A compartmental model for the prediction of breath concentration and absorbed dose of chloroform after exposure while shwoering." Risk Anal **13**: 51-62.

Cleek, R. L. and A. L. Bunge (1993). "A new method for estimating dermal absorption from chemical exposure.1. General approach." Pharmaceutical Research **10**: 497-506.

Cleek, R. L. and A. L. Bunge (1993). "A new method for estimating dermal absorption from chemical exposure. 1. General approach." Pharmaceutical Research **10**(4): 497-506.

Cogswell, S., S. Berger, et al. (2006). "A Parenteral Econazole Formulation Using a Novel Micelle-to-Liposome Transfer Method: <i>In Vitro</i> Characterization and Tumor Growth Delay in a Breast Cancer Xenograft Model." Pharmaceutical Research **23**(11): 2575-2585.

Cross, S., B. M. Magnusson, et al. (2003). "Determination of the effect of lipophilicity on the in vitro permeability and tissue reservoir characteristics of topically applied solutes in human skin layers." Journal of Investigative Dermatology **120**: 759-764.

Cross, S., B. M. Magnusson, et al. (2003). "Determination of the effect of lipophilicity on the in vitro permeability and tissue resevoir characteristics of topically applied solutes in human skin layers." J Invest Dermatol **120**: 759-764.

Cross, S. E., Y. G. Anissimov, et al. (2003). "Bovine-serum-albumin-containing receptor phasse better predicts transdermal absorption parameters for lipophilic compounds " J Invest Dermatol **120**(589-591).

Cross, S. E. and M. S. Roberts (1993). "Subcutaneous absorption kinetics and local tissue distribution of interferon and other solutes." J Pharm Pharmacol **45**: 606-609.

Cross, S. E. and M. S. Roberts (2006). Dermal blood flow, lymphatics, and binding as determinates of topical absorption, clearance and distribution. Dermal absorption models in toxicology and pharmacology. J. E. Riviere. Boca raton, CRC Press**:** 251-282.

Curry, F. E. (1983). Mechanics and thermodynamics of transcapillary exhange. In: Handbook of physiology, the cardiovascular system. Microcirculation. Bethesda, MD, American Physiological Society.

Curry, F. E. (1983). Mechanics and thermodynamics of transcapillary exhange. In: Handbook of Physiology, the Cardiovascular System. Microcirculation. Bethesda, MD, American Physiological Society. **4:** 309-374.

Curry, F. E. (2005). "Microvascular Solute and Water Transport." Microcirculation **12**: 17-31.

Curry, F. E. and C. C. Michel (1980). "A fiber matrix model of capillary permeability." Microvasc Res **20**: 96-99.

Cussler, E. L. (1997). Diffusion: Mass Transfer in Fluid Systems. Cambridge, Cambridge University Press.

Cussler, E. L. (1997). Diffusion: mass transfer in fluid systems. NY, Cambridge University Press.

Dabareiner, R. M., N. A. White, et al. (2005). "Effects of carolina rinse solution, dimethyl sulfoxide, and the 21-aminosteroid, U-74389G, on microvascular permeability and morphology of the equine jejunum after low-flow ischemia and reperfusion." Am J Vet Res **66**: 525-536.

Dancik, Y., M. A. Miller, et al. (2012). "Design and performance of a spreadsheet-based model for estimating bioavailability of chemicals from dermal exposure " Advanced Drug Delivery Reviews **in press**.

Danielli, J. F. (1940). "Capillary permeability and oedema in the perfused frog." J Physiol **98**: 109-129.

Dechadilok, P. and W. M. Deen (2006). "Hindrance factors for diffusion and convection in pores." Ind Eng Chem Res **45**(24): 6953-6959.

Deen, W. M. (1987). "Hindered transport of large molecules in liquid-filled pores." AIChEJ **33**(9): 1409-1425.

Ellis, J. P., R. Marks, et al. (1970). "Lymphatic function: the disappearance rate of ^{131}I-albumin from the dermis." Brit J Dermatol **82**: 593-599.

Ellis, J. P., R. Marks, et al. (1970). "Lymphatic function: the disapperance rate of ^{131}I-albumin from the dermis." Br J Derm **82**: 593-599.

Ellis, J. P., R. Marks, et al. (1970). "Lymphatic Function: The Disapperance Rate of ^{131}I Albumin from the Dermis." Br J Derm **82**: 593-599.

Enhanced_Medical_Decisions (2009). DoubleCheckMD.

Fardet, A., C. Hoebler, et al. (1998). "Restricted bovine serum albumin diffusion through the protein network of pasta." Journal of Agricultural and Food Chemistry `**46**: 4635-4641.

Fardet, A., C. Hoebler, et al. (1998). "Restricted bovine serum albumin diffusion throught the protein network of pasta." J Agric Food Chem **46**: 4635-4641.

Fedorowicz, A., M. A. Milller, et al. (2011). Finite dose skin permeation calculator, NIOSH.

Fernandez, M. J., W. T. Davies, et al. (1983). "Lymphatic flow in humans as indicated by the clearance of ^{125}I-labeled albumin from the subcutaneous tissue of the leg." J Surg Res **35**: 101-104.

Flessner, M. F. (2008). "Endothelial glycocalyx and the peritoneal barrier." Perit Dial Int **28**: 6-12.

Flynn, G. L. (1990). Physicochemical determinants of skin absorption. Principles of route-to-route extrapolarion for risk assessmemt. T. R. Gerrity and C. J. Henry. New York, Elsevier**:** 93-127.

Friedli, G.-L. (1996). Interaction of deamidated soluble wheat protein (SWP) with other food proteins and metals. Surrey, UK, University of Surrey. **PhD**.

Gabel, J. C. and R. E. Drake (1979). "Pulmonary capillary pressure and permeability." Crit Care Med **7**(9): 92-97.

Gao, X., M. G. Wientjes, et al. (1995). "Use of Drug Kinetics in Dermis to Predict In Vivo Blood Concentration after Topical Application." Pharmaceutical Research **12**: 2012-2017.

Garlick, D. G. and E. M. Renkin (1970). "Transport of large molecules from plasma to interstitial fluid and lymph in dogs." Am J Physiol **219**(6): 1595-1605.

Goi, N., K. Morishita, et al. (2010). "Evaluation of percutaneous permeation of flurbiprofen and ketoprofen after application of transdermal patches using a lateral sectioning approach in hairless rats." Pharmaceutical Development and Technology **16**(6): 658-665.

Grams, Y. Y., S. Alaruikka, et al. (2003). "Permeant lipophilicity and vehicle composition influence accumulation of dyes in hair follicles of human skin." Eur J Pharm Sci **18**(329-336).

Grams, Y. Y. and J. A. Bouwstra (2002). "Penetration and distribution of three lipophilic probes in vitro in human skin focusing on the hair follicle." J Control Releas **83**: 253-262.

Gupta, E., M. G. Wientjes, et al. (1995). "Penetration kinetics of 2'3'-dideoxyinosine in dermis is described by the distributed model." Pharmaceutical Research **12**: 108-112.

Guy, R. H. and J. Hadgraft (1985). "Transdermal drug delivery: a simplified pharmacokinetic approach." Int J Pharma **24**: 267-274.

Guy, R. H. and J. Hadgraft (1988). "Physicochemical aspects of percutaneous penetration and its enhancement." Pharmaceutical Research **5**(12): 753-758.

Guy, R. H., J. Hadgraft, et al. (1982). "A pharmacokinetic model for percutaneous absorption." Int J Pharma **11**: 119-129.

Hansen, S., A. Henning, et al. (2008). "In-silico model of skin penetration based on experimentally determined input parameters. Part I: experimental determination of partition and diffusion coefficients." Eur J Pharm BioPharm **68**: 267-274.

Happel, J. and H. Brenner (1973). Low Reynolds Number Hydrodynamics. Lyden, The Netherlands, Noordhoff International.

Harake, B. and G. G. Power (1986). "Thoracic duct lymph flow: a comparative study in newborn and adult sheep." J Develop Physiol **8**: 87-95.

Harake, B. and G. G. Power (1986). "Thoracic duct lymph flow: a comparitive study in newborn and adult sheep." J Develop Physiol **8**: 87-95.

Hardman, J. G., L. E. Limbird, et al. (2001). Goodman and Gilman's the Pharmacological Basis of Therapeutics. New York, NY, McGraw Hill.

Havas, E., T. Parviainen, et al. (1997). "Lymph flow dynamics in exercising human skeletal muscle as detected by scintigraphy." J Physiol **504**: 233-239.

Hayduk, W. and H. Laudie (1974). "Prediction of diffusion coefficients for nonelectrolytes in dilute aqueous solutions." Am Inst Chem Eng J **20**(3): 611-615.

Higaki, K., M. Asai, et al. (2002). "Estimation of intradermal disposition kinetics of drugs:II. Factors determining penetration of drugs from viable skin to muscular layer." Int J Pharma **239**: 129-141.

Hollander, W., P. Reilly, et al. (1961). "Lymphatic flow in human subjects as indicated by the disappearance of I^{131}-albumin from the subcutaneous tissue." J Clin Invest **40**: 222-233.

Hollander, W., P. Reilly, et al. (1961). "Lymphatic Flow in Human Subjects as Indicated by the Disapperance of I^{131}-Albumin from the Subcutaneous Tissue." J Clin Invest **40**: 222-233.

Hu, X. and S. Weinbaum (1999). "A new view of Starling's hypothesis at the microstructural level." Microvasc Res **58**(3): 281-304.

Hueber, F., J. Wepierre, et al. (1992). "Role of transepidermal and transfollicular routes in percutaneous absorption of hydrocortisone and testosterone: in vivo study in the hairless rat." Skin Pharmacology **5**: 99-107.

Ibrahim, R. and G. B. Kasting (2010). "Improved method for determining partition and diffusion coefficients in human dermis." Journal of Pharmaceutical Sciences **99**(12): 4928-4939.

Illel, B., H. Schaefer, et al. (1991). "Follicles play an important role in percutaneous absorption." J Pharm Sci **80**: 424-427.

Imayama, S. (1981). "Scanning and Transmission Electron-Microscope Study on the Terminal Blood-Vessels of the Rat Skin." Journal of Investigative Dermatology **76**(3): 151-157.

Imayama, S. (1981). "Scanning and transmission electron-microscope study on the terminal blood-vessels of the rat skin." J Invest Dermatol **76**(3): 151-157.

Jacobsson, S. and I. Kjellmer (1964). "Flow and protein content of lymph in resting and exercising skeletal muscle." Acta Physiol Scand **60**: 278-285.

Jain, N. and S. H. Yalkowsky (2001). "Estimation of the aqueous solubility I: Application to organic nonelectrolytes." Journal of Pharmaceutical Sciences **90**(2): 234-252.

Joory, K. D. (2004). "OC15 Lymphatic vessel distribution in human skin." Microcirculation **11**(6): 534.

Kammerau, B., A. Zesch, et al. (1975). "Absolute concentrations of dithranol and triacetyl-dithranol in the skin layers after local treatment: in vivo investigations with four different types of pharmaceutical vehicles." J Invest Dermatol **64**: 145-149.

Kasting, G. B., M. Miller, et al. (2008). "A spreadsheet-based method for estimating the skin disposition of volatile compounds: application to N,N-diethyl-m-toluamide (DEET)." Journal of Occupational and Environmental Hygiene **10**: 633-644.

Kasting, G. B., M. Miller, et al. (2008). "A spreadsheet-based method for estimating the skin disposition of volatile compounds: application to N,N-diethyl-m-toluamide (DEET)." J Occup Environ Hyg **10**: 633-644.

kasting, G. B., M. A. Miller, et al. (2008). Absorption and evaporation of volatile compounds applied to skin. Dermatologic, Cosmeceutic and Cosmetic Development. K. A. Walters and M. S. Roberts. New York, Informa Healthcare**:** 385-400.

Kasting, G. B., R. L. Smith, et al. (1992). Prodrugs for dermal delivery: solubility, molecular size, and functional group effects. Prodrugs: topical and ocular drug delivery. K. B. Sloan. New York, Marcel Dekker.

Kasting, G. B., R. L. Smith, et al. (1987). "Effect of lipid solubility and molecular size on percutaneous absorption." Pharmacol Skin **1**: 138-153.

Kedem, O. and A. Katchalsky (1958). "Thermodynamic analysis of the permeability of biological membranes to non-electrolytes." Biochim Biophys Acta **27**: 229-246.

Khakpour, M. and K. Vafai (2008). "Critical assessment of arterial transport models." Int J Heat Mass Transfer **51**: 807-822.

Khalil, E., K. Kretsos, et al. (2006). "Glucose partition coefficient and diffusivity in the lower skin layers." Pharmaceutical Research **23**: 1227-1234.

Khalil, E., K. Kretsos, et al. (2006). "Glucose partition coefficient and diffusivity in the lower skin layers." Pharmaceutical Research **23**(6): 1227-1234.

Kilgman, A. M. and E. Christophers (1963). "Preparation of isolated sheets of human startum corneum." Arch Dermatol **88**: 702-705.

Kligman, A. M. and E. Christophers (1963). "Preparation of isolated sheets of human stratum corneum." Archives of Dermatology **88**: 702-705.

Klitzman, B. and B. R. Duling (1979). "Microvascular hematocrit and red cell flow in resting and contracting striated muscle." Am J Physiol **237**: H481-490.

Kratochwil, N. A., W. Huber, et al. (2002). "Predicting plasma protein binding of drugs: a new approach." Biochemical Pharmacology **64**: 1355-1374.

Kretsos, K. and G. B. Kasting (2005). "Dermal capillary clearance: physiology and modeling." Skin Pharmacol Physiol **18**: 55-74.

Kretsos, K., G. B. Kasting, et al. (2004). "Distributed diffusion-clearance model for transient drug distribution within the skin." J Pharm Sci **93**: 2820-2835.

Kretsos, K., M. A. Miller, et al. (2008). "Partioning, diffusivity and clearance of skin permeants in mammalian dermis." Int J Pharma **346**: 64-79.

Kretsos, K., M. A. Miller, et al. (2008). "Partitioning, diffusivity and clearance of skin permeants in mammalian dermis." Int J Pharm **346**: 64-79.

Kretsos, K., M. A. Miller, et al. (2008). "Partitioning, diffusivity and clearance of skin permeants in mammalian dermis." International Journal of Pharmaceutics **346**(1-2): 64–79.

Kruse, J., D. Golden, et al. (2007). "Analysis, interpretation, and extrapolation of dermal permeation data using diffusion-based mathematical models." J Pharm Sci **96**(3): 682-703.

Kubota, K. and H. I. Maibach (1992). "A compartment model for percutaneous absoprtion: compatibility of lag time and steady-state flux with diffusion model." J Pharm Sci **8**: 863-865.

Kubota, K. and H. I. Maibach (1994). "Significance of viable skin layers in percutaneous permeation and its implication in mathematical models: theoretical consideration based on parameters for betamethasone 17-valerate." J Pharm Sci **83**: 1300-1306.

Laine, G. A., S. J. Allen, et al. (1987). "Outflow pressure reduces lymph flow rate from various tissues." Microvasc Res **33**: 135-142.

Landis, E. M. and J. R. Pappenheimer (1963). Exchange of substances through the capillary wall. Handbook of Physiology: Sect. 2; Circulation. Washington, DC, Am Physiol Soc. **II:** 961-1034.

Lesser, K. A. (1871). "Eine methode um grosse lymphmengen vom lebenden hunde zu gewinnen. Berichte über die verhandlungen der königlich schsischen gesellschaft der wissenschaften zu leipzig. ." Mathematisch-Physische Classe **23**: 590-616.

Leu, A., H. MJW., et al. (2001). "Measurement of the lymphatic clearance of the human skin using a fluorescent tracer." J Vascular Res **38**: 423-431.

Levick, J. R. and C. C. Michel (2010). "Microvascular fluid exchange and the revised starling principal." Cardiovascular Research.

Levick, J. R. and C. C. Michel (2010). "Microvascular fluid exchange and the revised Starling principle." Cardiovascular Res **87**: 198-210.

Liu, P., W. I. Higuchi, et al. (1994). "Transport of beta-estradiol in freshly excised human skin in vitro: diffusion and metabolism in each skin layer." Pharmaceutical Research **11**: 1777-1786.

Luft, J. H. (1966). "Fine structure of capillary and endocapillary layer as revealed by ruthenium red." Federation Proc **25**: 1773.

McCarley, K. D. and A. L. Bunge (1998). "Physiologically relevant one-compartment pharmacokinetic models for skin. 1. Development of models." J Pharm Sci **87**: 470-481.

McCarley, K. D. and A. L. Bunge (2001). "Pharmacokinetic models for dermal absorption." J Pharm Sci **90**: 1669-1719.

McDougal, J. N., G. W. Jepson, et al. (1986). "A physiological pharmacokinetic model for dermal absorption of vapors in the rat." Toxicol Appl Pharmacol **85**: 286-294.

McKone, T. E. (1993). "Linking a PBPK model for chloroform with measured breath concentrations in showers: implications for dermal exposure models." J Exp Anal Environ Epidemiol **3**: 339-365.

Mehta, S. C., M. I. Afouna, et al. (1997). "Relationship of skin target site free drug concentration (C*) to the in vivo efficacy: an extensive evaluation of the predictive value of the C*concept using acyclovir as a model drug." J Pharm Sci **86**: 797-801.

Michaels, A. S., K. Chandrasekaran, et al. (1975). "Drug permeation through human skin: theory and in vitro experimental measurement." AIChE **21**(5): 985-996.

Michel, C. C. and F. E. Curry (1999). "Microvascular permeability." Physiol Rev **79**: 703-761.

Miller, M. A., V. A. Bhatt, et al. (2006). "Absorption and Evaporation of Benzyl Alcohol from Skin." J Pharm Sci **95**(2): 281-291.

Modi, S., A. W. B. Stanton, et al. (2005). "Regional distribution of epifascial swelling lymph drainage rate constants in breast cancer-related lymphedema." Lymphat Res Biol **3**(1): 1-15.

Modi, S., A. W. B. Stanton, et al. (2007). "Clinical assessment of human lymph flow using removal rate constants of interstitial macromolecules: a critical review of lymphoscintigraphy." Lymphatic Res Biol **5**(3): 183-202.

Monteiro-Riviere, N. A., A. O. Inman, et al. (1993). "Topical Penetration of Piroxciam is Dependent on the Distribution of the Local Cutaneous Vasculature." Pharmaceutical Research **10**: 1326-1331.

Nitsche, J. M. and G. B. Kasting (2008). Biophysical models for skin transport. Dermal Absorption and Toxicity Assessment. M. S. Roberts and K. A. Walters. New york, Informa Healthcare**:** 249-267.

Nitsche, J. M., T. F. Wang, et al. (2006). "A Two-Phase Analysis of Solute Partitioning into the Stratum Corneum." J Pharm Sci **95**(3): 649-666.

Nugent, L. J. and R. K. Jain (1984). "Extravascular diffusion in normal and neoplastic tissues." Cancer Research **44**: 238-244.

Obach, R. S. (1999). "Prediction of human clearance of twenty-nine drugs from hepatic microsomal intrinsic clearance data: an examination of in vitro half-life approach and nonspecific binding to microsomes." Drug Metab Dispos **27**: 1350-1359.

Ogston, A. G., B. N. Preston, et al. (1973). Proc R Soc London Ser **A 333**: 297-316.

Olszewski, W., A. Engeset, et al. (1977). "Flow and composition of leg lymph in normal men during venous stasis, muscular activity and local hyperthermia." Acta Physiol Scand **99**: 149-155.

Pain, S. J., R. W. Barber, et al. (2003). "Side-to-side symmetry of radioprotein transfer from tissue space to systemic vasculature following subcutaneous injection in normal subjects and patients with breast cancer." Eur J Nucl Med Mol Imaging **30**: 657-661.

Pappenheimer, J. R., E. M. Renkin, et al. (1951). "Filtration, diffusion and molecular sieving through peripheral capillary membranes; a contribution to the pore theory of capillary permeability." Am J Physiol **167**(1): 13-46.

Parry, G. E., A. L. Bunge, et al. (1990). "Percutaneous absorption of benzoic acid across human skin, I. In vitro experiments and mathematical modeling." Pharmaceutical Research **7**: 230-236.

Pohl, P., S. M. Saparov, et al. (1998). "The size of the unstirred layer as a function of the solute diffusion coefficient." Biophys J **75**: 1403-1409.

Poling, B. E., J. M. Prausnitz, et al. (2001). The properties of gases and liquids. New York, McGraw-Hill.

Porter, C. J. H. and S. A. Charman (2000). "Lymphatic transport of proteins after subcutaneous administration." J Pharm Sci **89**: 297-310.

Potts, R. O. and R. H. Guy (1992). "Predicting skin permeability." Pharmaceutical Research **9**: 663-669.

Pries, A. R., T. W. Secomb, et al. (1994). "Microvascular blood flow resistance: role of endothelial surface layer." Am J Physiol **273**: H2272-H2279.

Rao, H. V. and D. R. Brown (1993). "A physiologically based pharmacokinetic assessment of tetrachloroethylene in groundwater for a bathing and showering determination." Risk Anal **13**: 37-49.

Renkin, E. M. (1964). "Transport of large molecules across capillary walls." Physiologist **60**: 13-28.

Renkin, E. M. (1977). "Multiple pathways of capillary permeability." Circulation Res **41**(6): 735-743.

Renkin, E. M. (1985). "Capillary transport of macromolecules: pores and other endothelial pathways." J Appl Physiol **58**(2): 315-325.

Renkin, E. M. and F. E. Curry (1982). "Endothelial permeability: pathways and modulations." Ann N Y Acad Sci **401**: 248-259.
Renkin, E. M., P. D. Watson, et al. (1977). "Transport pathways for fluid and large molecules in microvascular endothelium of the dog's paw." Microvasc Res **14**(2): 205-214.
Rheosense, I. (2008). Application note: Viscosity measurement of a model protein solution of BSA. **VROC-APP-04**.
Richardson, C. J., K. L. N. Blocka, et al. (1987). "Piroxicam and 5'-hydroxypiroxicam kinetics following multiple dose administration of piroxicam." Eur J Clin Pharmacol **32**: 89-91.
Richardson, C. J., K. L. N. Blocka, et al. (1987). "Piroxicam and 5'-hydroxypiroxicam kinetics following multiple dose administration of piroxicam." European Journal of Clinical Pharmacology **32**(1): 89-91.
Rippe, B. (1993). "A Three-Pore Model of Peritoneal Transport." Perit Dial Int **13 Suppl 2**: S35-38.
Rippe, B. (2008). "Does an endothelial surface layer contribute to the size selectivity of the permeable pathways of the three-pore model?" Perit Dial Int **28**(1): 20-24.
Rippe, B. and B. Haraldsson (1987). "Fluid and protein fluxes across small and large pores in the microvasculature. Application of two-pore equations." Acta Physiol Scand **131**: 411-428.
Rippe, B. and B. Haraldsson (1994). "Transport of macromolecules across microvascular walls: the two-pore theory." Physiol Rev **74**(1): 163-219.
Rippe, B., B. I. Rosengren, et al. (2002). "Transendothelial Transport: The Vesicle Controversy." J Vasc Res **39**(5): 375-390.
Rippe, B., B. I. Rosengren, et al. (2002). "Transendothelial transport: the vesicle controversy." J Vascular Res **39**(5): 375-390.
Rippe, B. and D. Venturoli (2007). "Simulations of Osmotic Ultrafiltration Failure in CAPD Using a Serial Three-Pore Membrane/ Fiber Matrix Model." Am J Physiol Renal Physiol **292**: F1035-F1043.
Roberts, M. S. and S. E. Cross (1999). "A physiological pharmacokinetic model for solute disposition in tissues below a topical application site." Pharmaceutical Research **16**: 1392-1398.
Rosengren, B. I., A. Rippe, et al. (2006). "Transvascular Protein Transport in Mice Lacking Endothelial Caveolae." Am J Physiol Heart Circ Physiol **291**: H1371-H1377.
Ryan, T. J. (1978). The lymphatics of the skin. The physiology and pathophysiology of the skin
A. Jarrett. New York, Academic Press. **5:** 1755-1811.
Sarin, H. (2010). "Physilogic upper limits of pore size of different blood capillary types and another perspective on the dual pore theory of microvascular permeability." Journal of Angiogenesis Research **2**.
Sarin, H. (2010). "Physiologic upper limits of pore size of different blood capillary types and another perspective on the dual pore theory of microvascular permeability." J Angiogen Res **2**: 14-32.

Sarin, H. (2010). "Physiologic upper limits of pore size of different blood capillary types and another perspective on the dual pore theory of microvascular permeability." Journal of Angiogenesis Research **2**: 14-32.

Sawada, G. A., N. F. H. Ho, et al. (1994). "Transcellular permeability of chlorpromazine demonstrating the roles of protein binding and membrane partitioning " Pharmaceutical Research **11**: 665-673.

Schad, H. and H. Brechtelsbauer (1977). "Thoracic duct lypmph in conscious dogs at rest and during changes of physical activity." Pflugers Arch **367**: 235-240.

Schaefer, H. and G. Stuttgen (1976). "Absolute Concentrations of an Antimycotic Agent, Econazole, in the Human Skin after Local Application." Arzneimittelforschung **26**: 432-435.

Schaefer, H., G. Stuttgen, et al. (1978). "Quantitative Determination of Percutaneous Absorption of radiolabeled Drugs In Vitro and In Vivo by Human Skin
" Curr Probl Dermatol **7**: 80-94.

Schaefer, H. and A. Zesch (1975). "Penetration of Vitamin A Acid into Human Skin." Acta Derm Venereol Suppl **74**: 50-55.

Schaefer, H., A. Zesch, et al. (1977). "Penetration, Permeation, and Absorption of Triamcinolone Acetonide in Normal and Psoriatic Skin." Arch Dermatol Res **258**: 241-249.

Scheuplein, R. J. (1965). "Mechanism of percutaneous absorption. I. Routes of penetration and influence of solubility." J Invest Dermatol **45**(5): 334-346.

Scheuplein, R. J. (1967). "Mechanism of percutaneous absorption. II. Transient diffusion and the relative importance of various routes of skin penetration." J Invest Dermatol **48**(1): 79-88.

Scheuplein, R. J. (1978). Skin permeation. The physiology and pathophysiology of the skin. A. Jarrett. New York, Academic Press. **5:** 1669-1752.

Schmid-Schonbein, G. W. (1990). "Microlymphatics and lymph flow." Physiol Rev **70**: 987-1028.

Shatkin, J. A. and H. S. Brown (1991). "Pharmacokinetics of the dermal route of exposure to volatile organic chemicals in water: a computer simulation model." Environ Res **56**: 90-108.

Siddiqui, O., M. S. Roberts, et al. (1989). "Percutaneous absorption of steroids: relative contributions of epidermal penetration and dermal clearance." J Pharmaco Biopharm **17**: 405-424.

Singh, P. and M. S. Roberts (1994). "Skin permeability and local tissue concentration of nonsteroidal anti-inflammatory drugs after topical application." J Pharmacol Exp Ther **268**: 144-151.

Sinko, P. A. (2011). Martin's Physical Pharmacy and Pharmaceutical Sciences. Philadelphia, PA, Lippincott Williams & Wilkins.

Staberg, B., P. Klemp, et al. (1983). "Lymphatic albumin clearance from psoriatic skin." J Am Acad Derm **9**(6): 857-861.

Staverman, A. J. (1951). "The theory of measurement of osmotic pressure." Rec Trav Chimi Pays-Bas **70**: 344-352.

Strand, S. E. and L. Bergqvist (1989). Critical reviews in therapeutic drug carrier systems.

Sugihara-Seki, M. and B. M. Fu (2005). "Blood flow and permeability in microvessels." Fluid Dynam Res **37**: 82-132.
Sugihara-Seki, M. and B. M. Fu (2005). "Blood flow and permeability in microvessels." Fluid Dynamics Research **37**: 82-132.
Supersaxo, A., W. R. Hein, et al. (1990). "Effect of molecular-weight on the lymphatic absorption of water-soluble compounds following subcutaneous administration." Pharmaceutical Research **7**(2): 167-169.
Supersaxo, A., W. R. Hein, et al. (1990). "Effect of molecular weight on the lymphatic absorption of water-soluble compounds following subcutaneous administration." Pharmaceut Res **7**(2): 167-169.
Swartz, M. A. (2001). "The physiology of the lymphatic system." Adv Drug Deliv Rev **20**: 3-20.
Taylor, A. E. and D. N. Granger (1984). Exchange of macromolecules across the microcirculation. Handbook of Physiology. The Cardiovascular System. Microcirculation. Bethesda, MD, Am Physiol Soc. **IV:** 467.
Taylor, G. W., J. B. Kinmonth, et al. (1957). "Lymphatic circulation studied with radioactive plasma protein." Br Med J **1**: 133-137.
Tojo, K., J. A. Masl, et al. (1985). "Hydrodynamic characteristic of an in vitro drug permeation cell." Ind. Eng. Chem. Fundam. **24**: 368-373.
Touitou, E., V. M. Meidan, et al. (1998). "Methods for quantitative determination of drug localized in the skin." J Control Releas **56**: 7-21.
Tsay, R. and S. Weinbaum (1991). "Viscous flow in a channel with periodic cross-bridging fibers of arbitrary aspect ratio and spacing." J Fluid Mech **226**: 126-148.
US_EPA (2009). Estimation Programs Interface Suite™ for Microsoft® Windows. Washington, DC, USA, United States Environmental Protection Agency.
van der Merwe, D., J. D. Brooks, et al. (2006). "A physiologically based pharmacokinetic model of organophosphate dermal absorption." Toxicol Sci **89**: 188-204.
Wang, T.-F., G. B. Kasting, et al. (2007). "A multiphase microscopic model for stratum corneum permeability. II. Estimation of physicochemical parameters and application to a large permeability database." Journal of Pharmaceutical Sciences **96**(11): 3024-3051.
Wang, T. F., G. B. Kasting, et al. (2006). "A Multiphase microscopic model for stratum corneum permeability.I. Formulation, solution and illustrative results for representative compounds." J Pharm Sci **95**(3): 620-648.
Wang, T. F., G. B. Kasting, et al. (2007). "A Multiphase microscopic model for stratum corneum permeability. II. Estimation of physicochemical parameters and application to a large permeability database." J Pharm Sci **96**(11): 3024-3051.
Weinbaum, S., J. M. Tarbell, et al. (2007). "The structure and function of the endothelial glycocalyx layer." Annu Rev Biomed Eng **9**: 121-167.
Weinbaum, S., J. M. Tarbell, et al. (2007). "The structure and function of the endothelial glycocalyx layer." Annu Rev Biomed Eng **9**: 121-167.
Weinbaum, S., R. Tsay, et al. (1992). "A three-dimensional junction-pore-matrix model for capillary permeability." Microvasc Res **48**: 85-111.
Weiss, H. M., M. Fresneau, et al. (2008). "Binding of pimecrolimus and tacrolimus to skin and plasma porteins: implications for systemic exposure after topical application." Drud Metabolism and Disposition **36**(9): 1812-1818.

Weiss, H. M., M. Fresneau, et al. (2008). "Binding of pimecrolimus and tacrolimus to skin and plasma proteins: implications for systemic exposure after topical application." Drug Metabolism and Disposition **36**(9): 1812-1818.

Weiss, H. M., M. Fresneau, et al. (2008). "Binding of pimecrolimus and tacrolimus to skin and plasma proteins: implications for systemic exposure after topical application." Drug Metab Dispos **36**(9): 1812-1818.

Wilschut, A., W. F. ten Berge, et al. (1995). "Estimating skin permeation. The validation of five mathematical skin penetration models." Chemosphere **30**: 1275-1296.

Xiang, T.-X. and B. D. Anderson (1995). "Phospholipid surface density determines the partitioning and permeability of acetic acid in DMPC:cholesterol bilayers." J. Membrane Biol. **148**: 157-167.

Xiang, T.-X. and B. D. Anderson (1997). "Permeability of acetic acid across gel and liquid-crystalline lipid bilayers conforms to free-surface-area theory." Biophys. J. **72**: 223-237.

Xiang, T. X. and B. D. Anderson (1994). "The relationship between permeant size and permeability in lipid bilayer membranes." J Membrane Biol **140**: 111-122.

Yalkowski, S. H. (1993). AQUASOL database. Tucson, University of Arizona.

Yamashita, S., T. Furubayashi, et al. (2000). "Optimized conditions for prediction of intestinal drug permeability using Caco-2 cells." Eur J Pharm Sci **10**: 195-204.

Yamazaki, K. and M. Kanaoka (2004). "Computational prediction of the plasma protein-binding percent of diverse pharmaceutical compounds." Journal of Pharmaceutical Sciences **93**(6): 1480-1494.

Zesch, A. and H. Schaefer (1975). "Penetration of Radioactive Hydrocortisonein Human skin from Various Ointment Bases." Arch Dermatol Forsch **252**: 245-256.

Zhang, X., R. H. Adamson, et al. (2006). "A 1-D model to explore the effects of tissue loading and tissue concentration gradients in the revised starling principle." Am J Physiol Heart Circ Physiol **291**: H2950-H2964.

University of Cincinnati

Date: 10/26/2012

I, Rania Ibrahim , hereby submit this original work as part of the requirements for the degree of Doctor of Philosophy in Pharmaceutical Sciences/Biopharmaceutics.

It is entitled:

Improved Estimation of Transport Parameters in the Dermis

Student's name: **Rania Ibrahim**

This work and its defense approved by:

Committee chair: Gerald Kasting, PhD

Committee member: Pankaj Desai, PhD

Committee member: Joel Fried, PhD

Committee member: Kevin Li, PhD

Committee member: R. Randall Wickett, PhD

3060